

# Garcia Center

Polymers at Engineered Interfaces

## Summer Program 2014



**“The program has no set time limits. Research is a lifelong experience and we hope to remain a resource to our students long after ‘graduation’.”**



The Garcia Center for Polymers at Engineered Interfaces was founded in 1996 and is named after the late Queens College professor Narciso Garcia, who was a pioneer in the integration of education and research. The Center focuses on the integration of materials research with tissue engineering, biomaterials, drug delivery systems, sustainable energy, nanocomposites, and recently, additive manufacturing. The Center also supports innovation through entrepreneurship and has multiple collaborations with industry and national laboratories, both in the US and abroad.

For information on the numerous programs that are available please see our website at:

<http://polymer.matscieng.stonybrook.edu>



The research scholar program offers the opportunity for high school teachers and students to perform research on the forefront of polymer science and technology together with the Garcia faculty and staff. Students work as part of focus research teams are taught to make original contributions of interest to the scientific community. In addition to entering national competitions, the students are encouraged to publish in refereed scientific journals, present their results at national conferences, and develop patents to protect their intellectual property.

Our goal is to convey to the students the excitement we enjoy daily in research and provide for them a supportive network within the scientific community. Research is a lifelong experience and we hope to remain a resource to our students long after “graduation”.

*Miriam Rafailovich and Jonathan Sokolov*

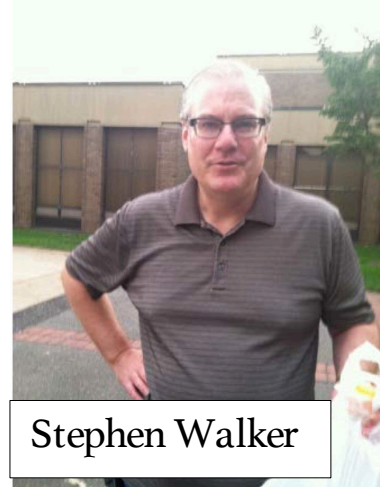
# *Faculty & Staff*



John Jerome



Jerell Aguila



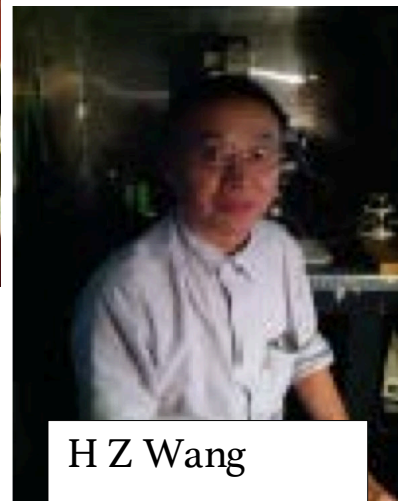
Stephen Walker



Ying Liu



Chris Gordon



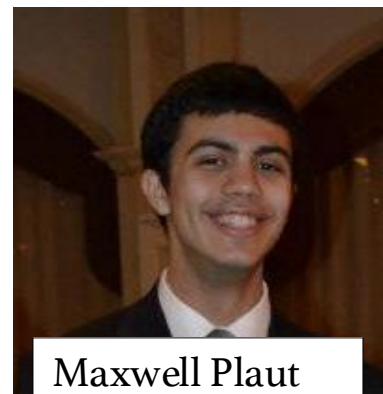
H Z Wang



Chung-Chueh  
(Simon) Chang



Adriana Pinkas-  
Sarafova



Maxwell Plaut



Marcia  
Simon



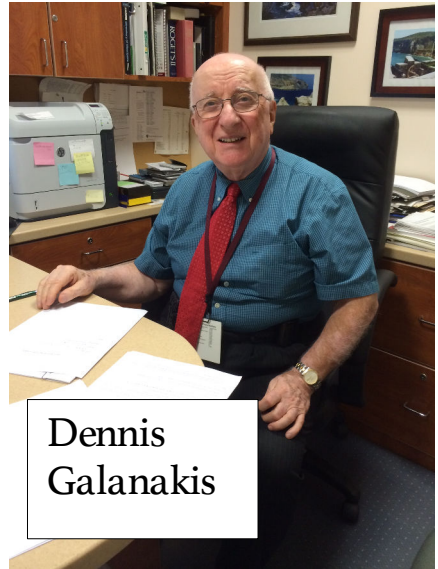
Maya Endoh



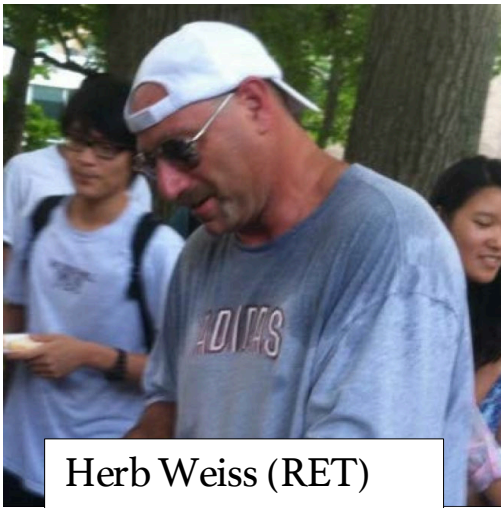
Tatsiana Mironava



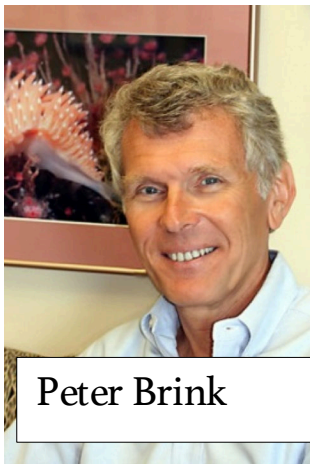
Molly Gentleman



Dennis Galanakis



Herb Weiss (RET)



Peter Brink



Dilip Gersappe



Julie Arslanoglu



David Perraglia



Rebecca Isseroff (RET)



Terrence Bissoondial (RET)



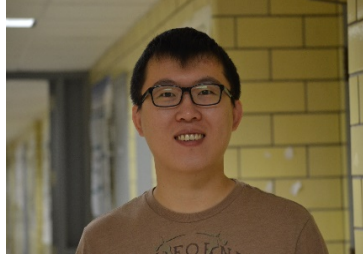
Mariah Geritano

Not Pictured:  
Manju Prakash (RET)

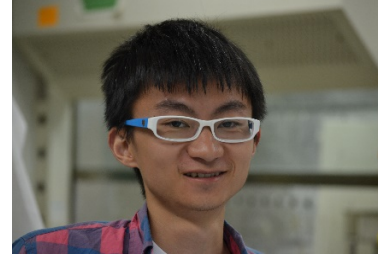
# *Graduate Students*



*Clement Marmorat*



*Hongfei Li*



*Juyi Li*



*Kai Yang*



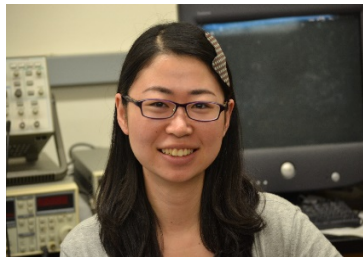
*Ke Zhu*



*Kuan-Che Feng*



*Linxi Zhang*



*Liudi Zhang*



*Longtao Han*



*Na Hyun Cho*



*Shan (Harry) He*



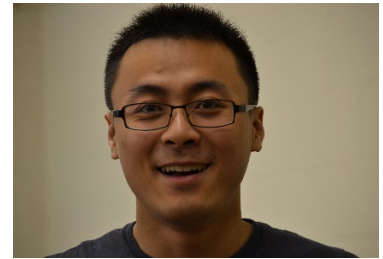
*Sisi Qin*



*Vincent Ricotta*



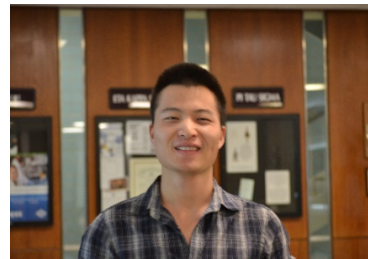
*Yan Xu*



*Yichen Guo*



*Yingjie Yu*



*Zhenhua Yang*

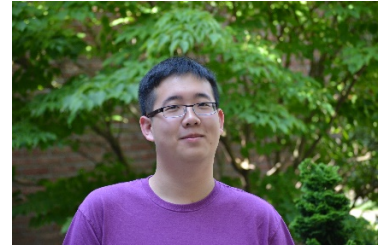
# *Research Experience for Undergraduates*



*Aaron Gochman*



*Allison Lee*



*Andrew Chen*



*Evelyn Kandov*



*Greta Huang*



*Gurkirat Singh*



*Jake Plaut*



*Jinying Lin*



*John Mele*



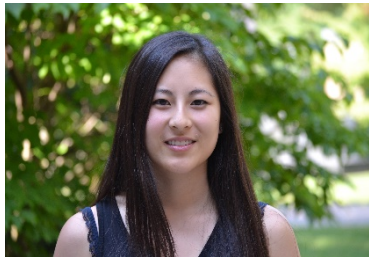
*Julia Landsberg*



*Monika Batra*



*Priyanka Talwar*



*Rachel Yang*



*Ruiyi Gao*



*Sneha Chittabathini*



*Steven Krim*



*Tehila Stone*

# *High School Students*



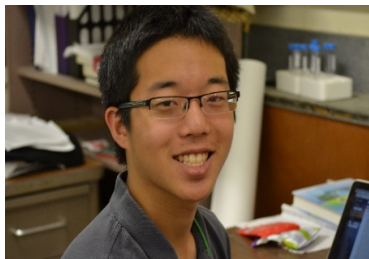
*Abigail Wax*



*Adina Singer*



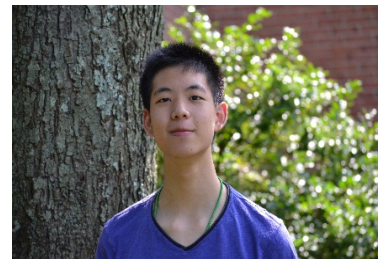
*Akash Wasil*



*Albert Tung*



*Anna Vaynrub*



*Arthur Chen*



*Arun Soni*



*Benjamin Golbin*



*Constance Lam*



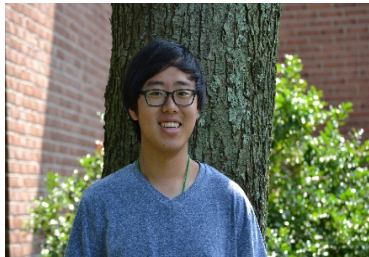
*Dan Kim*



*Daniel Foreman*



*Daphne Chen*



*David Choi*



*David Lin*



*Devorah Saffern*



*Elaina Zodiatis*



*Eliana Krim*



*Elizabeth Varghese*



*Emily Braverman*



*Eric Weitschner*



*Evan Hochhauser*



*Evan Lander*



*Gina Yuan*



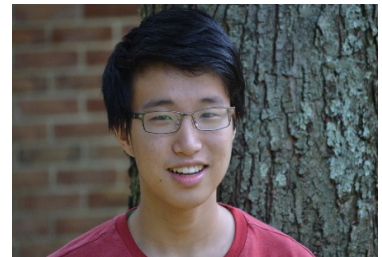
*Henry Dong*



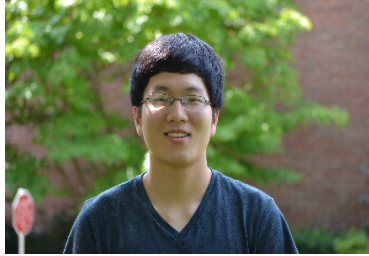
*Ilana Radinsky*



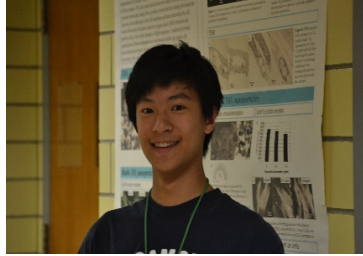
*Jacqueline Barash*



*Jay Cho*



*Jaymo Kang*



*Jeffrey Cheng*



*Jessica Kim*



*Joshua Goldstein*



*Joshua Lederer*



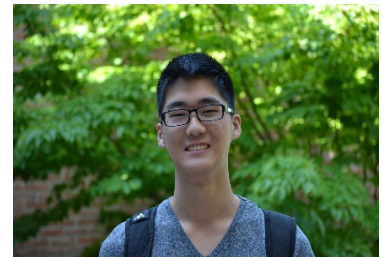
*Julie Vaughn*



*Justin Lish*



*Karena Etwaru*



*Luke Shin*



*Laura Pang*



*Lee Blackburn*



*Leeson Chen*



*Levy Sominsky*



*Mairead Milan*



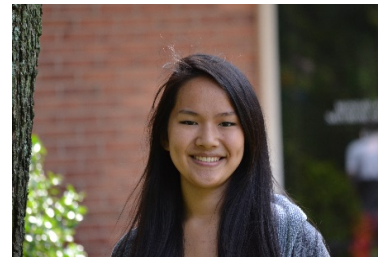
*Mason Zhang*



*Matthew Wu*



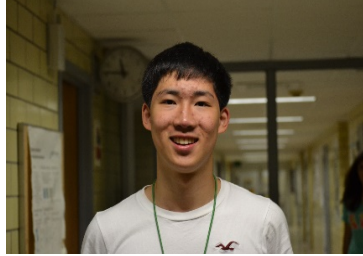
*Meena Jagadeesan*



*Meghan Bialt-DeCelie*



*Michael Meng*



*Michael Qu*



*Naomi Shapiro*



*Nicholas Han*



*Noah Davis*



*Pinelopi Margeti*



*Roshan Patel*



*Russell Charnoff*



*Ruth Kopyto*



*Ryan McCaffrey*



*Sal Fu*



*Sanket Desai*



*Sanket Mehta*



*Scarlett Guo*



*Shira Li*



*Taicheng Song*



*Tiffanie Yang*



*Vivek Subramaniam*



*William Berger*



*William Fried*



*Won Park*



*Zechariah Rosenthal*

*Not Pictured: Omkar Sreekanth*

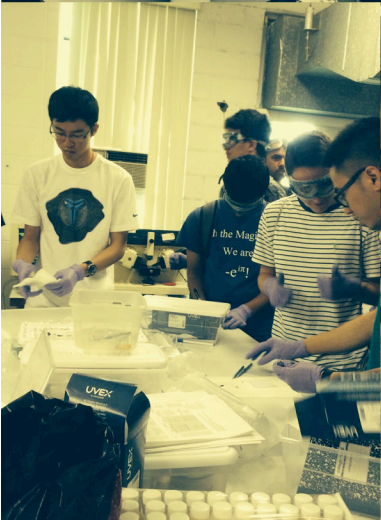
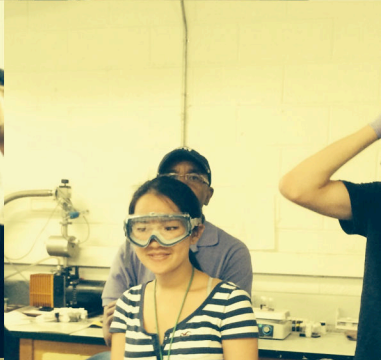
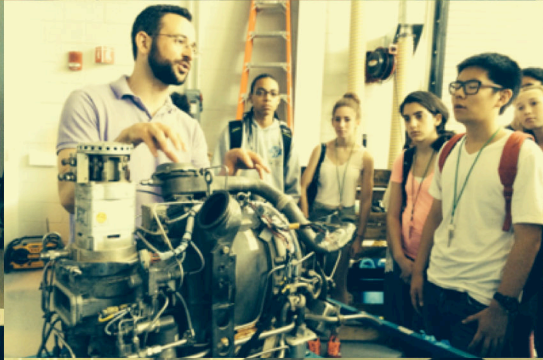
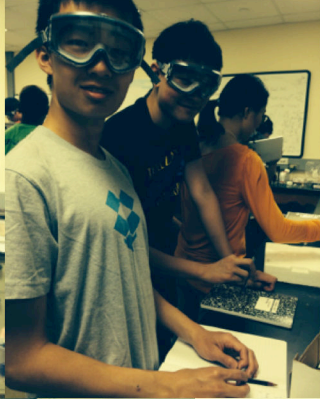
# Garcia Research Scholars Summer Program 2014

June 30 – August 12

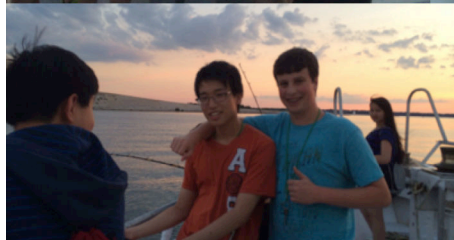
Sunday	Monday	Tuesday	Wednesday	Thursday	Friday	Saturday
	30	1	2	3	4	5
	<p><b>Anne Scheidt:</b> Welcome to Garcia!</p> <p><b>Dr. Srinivas Pentyala:</b> Intro to Research</p> <p><b>Dr. Dennis Galanakis:</b> Fibrinogen and Clots</p> <p><b>Dr. Lenny Poveromo:</b> Composite Prototype Center</p> <p><b>Allan Sachs:</b> Preparing for paper competitions and ISEF/LISEF</p> <p><b>Dr. Ron Tabitas:</b> DSA: Distributed Energy Project</p>	<p><b>Dr. Jason Trelowitz:</b> Nano-mechanics</p> <p><b>Dr. Peter Brink:</b> Cell Biophysics</p> <p><b>Dr. Rina Tannenbaum:</b> Characterization with Nanoscale Precision</p> <p><b>Dr. Jon Sokolov:</b> DNA Research Methods</p>	<p>Safety Training &amp; Facilities Tour</p>	<p><b>Dr. Jerry Yang:</b> Stem Cells</p> <p><b>Dr. Steven Schwartz:</b> Physics of Thin Film Processing</p> <p><b>Rebecca Isseroff:</b> Graphene Chemistry and Laboratory Notebooks</p> <p><b>Dr. Alvin Silverstein:</b> LEED Buildings and tour or Energy Center</p>	<p>Happy 4<sup>th</sup> of July!!</p> 	

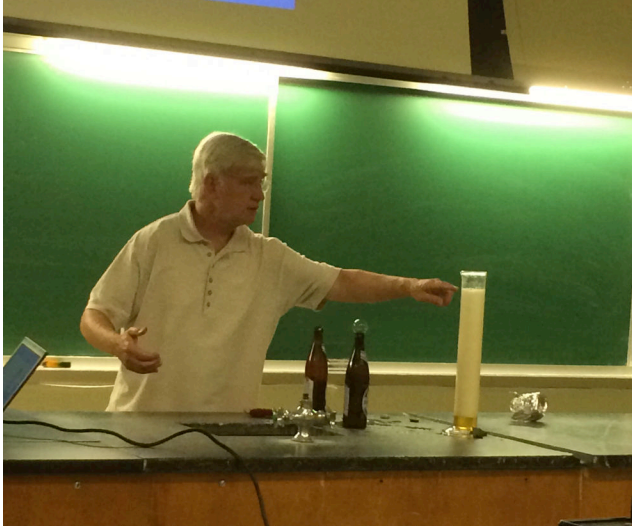
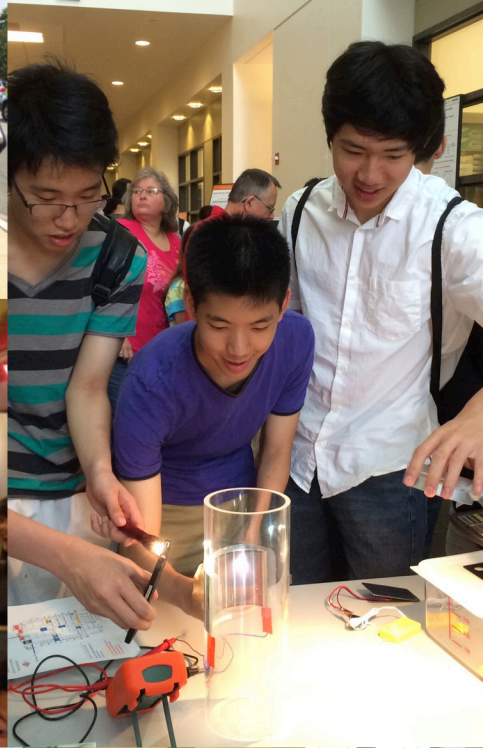
6	7	8	9	10	11	12
	<b>Dr. Marcia Simon:</b> Wound Healing and Stem Cells  Spin casting Experiment	<b>Dr. Dillip Gersappe::</b> Theoretical Modeling  Spin casting Experiment	<b>Dr. Chris Joubert</b> Stem Cells in Endodontics  <b>Dr. Molly Gentleman:</b> Super-Hydrophobic Materials  <b>Dr. Myungwoong Kim:</b> Electroresponsive Polymers  Journal Club	<b>Dr. Steven Walker:</b> Microbiology  <b>Dr. Tatsiana Mironova:</b> Nanotoxicology  <b>Dr. Adriana Pinkas-Sarafova:</b> Working with Dental Pulp Stem Cells	<b>Dr. Terrence Bissoondial:</b> Working with a partner  <b>Dr. Scheidt:</b> Starting a Business  Pizza Lunch	
13	14	15	16	17	18	19
		<b>Brooke Ellison:</b> Ethics of Stem Cell Research		Celtic Quest Fishing Trip 	Pizza Lunch	
20	21	22	23	24	25	26
BNL Science Sundays Trip				<b>Katherine Vorvalkos:</b> Working for the Government	Canoe Trip 	
27	28	29	30	31	1	2
		Softball Game 		Soccer Game	Pizza Lunch	
3	4	5	6	7	8	9
		Basketball Game 	<b>Dr. Eberhardt Mahnke:</b> Science for Artwork	Met and Art Science Center Trip	Pizza Lunch	
10	11	12				
		End-of-Summer Symposium				

# Spin Casting Experiment



# Celtic Quest Fishing Trip





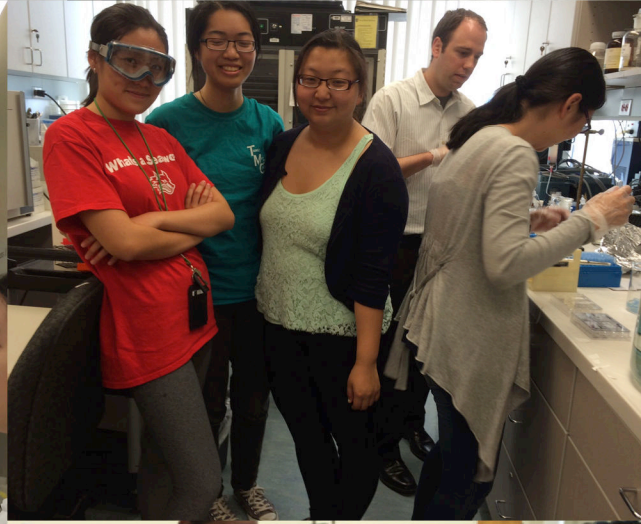
# BNL Science Sundays and Met trip

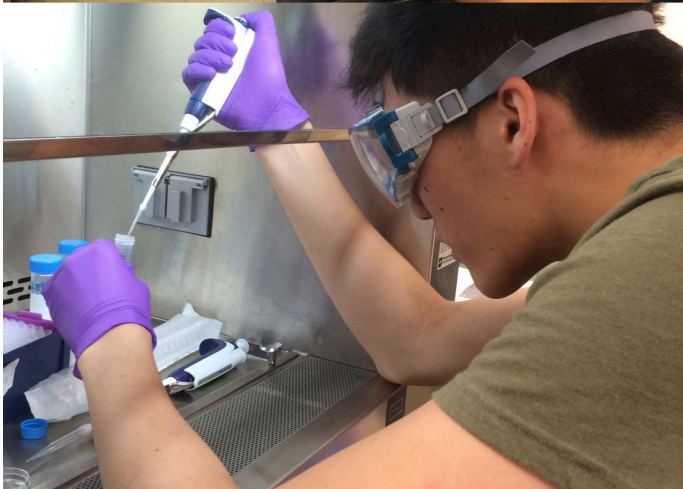
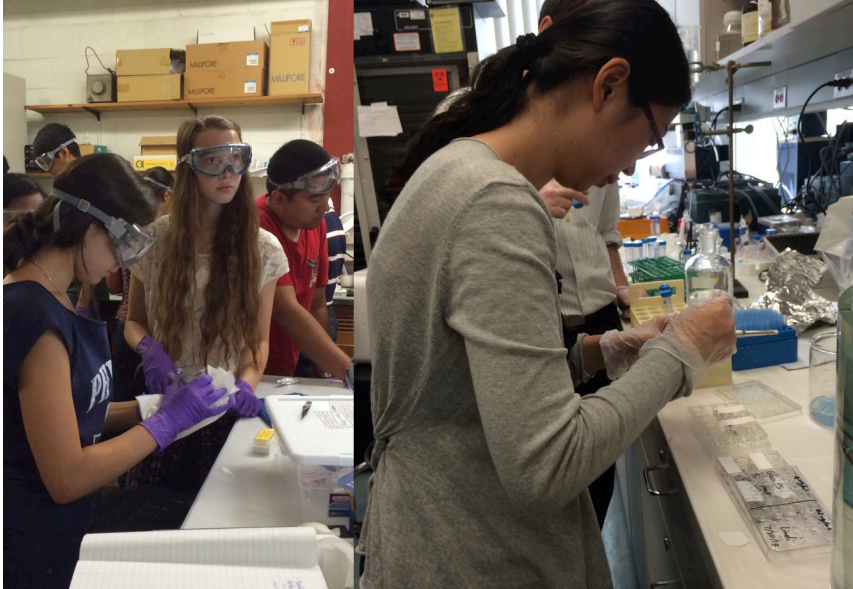
# Canoe Trip





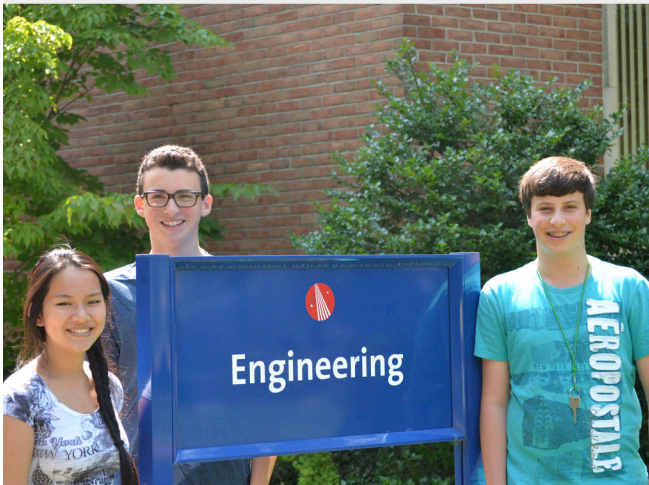
# In the Lab







# Out of the Lab



# SUMMER RESEARCH SYMPOSIUM 2014

**10:30 -10:38**

**SESSION 1 – ENVIRONMENTAL REMEDIATION**

**Chairs: Jacob Plaut, *Baruch College* & John Mele, *Stony Brook University***

Developing a Novel Nanoparticle-Infused Cream to Impede the Feeding Mechanisms of *Aedes Aegypti*

**Evan Hochhauser, Albert Tung, Eric Wietschner**

Exploring the Phytotoxicity of ZnO Nanoparticles and the Mechanisms of Transport in the Prothallial Cells of *Ceratopteris richardii*

**Meghan Bialt-DeCelie, Benjamin Golbin, Levy Sominsky**

Analysis and Comparison of Various Polymer Fibers for Use in Prototyping *Cimex lectularius* Trapping Mechanism

**Won Park, Zechariah Rosenthal**

**10:40-10:46**

**SESSION 2 – BIOPOLYMERS ON SURFACES**

**Chairs: Ruiyi Gao, *Yale University* and Priyanka Talwar, *Georgia Institute of Technology***

A Novel DNA Sequencing Method: Using Soft Lithography to Cut DNA and Extracting DNA from the Enzyme Stamped Surface

**Meena Jagadeesan, Adina Singer**

Investigating the Effect of Variable Polymer Surfaces and Soluble Protein Factors on Fibrin Formation and Platelets Aggregation

**Scarlett Guo, Laura Pang**

**10:48-10:56**

**SESSION 3 – FLAME RETARDANTS**

**Chair: Tehila Stone, *Princeton University***

Investigating the Application of Cellulose in Biodegradable Flame Retardant Polymer Blends

**Shira Li, David Lin**

Biodegradable, Flame Retardant Wood-Plastic Composites Via *In Situ* Polymerization of Lactide Monomer

**Noah Davis, Dan Kim**

Halogen Free Flame Retardant Polymer Nanocomposites

**William Berger, Elaina Zodiatis**

**10:58-11:03**

**SESSION 4 – NANOCOMPOSITES**

**Chair: Gurkirat Singh, *Stony Brook University***

Synthesis and Characterization of Graphene Nanoparticle Infused Polyethylene Nanocomposite Material for Enhanced Mechanical and Conductivity Properties  
**David Choi, Arun Soni, Russell Charnoff**

Effect of Clay on High Density Polyethylene: Oxygen Permeability  
**Taicheng Song**

**11:05-11:15**

**SESSION 5 – DENTAL PULP STEM CELLS ON SURFACES**

**Chairs: Greta Huang, *UC Berkeley*, Monika Batra, *Stony Brook University*, and Rachel Yang, *Cornell University***

**Part 1: 3D Surfaces**

Characterization of 3D Printed PLA Cell Scaffolds Versus Compressed PLA Scaffolds and Effect on DPSC Differentiation

**Leeson Chen**

Creation of a Drug Delivery Mechanism for Dexamethasone Differentiation of Dental Pulp Stem Cells

**Ryan McCaffrey**

**Part 2: 2D Surfaces**

Investigating Proliferation and Differentiation of Dental Pulp Stem Cells on Polystyrene/Polybutadiene Blends and Graphene/Polybutadiene Substrates

**Sanket Mehta, Vivek Subramaniam**

Effects of Stimulated Photovoltaic Substrate and Static Magnetic Fields on Dental Pulp Stem Cell Proliferation and Differentiation

**Jay Cho, Mason Zhang**

Dental Pulp Stem Cell Mobility on Cornell Polymer Films

**Sanket Desai**

**11:17- 11:27**

**SESSION 6 – CELL JUNCTIONS AND CELL MIGRATION**

**Chairs: Sneha Chittabathini and Evelyn Kandov: *Stony Brook University***

Sustained drug delivery of silver curcumin nanoparticles for wound healing in dermal fibroblasts

**Daphne Chen**

Increased Junctional Conductance and Intercellular Channel Formation in CX43 HeLa Cells Exposed to Graphene

**Abigail Wax, Karena Etwaru**

Identifying the Age-Dependency of Human Dermal Fibroblast Uptake and the Cytotoxic Response to Gold Nanoparticles of Varying Concentrations

**Emily Braverman, Elizabeth Varghese, Anna Vaynrub**

Mechanisms of Migration of Human Dermal Fibroblasts on various topographically distinct scaffolds and when treated with the p12 peptide

**Eliana Krim, Mairead Milan, Naomi Shapiro**

**11:29-11:39**

**SESSION 7 – THE INFLUENCE OF HYDROGEL SCAFFOLDS ON CELL BEHAVIOR**

**Chair: Aaron Gochman, Stony Brook University**

Engineering Hydrogel Scaffolds for the Culture of Endothelial Cells and Applying Titanium Dioxide Nanoparticles to Regulate Proliferation

**Pinelopi Margeti**

The Modelization and Characterization of Hydrogel Cross-linking Using Microbial Transglutaminase as a Cross-linking agent

**Jaymo Kang, Joshua Lederer**

Crosslinked Hydrogels as a Platform for Mineralization with Dental Pulp Stem Cells

**Tiffany Yang, Heesu Shin**

Optimizing Conditions to Proliferate Hematopoietic Stem Cells without Differentiation

**Ruth Kopyto**

The Effects of Various Substrate Interfaces and Stemregenin1 on Hematopoietic Stem Cell Proliferation and Stemness *in vitro*

**Henry Dong**

**11:41- 11:46**

**SESSION 8 – FUEL CELLS**

**Chair: Jinying Lin, Stony Brook University**

Increasing the Performance of PEM Fuel Cells with Nanoparticle Alloys on the Nafion Membrane

**Akash Wasil, Roshan Patel, William Fried**

Effects of Carbon Chain Length in Thiol-Functionalized Gold Nanoparticles Coating a Nafion® Membrane on PEM Fuel Cell Efficiency

**Ilana Radinsky**

**11:48-11:54**

**SESSION 9 – SOLAR POWER**

**Chair: Steven Krim, *Stony Brook University***

Construction of the OPB Active Layer Using the LB Trough or Inducing Polymer Phase Separation to Improve Morphology and Efficiency

**Wanying Fu, Nicholas Han**

Creating a Solar-Powered Water Filtration System

**Josh Goldstein, Daniel Foreman**

**11:56-12:08**

**SESSION 10 – GRAPHENE**

**Chairs: Andrew Chen, *Rice University* and Allison Lee, *University of Maryland***

Characterizing and Utilizing Silver Graphene and Iron Graphene Nanoparticles

**Jaqueline Barash**

Enhancing the Power Conversion Efficiency of Organic Photovoltaics via Exciton Gap Reduction through the Integration of Functionalized Reduced Graphene Oxide and Phase Separated Polymer Morphology

**Jessica Kim**

Optimizing Hole Extraction Layers of OPV Cells with Functionalized Graphene Derivatives

**Michael Meng, Jeffrey Cheng, Michael Qu**

Investigating Novel Antibacterial Properties of Graphene, TiO<sub>2</sub> nanoparticles, and PDMS and EVA-based Phase Separated Polymer Blends

**Devorah Saffern, Julie Vaughn**

Coating Fuel Cell Membranes with Different Functionalization of Graphene Oxide and Reduced Graphene Oxide to Enhance PEM Fuel Cell Efficiency

**Lee Blackburn, Arthur Chen, Justin Lish**

Compatibilization of Thin Films Binary Polymer Blend Using Pure and Oxidized Graphene

**Evan Lander, Omkar Sreekanth**

**12:10-12:15**

**SESSION 11 – SIMULATION AND MODELLING**

**Chair: Julia Landsberg, *Queens College of CUNY***

Using Nanofillers to Strengthen Polymer Blends

**Matthew Wu**

Designing Tablets for Personalized Medicine

**Gina Yuan**

Optimizing the Morphology of Solar Cells

**Constance Lam**

# SESSION I:

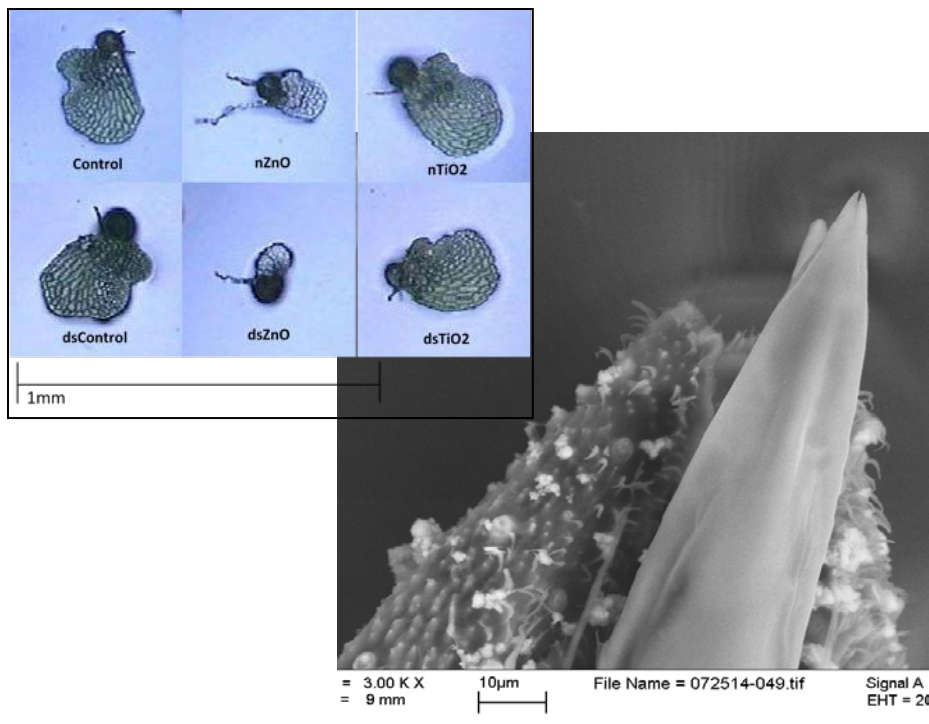
# ENVIRONMENTAL

# REMEDIATION

MENTORS: TERRENCE BISSOONDIAL

HARRY SHAN HE

LINXI ZHANG



# Developing a Novel Nanoparticle-Infused Cream to Impede the Feeding Mechanisms of *Aedes Aegypti*

**Evan Hochhauser**, Half Hollow Hills High School West, Dix Hills, NY 11746

**Eric Wietschner**, Hebrew Academy of the Five Towns and Rockaway, Cedarhurst, NY 11516

**Albert Tung**, University High School, Irvine, CA 92612

**Harry Shan He and Linxi Zhang**, Stony Brook University, Stony Brook NY 11790

**Dr. Miriam Rafailovich**, Stony Brook University, Stony Brook NY 11790

The *Aedes aegypti* mosquito is a carrier of many vectors responsible for numerous diseases including dengue fever, chikungunya, and yellow fever. Current measures to repel mosquitoes involve using repellent such as N,N-Diethyl-3-methylbenzamide (or DEET) which interferes with the chemical receptors of mosquitoes<sup>1</sup>. However, DEET is toxic if ingested and has many side effects<sup>2</sup>. Our work focuses on developing and optimizing a nanoparticle infused cream to inhibit the feeding process of *Aedes Aegypti*. Moisturizing creams were prepared containing either bentonite sodium clay nanoparticles, halloysite clay nanoparticles, rutile titanium dioxide (TiO<sub>2</sub>) nanoparticles, or rutile TiO<sub>2</sub> nanoparticles coated with poly(methyl vinyl ether-alt-maleic acid) and oligomeric proanthocyanidins in a 15% concentration. Female *Aedes aegypti* mosquitoes were exposed to feeding wells filled with bovine blood and covered with a collagen membrane coated with the various creams. The feeding of the mosquitoes was evaluated through live video, and the amount of blood ingested was determined post-mortem through optical microscopy. Statistically, the coated rutile TiO<sub>2</sub> particle cream significantly inhibited the feeding abilities of the yellow fever mosquito by 40 percent (Figure 1). Optical, confocal, and EdX spectroscopy revealed amounts of titanium dioxide near and in the proboscis of mosquitoes (Figure 2). Subsequent SEM analysis of the titanium dioxide nanoparticles showed that TiO<sub>2</sub> has a diameter of size  $15.0 \pm 3.5$  nm and that the nanoparticles frequently aggregate (Insert). As such, visual evidence of the presence of titanium dioxide nanoparticles on the proboscis of mosquitoes and of their ability to aggregate confirm that the nanoparticles are responsible for the inhibition.

Figure 1: 7/8/14 test on *Aedes Aegypti* mosquitoes with the average percentage of mosquitoes engorged with blood taken from three repetitions.

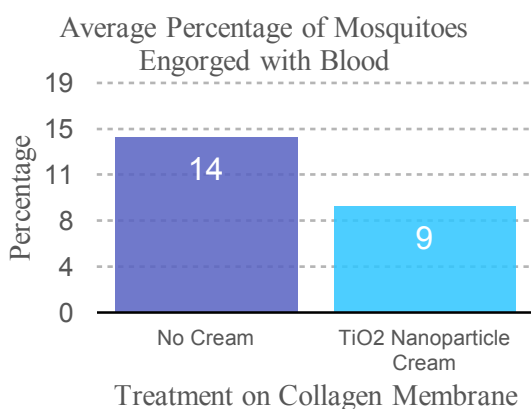
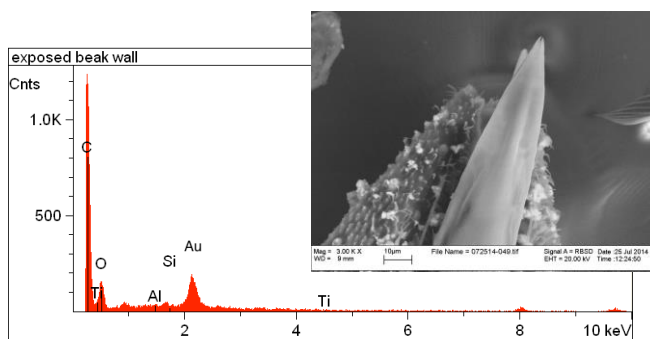


Figure 2. Energy-dispersive X-ray spectroscopy spectrum of the exposed beak wall of a partially fed mosquito which indicates the presence of titanium and oxygen, hence titanium dioxide nanoparticles



Insert: . SEM image of titanium dioxide infused cream depicting the aggregation of the titanium dioxide in the cream. Aggregates are approximately 1-2  $\mu$ m.

<sup>1</sup> Pellegrino, M., Steinbach, N., Stensmyr, M. C., Hansson, B. S., & Vosshall, L. B. (2011). A natural polymorphism alters odour and DEET sensitivity in an insect odorant receptor. *Nature*, 478(7370), 511-514.

<sup>2</sup> Robbins, P. J., & Cherniack, M. G. (1986). Review of the biodistribution and toxicity of the insect repellent- diethyl- - toluamide (DEET). *Journal of Toxicology and Environmental health*, 18(4), 503-525.

## Exploring the phytotoxicity of ZnO nanoparticles and the mechanism of transport in the prothallial cells of *Ceratopteris richardii*

Meghan Bialt-DeCelie, Benjamin Golbin, Levy Sominsky, and Dr. Terrence Bissoondial  
George W. Hewlett HS, Hewlett NY, 11557

Zinc ( $Zn^{2+}$ ) cation is an essential cofactor for numerous enzymes and is indispensable in stabilizing the structure and consequently the function of many proteins [1]. Heavy industrialization has led to increased contamination of agricultural fields with zinc, which in excess is cytotoxic [2]. The toxicity of this heavy metal is further amplified with the wide commercial usage of zinc oxide nanoparticles [3]. The ZIP (ZRT, IRT-like Protein) family of transporters plays an integral role in the uptake, translocation and subcellular distribution in seeded plants [4]. In non-seeded plants, the ZIP gene family remains uncharacterized. In this study, a full length orthologue of a ZIP gene (designated CrZIP1) was identified and isolated in the fern *Ceratopteris richardii* by screening the EST cDNA library and utilizing 3' RACE PCR. *In silico* analyses revealed that the gene codes for a putative membrane bound protein (plasma membrane or vacuolar) with 8 transmembrane domains and numerous post-translation modifications, characteristic of ZIP transporters in seeded plants. Phylogenetic studies showed that CrZIP1, as well as putative ZIP genes from the bryophyte *Phycomitrella patens* and the lycophyte *Selaginella moelendorfii* are more closely related to ZIP4/IRT3 in *Arabidopsis thaliana*. Analysis of the EST cDNA libraries of *Phycomitrella* and *Selaginella* suggests differential regulation of various paralogues or isoforms of the ZIP genes identified in these organisms. RT-PCR analysis on RNA isolated from spores of *Ceratopteris* showed that the CrZIP1 gene is more transcribed in zinc deficiency conditions and down-regulated in an excess of zinc. Knockdown of CrZIP1 by RNA interference (RNAi) resulted in gametophytes with reduced cell division and chlorophyll production in the prothalli when grown on C-Fern media containing ZnO nanoparticles (Figure1). Cell elongation and rhizoid formation were however promoted under these conditions. The results from this study suggest that CrZIP1 may be the primary zinc transporter of prothallial cells and an initial knockdown of CrZIP may lead to an alternative transport of Zn into the cell. The use of this secondary transport may result in higher level of cytosolic zinc, explaining the observed increase in toxicity.

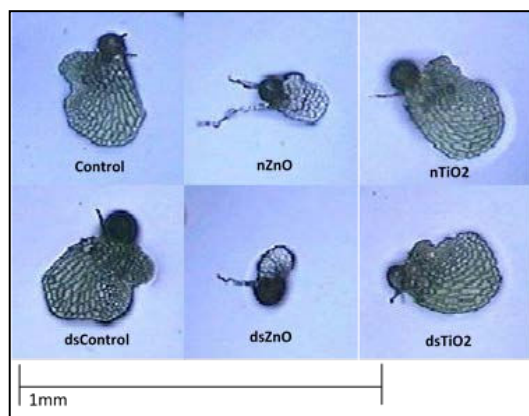


**Figure 1. RNAi of CrZIP1 in the *Ceratopteris richardii*.** Spores were incubated with double stranded RNA (ds) to knockdown the level of CrZIP1 transcripts. After knockdown, spores were plated C-Fern Media containing 100mg/L of ZnO or TiO<sub>2</sub> nanoparticles (<100nm). Control plates had no nanoparticles. Gametophytes shown are 10 days old.

<sup>1</sup> Sharma, Ashish, et al. "Zinc—an indispensable micronutrient." *Physiology and Molecular Biology of Plants* 19.1 (2013): 11-20.

<sup>2</sup> Clemens, S. "Toxic metal accumulation, responses to exposure and mechanisms of tolerance in plants." *Biochimie* 88.11 (2006): 1707-1719.

<sup>3</sup> Stampoulis, Dimitrios, Saion K. Sinha, and Jason C. White. "Assay-dependent phytotoxicity of nanoparticles to plants." *Environmental science & technology* 43.24 (2009): 9473-9479.

<sup>4</sup> Guerinot, Mary Lou. "The ZIP family of metal transporters." *Biochimica et Biophysica Acta (BBA)-Biomembranes* 1465.1 (2000): 190-198.

# Analysis and Comparison of Various Polymer Fibers for Use in Prototyping a *Cimex lectularius* Trapping Mechanism

Won Park, Herricks HS, New Hyde Park NY, 11040, Zechariah Rosenthal, Rambam Mesivta HS, Lawrence NY, 11559, John Mele, Stony Brook University, Stony Brook NY, 11794, Jacob Plaut, Rambam Mesivta HS, Lawrence NY, 11559, Harry Shan He, Stony Brook University, Stony Brook NY, 11794, Linxi Zhang, Stony Brook University, Stony Brook NY, 11794

Bed bug infestations have become a widespread problem throughout the world. In the past few decades, bed bugs have developed a resistance to many pesticides making them very difficult to exterminate[1,2]. Current treatments are often expensive and use environmentally harmful chemicals. Our goal is to understand, improve, and prototype the novel trapping mechanism which uses electrospun recycled polymers to create a more efficient and pesticide free solution to the bed bug problem.

Fibers were prepared for electrospinning by dissolving the recycled polystyrene, otherwise known as Styrofoam, in a tetrahydrofuran dimethylformamide solution. Many other polymers at varying concentrations were electrospun[3] as well for comparison including poly-(butylene adipate-co-terephthalate), polystyrene, polylactic acid, polypropylene, and polyethylene terephthalate. After the fibers were electrospun they were used for several analytical procedures. The first of these procedures was optical microscopy which was used in order to determine fiber diameter and interfiber spacing. The fibers must be wide enough to let the bed bug leg into the mesh, but concentrated enough to tangle its leg hairs, as seen in Figure 1. Next we tested the relative shear modulus comparing polystyrene and recycled polystyrene fibers using Atomic Force Microscopy (Figure 2). Comparing the fibers' shear moduli is essential in finding the optimal rigidity that matches the strength of the bed bug: hard enough so that the bed bug cannot break the fiber, but soft enough to allow its leg into the mesh. Other analysis of the fibers included composition analysis using FTIR and calculating the dielectric constant as well as the zeta potential.

Understanding which characteristics of our fiber contribute to its ability to trap bed bugs could then be used to figure out how to capture other insects. By altering the aforementioned attributes of the fibers, improvements can be made on the mechanism's efficiency and specificity when used with each insect. This information can be used to assist in synthesizing fibers for mass production and to help encourage further utilization for other areas of pest control.

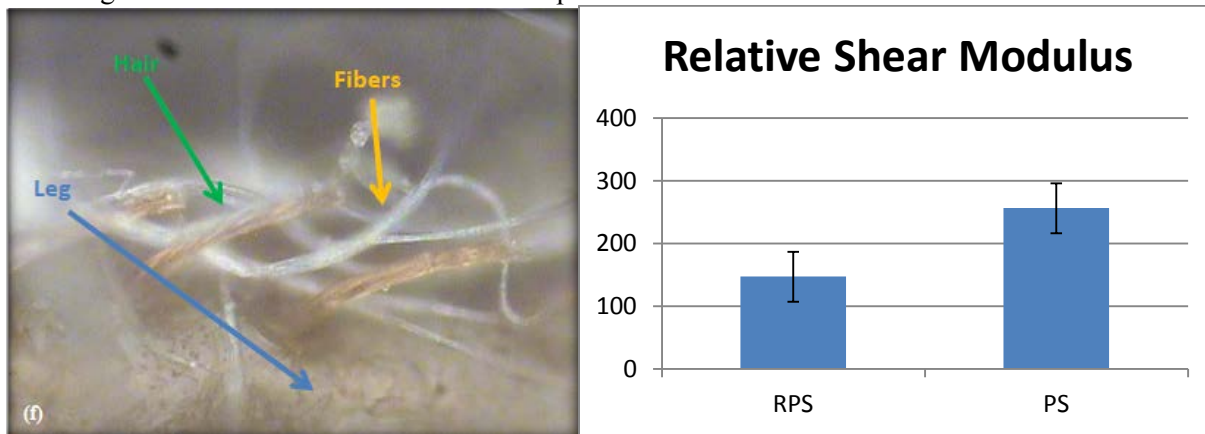


Figure 1: Bed bug leg hairs trapped in RPS fibers. 50x mag [4]

Figure 2: Relative Shear Modulus of polystyrene and recycled polystyrene from Atomic Force Microscopy

[1] Usinger RL. *Monograph of Cimicidae*. Vol 7. College Park, MD: Thomas Say Foundation; 1966

[2] Harlan, Harold. "Improved Strategies Necessary to Combat Bed Bug Resurgence." *Infectious Disease News* n.d.: n. pag. *Infectious Disease News*. Healio.com, Jan. 2012. Web. 27 Aug. 2013.

[3] Doshi, Jayesh, and Darrell H Reneker. "Electrospinning process and applications of electrospun fibers." *Journal of electrostatics* 35.2 (1995): 151-160.

[4] Jacob Plaut, Michal Liebowitz, Daniel Rudin, Timothy Hart, Harry Shan He, and Linxi Zhang. "Engineering a Novel Cimex Lectularis Trapping Mechanism Utilizing Electrospun Recycled Polymers." (2013)

# **SESSION 2 :**

# **BIOPOLYMERS ON**

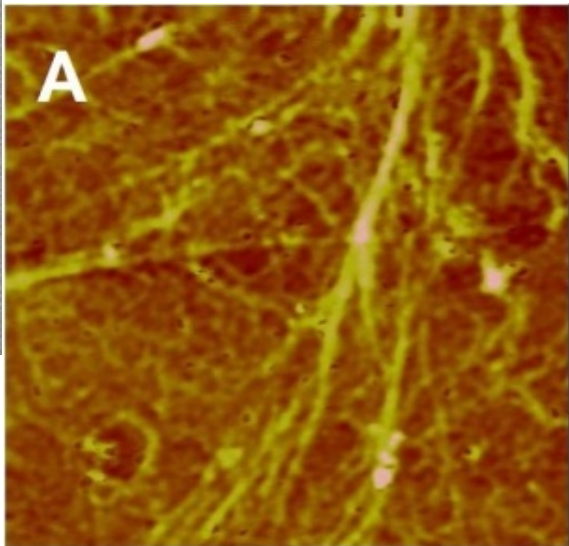
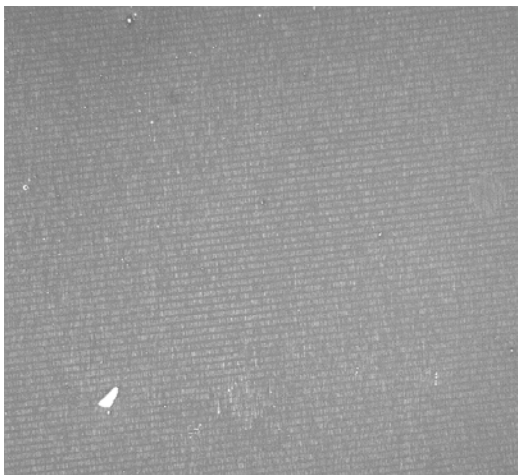
# **SURFACES**

**MENTORS: LIUDI ZHANG**

**NA HYUN CHO**

**KE ZHU**

**TERRENCE BISSOONDIAL**



## A Novel DNA Sequencing Method: Using Soft Lithography to Cut DNA and Extracting DNA from the Enzyme Stamped Surface

Meena Jagadeesan, Phillips Exeter Academy, Exeter NH 03833, Adina Singer, Stella K. Abraham High School for Girls, Hewlett NY 11557

Dr. Terrence Bissoondial, Na Hyun Cho, Dr. Jonathan Sokolov, Ke Zhu

The last decade has seen an explosion in new DNA sequencing technologies<sup>1</sup>. Despite these advances, the cost and rate of sequencing has been limited by the need to reassemble short, randomly cut DNA fragments into a continuous strand. Canonical DNA sequencing methods are hindered because they do not retain the ordering of DNA fragments. Because multiple copies of repeated subsequences of nucleotides are scattered across DNA strands, arranging the fragments into complete strands is difficult and time-consuming<sup>2</sup>. However, if the position and order of the DNA fragments could be maintained, this problem could be avoided, and the length of the assembly process would be significantly reduced. This study shows a novel way of cutting DNA that maintains the order of the fragments.

To achieve this, DNA was stretched linearly (“combed”) out of solution of concentration 10 ng/microliter onto a polymethyl methacrylate coated silicon wafer. An electric field of 1.5 V/cm was applied within the solution, enabling more DNA to stick to the silicon wafer. The DNA on the surface was imaged by fluorescence microscopy of yoyo-stained DNA using a confocal microscope.

Excellent cutting of the absorbed DNA was achieved using the following optimized protocol: Using soft lithography, a polydimethylsiloxane stamp was prepared from a silicon template with grooves spaced every 3.5 micrometers. The stamp was placed in an ultraviolet ozone cleaner for fifteen minutes in order to change the surface from hydrophobic to hydrophilic. A solution of 10 microliters of DNase I enzyme, 20 microliters of DNase buffer, and 180 microliters of deionized water was prepared. 30 microliters of the solution was placed on a 3 cm square of Technicloth. The stamp was placed on the cloth for 30 seconds. Then, the enzyme-coated stamp was placed on the DNA-coated silicon wafer for 30 seconds.

Means to remove and optimize the cut DNA are currently being explored. Washing the DNA coated silicon wafers with deionized water or elution buffer does not pick up a significant amount of DNA. However, washing with a chloroform isoamyl solution effectively removes the DNA by dissolving the PMMA coating. Future work involves the purification of the cut DNA fragments from the solution.

1. David A. Wheeler, Maithreyan Srinivasan, Michael Egholm. The complete genome of an individual by massively parallel DNA sequencing. *Nature*, **452**, 872-876.

2. Elaine R. Mardis. A decade's perspective on DNA sequencing technology. *Nature*, **470**, 198-203.



**Figure 1:** A sample of DNA that was cut using the outlined soft lithography procedure.

## Investigation in the Effect of Variable Polymer Surfaces and Soluble Protein Factors on Fibrinogen Fiber Formation and Platelet Activation

Scarlett Guo<sup>⊙</sup>, Laura Pang<sup>♁</sup>, Ruiyi Gao<sup>♥</sup>, Priyanka Talwar<sup>♠</sup>, Liudi Zhang<sup>♠</sup>, Dennis Galanakis<sup>♠♠</sup> and Miriam Rafailovich<sup>♠</sup>

♠Department of Materials Science and Engineering, Stony Brook University, Stony Brook, NY, 11794

♠♠ Blood Bank, Stony Brook University Hospital, Stony Brook, NY 11794

⊙ Dougherty Valley High School, San Ramon, CA, 94582   ♥Georgia Institute of Technology, Atlanta, GA 30332

♁Texas Academy of Mathematics and Science, Denton, TX, 76203   ♥Yale University, New haven, CT, 06520

A typical response to injury includes the formation of a blood clot, or thrombus, which prevents further bleeding, but such a clot can also lead to adverse effects like thrombosis, the obstruction of a circulatory vessel. Late stent thrombosis (ST), in which a blood clot is formed after implantation of the biomedical device, occurs in fewer than 5% of patients, but the incidence of such an event may be conducive toward lethal conditions such as heart attack and stroke<sup>1</sup>. In order to clarify the interaction of proteins with implant devices at the phase boundary, we investigated the effect of the surface chemistry of polymers commonly used in implant devices on the conformation of fibrinogen, a protein crucial in the formation of the platelet plug in the clotting process. The resultant platelet binding and activation on fibers formed in the absence of thrombin was also explored.

Polystyrene (PS), Polylactic Acid (PLA), and Poly (methyl methacrylate) (PMMA) at 15 mg/mL as well as Poly (4-vinyl pyrimidine) at 30 mg/mL were spun-cast, and Ellipsometry was used to determine the thickness of the spun-cast films. Samples were annealed and incubated in varying concentrations of fibrinogen and platelets and subsequently viewed under the optical microscope to confirm the presence of fibers. PS, P4VP, and PMMA surfaces were also incubated in fibrinogen with varying concentrations of P12, a derivative of fibronectin, which preliminary tests indicate to have some effect on the frequency of fiber formation.

AFM imaging was then used to characterize surface fibers on the surface and determine fiber diameter. P4VP exhibited large networks of fibers, and both P4VP and PS showed large fibers with a network of smaller fibers coating the surface. PMMA demonstrated the formation of large cables of fibers without smaller networks, while PLA exhibited little to no fiber formation. Platelets and fibers were then stained with fluorescent dyes and viewed under the EVOS microscope. It was found that platelets marginally preferentially bound onto fibrinogen fibers. SEM imaging was then used to deduce platelet binding sites and stages of activation. Platelets bound on fibrinogen fibers were observed to have a higher activation rate than those adsorbed onto polymer surfaces.

Our research demonstrates that uncleaved fibrinogen in the absence of thrombin interacts with different surfaces which instigate the formation of fiber matrices, providing further evidence of the surfaces' influence on the conformation and activation of fibrinogen aC domains<sup>2</sup>. P4VP and PS surfaces resulting in large fibrinogen networks as well as preferential platelet aggregation and activation on fiber matrices provide significant evidence towards the possibility of surface induced thrombosis of similar vascular device surfaces. The PLA surfaces demonstrated minimal fibrinogen and platelet adsorption, and therefore PLA presents the most promising candidature for further intravascular implant device design.

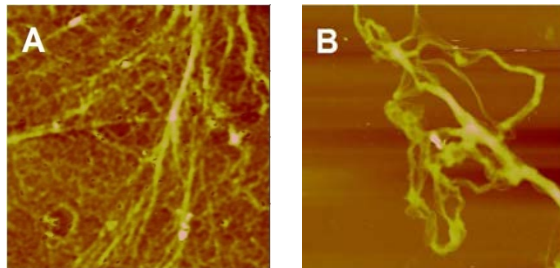


**Figure 1** The above are AFM images characterizing fiber deposition on polymer surfaces. (A) Fibers formed on P4VP included large branching fibers as well as smaller fibers that coated the polymer surface. (B) Fibers formed on PS surfaces were largely cable fibers with fewer branching points and small branching fibers to a lesser extent.

<sup>1</sup> Laurens N, Koolwijk P, de Maat MPM. Fibrin structure and wound healing. *J Thromb Haemost* 2006; 4: 932–9.

<sup>2</sup> Rafailovich, M. H., Galanakis, D., Liu, Y., Jaseung, K., Koo, J., Simon, M., et al. Control of Anti-Thrombogenic Properties: Surface-Induced Self-Assembly of Fibrinogen Fibers. *Biomacromolecules*, 1259-1268.

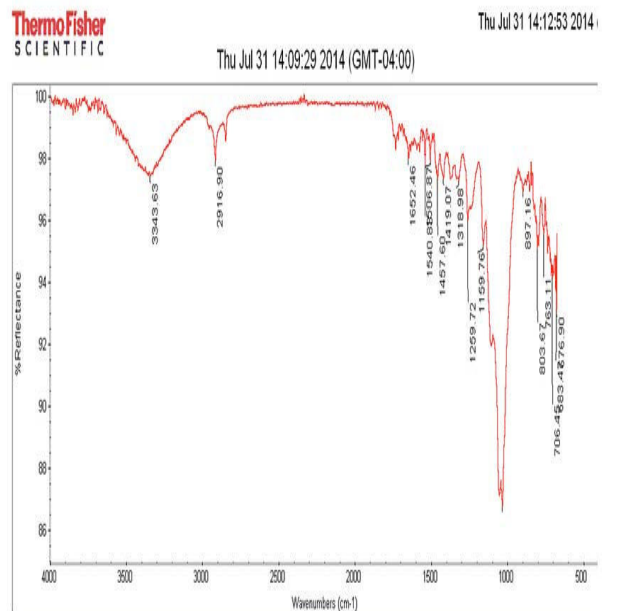
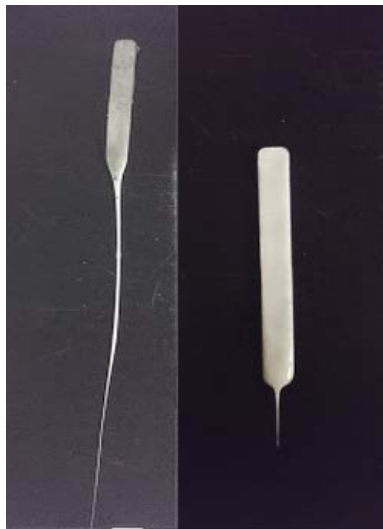
# SESSION 3:

# FLAME RETARDANTS

MENTORS: KAI YANG

YICHEN GUO

HARRY SHAN HE



Wood

**Investigating the Application of Cellulose in Biodegradable Flame Retardant Polymer Blends**  
**Shira Li**, Livingston High School, Livingston, NJ 07039; **David Lin**, Holmdel High School, Holmdel, NJ 07733;  
**Tehila Stone**, Princeton University, NJ 08544;  
**Harry Shan He, Dr. Miriam Rafailovich**, Stony Brook University, Stony Brook, NY 11790

Each year, there are thousands of deaths, tens of thousands of injuries, and billions of dollars lost because of fires in the US. Since common plastics are highly flammable, stringent legislative flame retardancy standards must be met in everyday products to protect consumers. Industries currently use halogenated flame retardant additives, but research has demonstrated that they are easily ingested and can cause hormonal, neural, and developmental problems.<sup>1</sup> Moreover, traditional plastics amount to 32 million tons of waste annually, equivalent to 13% of municipal solid waste stream.<sup>2</sup> With the plastics recycling rate hovering at a meager 9%, plastic waste pollutes the environment and oftentimes remains in landfills for over a century. Our goal is to create a completely biodegradable, flame retardant polymer for applications from consumer electronics to disposable eating utensils.

Our project focuses on combining cellulose, a stabilizing fiber found naturally in wood, with RDP, an organophosphorus intumescent flame retardant additive,<sup>3</sup> to a blend of PLA and PBAT, two biodegradable plastics have high elastic modulus and high impact strength,<sup>4</sup> respectively, in order to match the mechanical strength of existing plastics while also making them flame retardant and environmentally friendly. 50/50, 40/60, and 60/40 PLA/PBAT blends were kept as control groups but were also combined with 40/60 RDP/Cellulose blends to create 45/45/10, 36/54/10, and 54/36/10 PLA/PBAT/RDP-Cellulose experimental groups. PLA/PBAT/RDP and PLA/PBAT/Cellulose blends were also created in 45/45/10 percentages to determine the individual effects of each additive.

The blends containing the 10% RDP-Cellulose all had a V0 flame retardancy grade and in almost all trials,

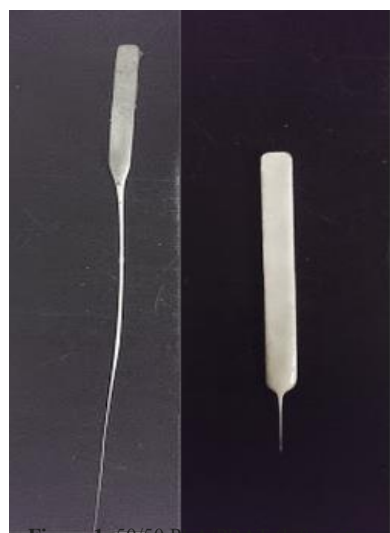


Figure 1: 50/50 PLA/PBAT (left) with extensive dripping vs. 45/45/10 PLA/PBAT/RDP-Cellulose (right) with minimal dripping

self-extinguished in less than one second (Table 1). PLA/PBAT blends that containing only cellulose additive

dripped less than the control

PLA/PBAT blends but remained highly flammable, while PLA/PBAT blends containing only RDP additive dripped the most but were flame retardant. In conjunction, PLA/PBAT/RDP-Cellulose blends had minimal dripping while simultaneously maintaining flame retardancy due to the cellulose fibers acting as thermomechanical stabilizers and RDP creating a thermal barrier to the fire (Figure 1).

We found that the addition of RDP-Cellulose to PLA/PBAT blends decreased mechanical properties such as the elastic modulus, yield strength, tensile toughness, and IZOD impact toughness as a result of microphase separation in the copolymer. As a result, we are continuing to research the minimal ratio of RDP-Cellulose in the PLA/PBAT/RDP-Cellulose blend to maintain a flame retardancy grade of V0 while enhancing the polymer's mechanical properties.

Sample	T1 (sec)	T2 (sec)	Cotton Ignition	Level	Drip
PLA.PBAT.50.50	8.7	>30	Yes	NG	Some
PLA.PBAT.50.50	8.7	17.4	Yes	V2	Some
PLA.PBAT.40.60	>30	-	Yes	NG	Some
PLA.PBAT.40.60	10	15.7	Yes	V2	Some
PLA.PBAT.60.40	>30	-	Yes	NG	Some
PLA.PBAT.60.40	12.7	13.4	Yes	V2	Some
PLA.PBAT.Cellulose.45.45.10	>30	-	Yes	NG	Minimal
PLA.PBAT.Cellulose.45.45.10	>30	-	Yes	NG	Minimal
PLA.PBAT.RDP.45.45.10	<1	<1	No	V0	Extensive
PLA.PBAT.RDP.45.45.10	<1	<1	No	V0	Extensive
PLA.PBAT.RDPCellulose.45.45.10	<1	<1	No	V0	Minimal
PLA.PBAT.RDPCellulose.45.45.10	<1	<1	No	V0	Minimal
PLA.PBAT.RDPCellulose.36.54.10	<1	<1	No	V0	Minimal
PLA.PBAT.RDPCellulose.36.54.10	<1	<1	No	V0	Minimal
PLA.PBAT.RDPCellulose.54.36.10	<1	<1	No	V0	Minimal
PLA.PBAT.RDPCellulose.54.36.10	2.6	<1	No	V0	Minimal

Table 1: UL-94 Flame Test Results and Grades

<sup>[1]</sup> Betts, K. (2008). New Thinking on Flame Retardants. *Environmental Health Perspectives*, 116(5), A210-A213.

<sup>[2]</sup> Plastics, Common Wastes and Materials. (2014, February 28). Retrieved August 7, 2014.

<sup>[3]</sup> Bright, D., Dashevsky, S., Moy, P., & Williams, B. (1997). Resorcinol bis(diphenyl phosphate), a non-halogen flame-retardant additive. *Journal of Vinyl and Additive Technology*, 3(2), 170-174.

<sup>[4]</sup> Weng, Y., Jin, Y., Meng, Q., Wang, L., Zhang, M., & Wang, Y. (2013). Biodegradation behavior of poly(butylene adipate-co-terephthalate) (PBAT), poly(lactic acid) (PLA), and their blend under soil conditions. *Polymer Testing*, 32(5), 918-926.

## Biodegradable, Flame Retardant Wood-Plastic Composites Via *In Situ* Polymerization of Lactide Monomer

Noah Davis<sup>1</sup>, Dan Kim<sup>2</sup>, Tehila Stone<sup>3</sup>, Dr. Miriam Rafailovich<sup>4</sup>, Kai Yang<sup>4</sup>, Shane He<sup>4</sup>

1) Earl L. Vandermeulen High School, Port Jefferson, NY 11777 2) Smithtown West High School, Smithtown, NY 11787 3) Princeton University, Princeton, NJ 08544 4) Garcia MRSEC, SUNY Stony Brook, NY 11794

Wood materials are an abundant, low cost, highly used material. However it is evident in the \$9-10 billion dollars spent to correct construction defects each year that improvements are needed to fortify wood's properties<sup>1</sup>. In recent years there has been a push to increase the thermal and mechanical properties of wood through engineered wood composites. An increasing amount of synthetic polymers produces a lot of environmental pollution<sup>2</sup> and so biodegradable alternatives are becoming more popular. This project looked to optimize the mechanical and thermal properties of wood through *in situ* polymerization of lactide monomer, a biodegradable polymer, within the wood. We theorized that doing so would create a cross-linked network of polymers grafted to the wood fibers, which would strengthen the wood, while also allowing for better thermal properties. Additionally, another sample of polymerized wood would be impregnated with RDP, a chemical that has been shown to make wood flame retardant, but also takes away from its mechanical properties. We hypothesized that this sample would be slightly less strong than polymerized wood alone, but would be a better flame retardant. Plain wood and wood soaked in RDP were used as controls to compare to the polymerized samples.

The monomers were dissolved in water to allow for impregnation within the wood. A very small amount of sulfuric acid was added to this solution to act as a catalyst. Once the wood samples soaked in solution for two hours they were put in an oven at approximately 100°C for 92 hours to allow for a thorough polymerization to occur. The wood samples came out highly discolored, which could be accounted for by the monomer incorporation in combination with the heating. The samples were then measured to determine the percent by mass of polymer, which was approximately 15% on average. Half the wood was then soaked in RDP for 24 hours. Samples were then measured and on average showed 5% RDP by mass.

Numerous tests are necessary to show the mechanical and thermal properties of wood. An initial Fourier Infrared Transform Spectroscopy (FTIR) test was needed to show that the wood samples did in fact contain RDP and polymer. This test allows for the chemical composition of a material to be revealed. Figure 1 shows the

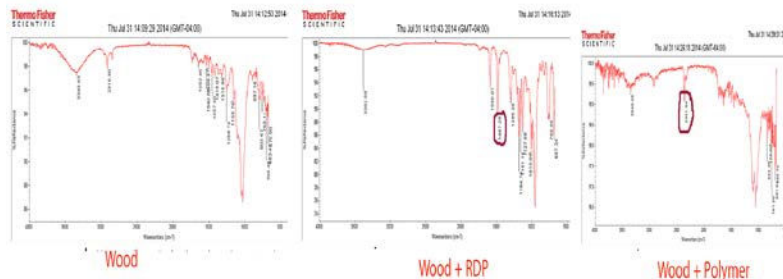


Figure 1) The highlighted peaks indicate bonds corresponding to addition of RDP and polymer.

peaks of wood, RDP soaked wood and polymerized wood, respectively. The peaks indicate that the samples were treated correctly and that the monomer did polymerize within the wood. After this, mechanical testing was done using izod impact testing. The polymerized wood samples showed much greater toughness and on average doubled the toughness of plain wood. Additionally using the UL-94 flame test it became apparent that polymerized wood extinguished itself after some time. Polymerized, RDP soaked wood extinguished itself right away, earning the highest V0 ranking on the test and exhibiting complete flame retardancy. More testing needs to be done to complete the mechanical and thermal profile for both polymerized and polymerized, RDP soaked wood, but results indicate enhanced performances across the board.

<sup>1</sup> Fitzgerald, J. (2007). Preventing Moisture-Related Problems in Residential Wood Framing. *Architectural Record*.

<sup>2</sup> Kaith, B.S., Mittal, H., Jindal, R., Maiti, M., & Kalia, S. (2011). Cellulose Fibers: Bio- and Nano-Polymer Composites. *Green Chemistry and Technology*, 426-446.

## Halogen Free Flame Retardant Polymer Nanocomposites

**William Berger**, Roslyn High School, Roslyn Heights, NY 11577, **Elaina Zodiatis**, Smithtown High School East, St. James, NY 11780, **Yichen Guo**, Stony Brook University, Stony Brook, NY 11790

Polymers have a wide variety of applications in many industries, due to their desirable mechanical properties, combined with low costs and weights. Adding flame retardancy would further expand the uses of many polymers, such as nylon and polystyrene (PS). However, halogens, which are normally used as an additive for flame retardancy, are toxic to humans (Darnarud,2003). Replacement materials that can maintain this level of flame retardancy that aren't toxic would expand possible uses even further. Melamine phosphate (MP) is a promising material to use as a replacement for halogens, as it is non-toxic. However, by itself it wouldn't be able to reach the required level of flame retardancy while maintaining any sort of strength within the polymer (Lv et. Al., 2005). We decided to test how to add melamine phosphate in order to enhance the flame retardancy of polymers while maintaining mechanical properties and keeping it non-toxic.

The main focus of our research was on Nylon 6.0 and PS, and increasing their flame retardancy while retaining their mechanical properties. We made samples of nylon with 20,30, and 40% MP and 20,30,and 40% MP with resorcinol bis(diphenyl phosphate) (RDP). In addition, samples of both nylon and PS were made with no additives, at 25% MP with 5% graphene, and 25% MP with RDP with 5% graphene. While the nylon was able to reach a V0 rating for flame retardancy at 40% MP-RDP (Figure 1), it was far too brittle to be of any use, as evidenced by the fact that it broke while being removed from the mold. The lowering of the amount of flame retardant additives and the addition of graphene to the sample aided in the maintaining of mechanical properties in the sample. We were able to achieve much better results for the samples when they contained MP with RDP, as the RDP allowed the MP to mix into the polymer much more easily, and without it, it would stay separated (Figure 2.1). In addition, with graphene to aid the char structure, the additives had synergy, with the MP producing nitrogen, while the RDP and graphene aided in the plasticity and strength of the char respectively, allowing bubbles to form and preventing further melting (Figure 2.2).

Sample	t <sub>1</sub> (s)	t <sub>2</sub> (s)	Dripping	Grade
100Nylon	>30	NA	Y	NG
60Nylon40MP	1	5	Y	V <sub>2</sub>
60Nylon40MP-RDP	1	3	Y (cannot ignite cotton)	V <sub>0</sub>
70Nylon25MP5G	1	11	N	V <sub>1</sub>
70Nylon25MP-RDP5G	1	6	N	V <sub>0</sub>
100PS	>30	NA	Y	NG
70PS25MP5G	3	>30	N	NG
70PS25MP-RDP5G	3	25	N	V <sub>1</sub>

Figure 1: Results of UL 94 Flame Test, numbers in sample names are percentages (%), G is graphene (H-5), NG is no grade.

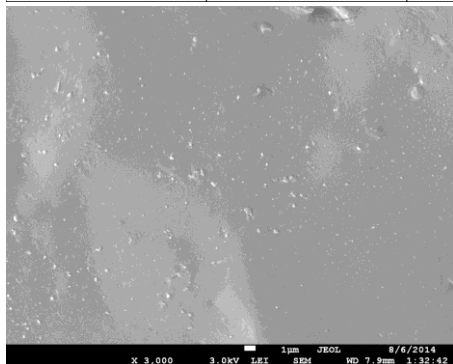


Figure 2.1

Figure 2: SEM images at 3000x magnification.  
 -Figure 2.1 is 70% PS, 25% MP, and 5% graphene  
 -Figure 2.2 is 70% nylon, 25% MP+RDP, and 5% graphene

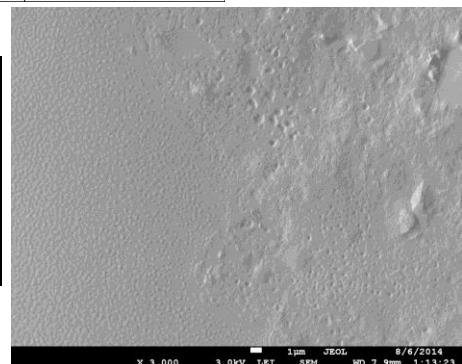


Figure 2.2

Darnarud, P.(2003). Toxic Effects of Brominated Flame Retardants in Man and in Wildlife.*Environment International*, 29(6),841-853.

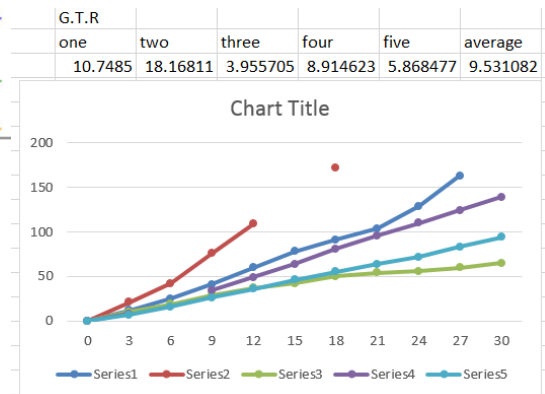
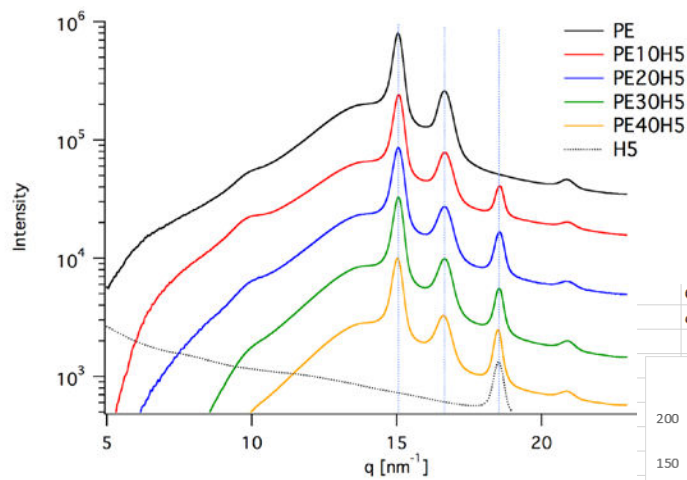
Lv, P., Wang, Z., Hu, K., & Fan, W. (2005). Flammability and thermal degradation of flame retarded polypropylene composites containing melamine phosphate and pentaerythritol derivatives. *Polymer Degradation and Stability*, 90(3), 523-534.

# SESSION 4 :

# NANOCOMPOSITES

MENTORS: KAI YANG

YICHEN GUO



# Synthesis and Characterization of Graphene Nanoparticle Infused Polyethylene Nanocomposite Material for Enhanced Mechanical and Conductivity Properties

David Choi, Canyon Crest Academy, San Diego, CA, 92130 , Arun Soni, Staples HS, Westport, CT, 06880 , Russell Charnoff, Hebrew Academy of the Five Towns and Rockaway, Cedarhurst, NY, 11516 , Kai Yang, Dr. Maya Endoh, Dr. Miriam Rafailovich, Stony Brook University, Stony Brook, NY, 11794

Graphene is a promising new material in materials engineering with its exceptionally high mechanical strength and conductivity (Geim et. al., 2007)<sup>1</sup>. Polymer nanocomposite materials incorporating graphene have traditionally been sought after for their enhanced thermal and electrical conductivity (Kim et. al., 2010)<sup>2</sup>. However, often times, the insertion of fillers into polymers cause significant decreases in mechanical strength (Lee et. al., 2003)<sup>3</sup>.

In this study, we explore the effect of H5 graphene nanoplatelets on low and high density polyethylene in varying concentrations and characterize the molecular structure of H-5 graphene/low-density polyethylene nanocomposite material. Graphene-polyethylene nanocomposite materials with concentrations 5%, 10%, 15%, 20%, 30%, and 40% for both high and low density polyethylene were prepared by melt blending using the Brabender and molded into desired shapes using the Carver Hot Press. The IZOD Impact Test determined that the 5% Graphene-Low Density Polyethylene composite material withstood an average force of 452 Joules per meter, while the 10% concentration withstood 384 J/m compared to pure polyethylene's 353 J/m. The Instron Tensile Test determined that the nanocomposite's Young's Modulus increased linearly as concentration of graphene increased, and the 5% and 10% concentrations saw a 13% and 88% increase respectively. Our research suggests that mechanical strength relative to H-5 graphene concentration in low-density polyethylene peaks around a concentration of 5%. In contrast to previous research with nanocomposite material, which showed decreased mechanical properties, the 5 and 10% concentrations displayed enhanced mechanical properties. The Unitherm Thermal Conductivity Test determined that the 5% and 10% concentrations conducted 0.34 Watts per meter Kelvin and 0.50 W/mK respectively compared to pure polyethylene's value of 0.24 W/mK. As such, graphene-polyethylene nanocomposite material displayed both increased mechanical properties and increased thermal conductivity at low concentrations. Wide Angle X-Ray Scattering Microscopy shows that lower concentrations of H5 graphene nanoplatelets in low-density polyethylene do not strongly affect the molecular structure of the polymer, unlike the behavior seen with graphene in polypropylene. Our study shows promise for nanocomposite materials that display both enhanced mechanical strength and thermal conductivity.

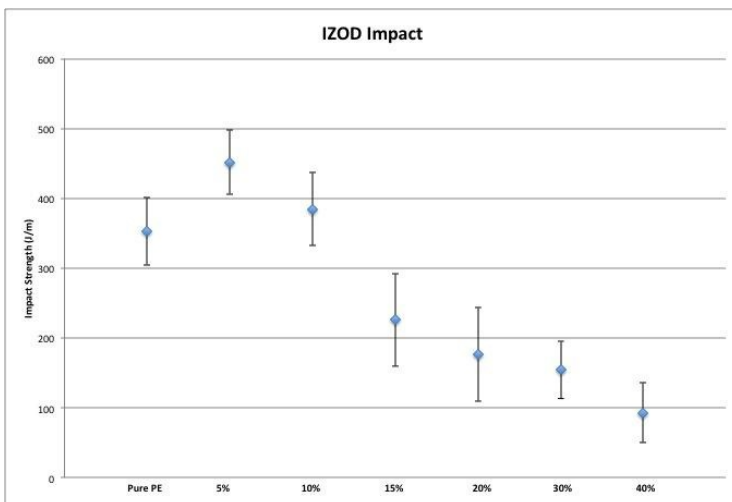


Figure 1: Impact strength of low density polyethylene with different graphene concentrations

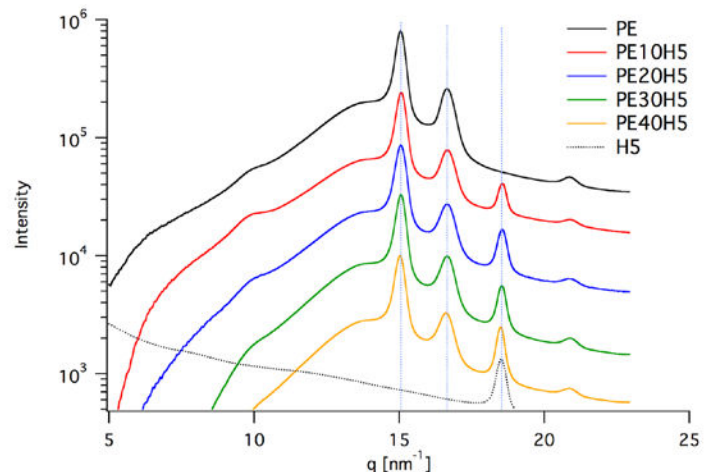


Figure 2: Wide Angle X-Ray Scattering Analysis of polyethylene-graphene composite material with different graphene concentrations.

<sup>1</sup>Geim, A. K., & Novoselov, K. S. (2007). The rise of graphene. *Nature Materials*, (6), 183- 191.

<sup>2</sup>Kim, H. W., Abdala, A. A., & Macosko, C. W. (2010). Graphene/Polymer Nanocomposites. *Macromolecules*, (43), 6515- 6530.

<sup>3</sup>Lee, J. H., Park, T. G., Park, H. S., Lee, D. S., Lee, Y. K., Yoon, S. C., & Nam, J. D. (2003). Thermal and mechanical characteristics of poly(L-lactic acid) nanocomposite scaffold. *Biomaterials*, (24) 2773- 2778.

## Effect of Clay on High Density Polyethylene: Oxygen Permeability

Taicheng Song, Dublin School, Dublin, NH, 03444, Kai Yang, Stony Brook University, Long Island, NY, 11794, and Dr. Miriam Rafailovich, Stony Brook University, Long Island, NY, 11794

High Density Polyethylene (HDPE) is widely used in the world due to its good ability to block humidity; However, HDPE has a great Oxygen permeability which causes it not able to accomplish some of the tasks. Nano-clay can provide stratified nacre like layer with a homogenous distribution of nanoplatelets within the polymer matrix (Christian et. Al., 2012)<sup>1</sup>. A reduction of Oxygen permeability can be observed after adding nano-clay to the polymer (Osman et. Al., 2004)<sup>2</sup>. This experiment primary focuses on finding what percentage of what type of clay create the best gas barrier.

We spent most of the time making HDPE sample with different concentration Cloisite Na+ clay. HDPE is mixed with 10%, 20% Cloisite Na+ clay and 10%, 20% Halloysite clay. We worked out a reliable way to obtain thin polymer sample with no air bubble. We run the samples through the gas permeability machine and obtained the rate of Oxygen flowing through the sample under pressure. The average flow rate (G.T.R) of pure HDPE is about twice faster than the HDPE sample with 10% Na+ clay. However due to the insufficiency of quantity of data, the standard deviation right now is very high and further experimentations is required to acquire a more accurate data.

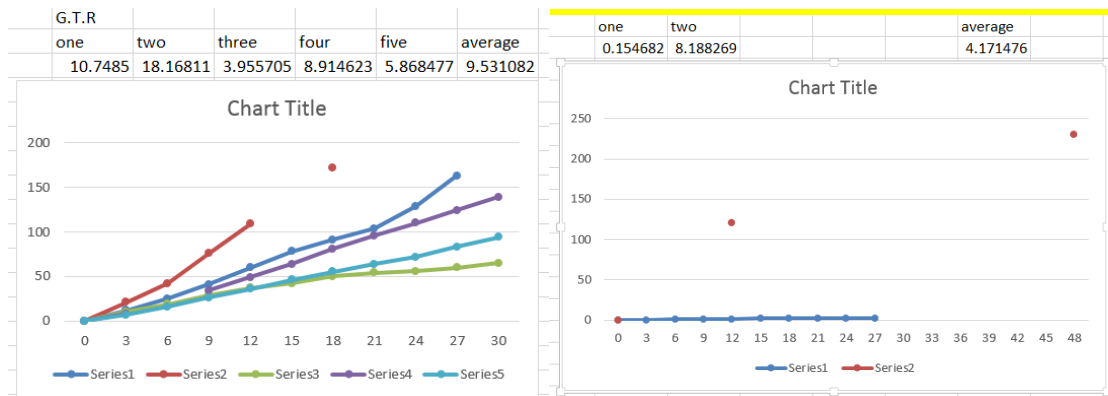


Figure 1: Five tests on the permeability of 100% HDPE sample

Figure 2: Two tests on the permeability of 90% HDPE + 10% Cloisite Na+ sample

<sup>1</sup> Christian Aulin b, German Salazar-Alvarez and Tom Lindström, High strength, flexible and transparent nanofibrillated cellulose–nanoclay biohybrid films with tunable oxygen and watervapor permeability . Stockholm, Sweden. Stockholm University., DOI: 10.1039/C2NR31726E (Paper) *Nanoscale*, 2012, 4, 6622–6628  
<sup>2</sup> Osman, M. A. and Atallah, A. (2004), High-Density Polyethylene Micro- and Nanocomposites: Effect of Particle Shape, Size and Surface Treatment on Polymer Crystallinity and Gas Permeability. *Macromol. Rapid Commun.*, 25: 1540–1544. doi: 10.1002/marc.200400254

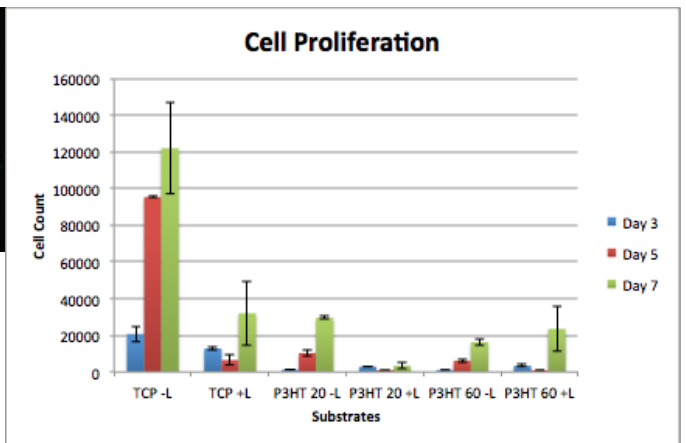
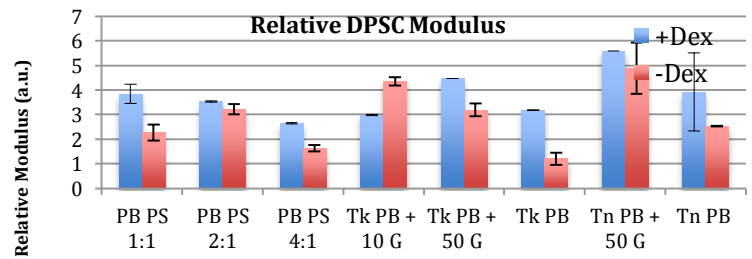
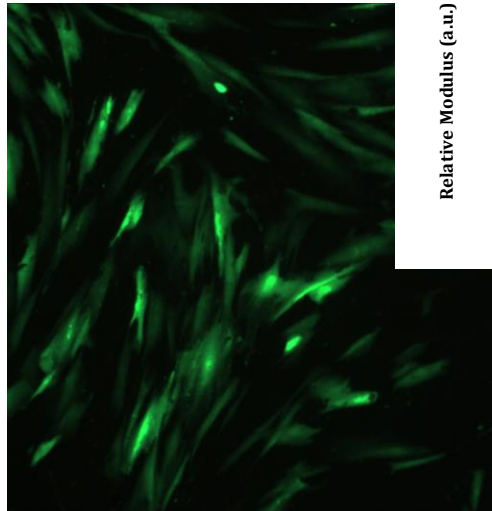
# SESSION 5 : DENTAL PULP STEM CELLS ON SURFACES

MENTORS: YINJIE YU

JUYI LI

VINCENT RICCOTA

KUANCHE FENG



# Characterization of 3D Printed PLA Cell Scaffolds Versus Compressed PLA Scaffolds and Effect on DPSC Differentiation

Leeson Chen, Palm Harbor University High School, Palm Harbor, Fla.

Professor Miriam Rafailovich, Andriana Pinkas-Sarafavo Ph.D, Ying Jie, Monika Batra, Stony Brook University, Stony Brook, NY, Rachel Yang, Cornell University, Ithaca, NY

The merging of three-dimensional printing (3DP) with medicine is a promising new field of biotechnology. 3DP can be used to create complex structures, such as medical implants with cell scaffolds.<sup>1,2</sup> Currently, the most common method of producing these implants involves compressing polymers into molds. In this study, we compared the methods of 3DP versus compression in terms of water contact angle, porosity, topography, and cell proliferation and calcification. Unpigmented polylactic acid (PLA) filament was used for both 3DP and compression. PLA has already been shown to be a suitable scaffold for breast cancer cells, and is used in modern medical implants.<sup>3,4</sup> Acrylonitrile butadiene styrene (ABS), a common polymer for 3DP, was also printed. The 3D printer, a Makerbot Replicator™ 2, was used to create circular flat scaffolds of 1.0 cm and 2.0 cm diameter. Two sets of scaffolds of identical dimensions were molded at 320° Fahrenheit from either the PLA filament or PLA pellets of discrete molecular weight [ ]. Two methods of sterilization were employed to test their potential reactions and effects on the polymers: 80% ethanol with ultraviolet light, and 24-hour exposure to ethylene oxide gas (EtO). After sterilization, scaffolds were plated with dental pulp stem cells (DPSCs) in dexamethasone. Cell medium without dexamethasone was compared against the control to test cell

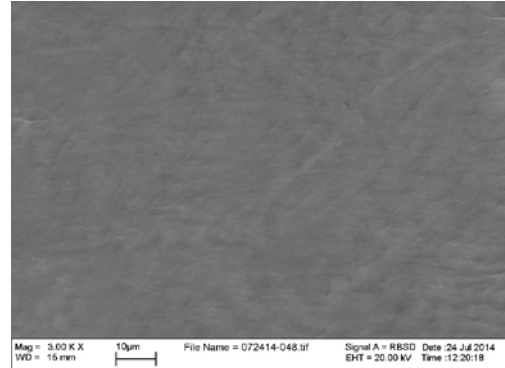


Figure 1: SEM view of 3DP PLA before sterilization

differentiation upon PLA. [Water contact angle], scanning electron microscope (SEM), Fourier-Transform Infrared spectroscopy (FTIR), reverse transcriptase-polymerase chain reaction (RT-PCR), and confocal microscopy were used to analyze differences in characterization of the scaffolds. SEM analysis revealed the texture of 3DP ABS as too rough to support cell growth, and was subsequently removed from further study. The two methods of sterilization displayed no difference in effect on porosity or topography from each other, and did not differ from the profile prior to sterilization (Fig. 1). <need more data> Further research in this study would involve tensile strength of 3DP versus compression, biodegradability, toxicology profiles, the use of different polymers, and using 3DP to create delicate structures such as cardiac stents.

1 Bergmann, Christian, et al. "3D printing of bone substitute implants using calcium phosphate and bioactive glasses." *Journal of the European Ceramic Society* 30.12 (2010): 2563-2567.

2 Curodeau, Alain, Emanuel Sachs, and Salvatore Caldarise. "Design and fabrication of cast orthopedic implants with freeform surface textures from 3-D printed ceramic shell." *Journal of biomedical materials research* 53.5 (2000): 525-535.

3 Sahoo, Sanjeeb K., Amulya K. Panda, and Vinod Labhasetwar. "Characterization of porous PLGA/PLA microparticles as a scaffold for three dimensional growth of breast cancer cells." *Biomacromolecules* 6.2 (2005): 1132-1139.

4 Lavik, Erin, et al. "Seeding neural stem cells on scaffolds of PGA, PLA, and their copolymers." *Neural Stem Cells: Methods and Protocols*. Humana Press, 2002. 89-96.

## Creation of a Drug Delivery Mechanism for Dexamethasone Differentiation of Dental Pulp Stem Cells

Ryan McCaffrey, Commack High School, Commack, NY 11725; Greta Huang, University of California, Berkeley, Berkeley, CA 94720; Kuan-Che Feng, Stony Brook University, Stony Brook, NY 11794; Clément Marmorat, Stony Brook University, Stony Brook, NY 11794; Dr. Miriam Rafailovich, Stony Brook University, Stony Brook, NY 11794

Biomaterial scaffolds are used to regenerate damaged tissue by acting as templates for stem cell growth and differentiation.<sup>1</sup> Dental pulp stem cells are becoming increasingly preferred for tissue engineering because like mesenchymal stem cells, they are multipotent, but do not present ethical concerns since they can be easily collected from discarded teeth.<sup>2</sup>

The purpose of this study is to create a mechanism that can deliver dexamethasone, an osteogenic inducing drug, to dental pulp stem cells over a period of 28 days, an ideal time period for dexamethasone activity. A hydrogel was entrapped in the pore network of a 3D printed poly-L-D-lactic acid (PLDLA) disc by crosslinking a ten percent gelatin solution with microbial transglutaminase (MTG) as the solution settled on the PLDLA surface. Observation and experimentation showed that the hydrogel was not absorbed into the PLDLA, but rather solidified on the surface of the PLDLA. As a result, PLDLA was rejected in favor of a polyurethane foam.

The polyurethane foam was chosen as a cell-plating surface material because of its high porosity and biocompatibility with stem cells. Polyurethane surfaces were created through a reaction of the isocyanate component of urethane resin and the hydroxyl component of urethane hardener, forming solid surfaces that could be molded into 34mm petri dishes. Observation of the polyurethane under an optical microscope confirmed the presence of pores within the polyurethane network, as shown in Figure 1.

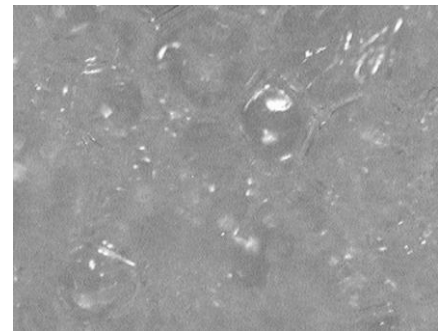


**Figure 1:** An optical microscope image of the surface of a polyurethane foam surface at 50x magnification.

A 1:25 MTG to gelatin hydrogel was created to calculate the release rate of dexamethasone into cell media. Red food coloring was used as a substitute for dexamethasone when calculating release rate for economical purposes. The hydrogel was placed in a 34mm petri dish and covered with 2 mL of deionized water (di-H<sub>2</sub>O). Over a period of 24 hours, the hydrogel released approximately 25 percent of its original content of red food coloring into the di-H<sub>2</sub>O, implying that a higher MTG concentration in the hydrogel solution is necessary to create a gel with a 28-day release period.

Future research entails finding the ideal MTG to gelatin ratio for a hydrogel that will be absorbed within the pore network of polyurethane discs. Dexamethasone will be impregnated into the resulting drug delivery mechanism, and dental pulp stem cells will be plated. A control group of cells will be fed dexamethasone periodically to induce osteoblast differentiation, which will be compared to the cells growing on the drug delivery mechanism to see if the dexamethasone escaping from the polyurethane pore network will have an effect on dental pulp stem cell differentiation.

<sup>1</sup> O'Brien, F. J. Biomaterials & Scaffolds for Tissue Engineering. *Materialstoday* **2011**, 14, pp 88-95.

<sup>2</sup> Graziano, A.; d'Aquino, R.; Cusella-De Angelis, M. G.; De Francesco, F.; Giordano, A.; Laino, G.; Piattelli, A.; Traini, T.; De Rosa, A.; Papaccio G. Scaffold's Surface Geometry Significantly Affects Human Stem Cell Bone Tissue Engineering. *J Cell Physiol* **2008**, 214, pp 166-172.

# Investigating Proliferation and Differentiation of Dental Pulp Stem Cells on Polystyrene/Polybutadiene Blends and Graphene/Polybutadiene Substrates

Sanket Mehta Walton High School, Atlanta, GA 30067; Vivek Subramaniam Westborough High School, Westborough, MA 01581

Yingjie Yu<sup>1</sup>, Vince Ricotta<sup>1</sup>, Kuanche Feng<sup>1</sup>, Shazim Farooq<sup>2</sup>, Dr. Adrianna Pinkas-Sarafova<sup>2</sup>, Dr. Miriam Rafailovich<sup>1</sup>

<sup>1</sup>Department of Material Sciences and Engineering, Stony Brook University, Stony Brook, NY 11790; <sup>2</sup>School of Dental Medicine, Stony Brook University, Stony Brook, NY 11790

There is an acute need to develop techniques that can optimally induce proliferation and differentiation of stem cells *in vitro* for regenerative therapy<sup>1</sup>. Dental pulp stem cells (DPSCs) are easily accessible, multipotent stem cells that can differentiate into osteocytes, chondrocytes, and adipocytes, making them applicable in various regenerative treatments<sup>2</sup>. Currently, differentiation can be induced in DPSCs through the use of biological growth factors and mechanical scaffolding. This study focuses on the latter, by examining the ability of graphene/polybutadiene and polystyrene/polybutadiene composites to induce osteogenic differentiation of DPSCs.

Various ratios of graphene/polybutadiene (thin PB – 3mg/mL, thick PB – 20mg/mL, thin PB + 50% graphene, thick PB + 10% graphene, and thick PB + 50% graphene) and polystyrene/polybutadiene copolymer (PB:PS 4:1, 2:1, and 1:1) solutions were

prepared. Polymer thin films were spun-coated onto silicon wafers, which were characterized using atomic force microscopy to ensure appropriate surface properties. DPSCs were plated onto both composite substrates and tissue culture plastic. For each concentration, samples were prepared with and without the growth factor dexamethasone as a positive control<sup>3</sup>.

Growth rate showed an increase in cell proliferation by Day 7 on prepared graphene/PB and PB/PS substrates (Fig. 1). Furthermore, cell modulus testing using atomic force microscopy indicated higher relative modulus for cells that were grown on graphene compared to non-graphene substrates, with and without dexamethasone (Fig. 2). Analysis using a phase contrast fluorescence microscope on day 14 indicated normal cell morphology, and xylenol orange dye staining on day 14 indicated preliminary calcification. Confocal microscopy and scanning electron microscopy tests will be conducted to verify calcification and biomineralization. In the future, we plan to conduct ELISA staining to analyze osteocalcin content and conduct RT-PCR to examine gene expression.

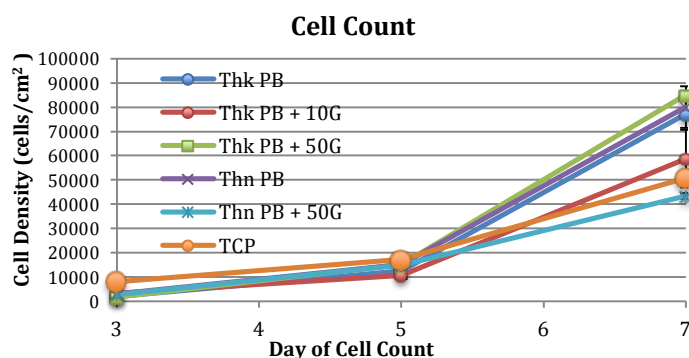


**Figure 1: Cell Proliferation Curve**  
Cells were counted using a hemacytometer over a period of seven days to analyze DPSC proliferation on varying substrates.

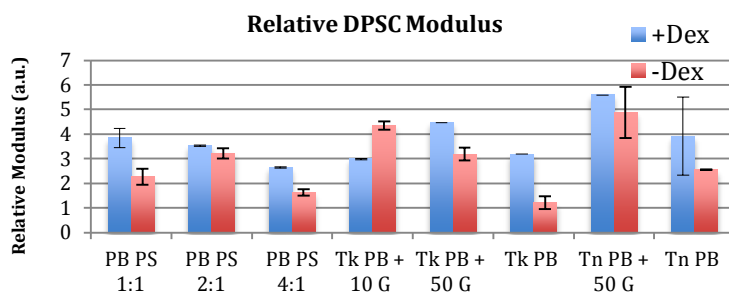


**Figure 2: Cell Relative Modulus on Different Polymer Thin Film Substrates**  
Relative moduli of cells were measured using atomic force microscopy to show hardness of extracellular matrix, indicative of osteogenic differentiation.

<sup>1</sup>Feng, R., & Lengner, C. (2013). Application of Stem Cell Technology in Dental Regenerative Medicine. *Advances in Wound Care*, 2(6), 296-305.

<sup>2</sup>D'aquino, Riccardo; Papaccio, Gianpaolo; Laino, Gregorio; Graziano, Antonio (2008). "Dental Pulp Stem Cells: A Promising Tool for Bone Regeneration". *Stem Cell Reviews* 4 (1): 21–6.

<sup>3</sup>McCulloch, C. A. G., & Tenenbaum, H. C. (1986). Dexamethasone induces proliferation and terminal differentiation of osteogenic cells in tissue culture. *The Anatomical Record*, 215(4), 397-402.

## Effects of Stimulated Photovoltaic Substrate and Static Magnetic Fields on Dental Pulp Stem Cell Proliferation and Differentiation

Jae Hee Cho<sup>1</sup>, Mason Zhang<sup>2</sup>, Yingjie Yu<sup>3</sup>, Vincent Ricotta<sup>3</sup>, Kuanche Feng<sup>3</sup>, Shazim Farooq<sup>3</sup>,  
Dr. Adriana Pinkas-Sarafova<sup>4</sup>, Dr. Marcia Simon<sup>4</sup>, Dr. Miriam Rafailovich<sup>3</sup>

<sup>1</sup>Westwood High School, Austin, TX, 55446, <sup>2</sup>Wayzata High School, Plymouth, MN, 78750

<sup>3</sup>Dept. of Material Sciences & Engineering and <sup>4</sup>Oral Biology & Pathology, Stony Brook University, Stony Brook, NY, 11794

Dental pulp stem cells [DPSCs] are highly proliferative multipotent stem cells that have the ability to differentiate into osteoblastic and odontoblastic cells and can be easily accessed for use in tissue engineering and regeneration<sup>1</sup>. However, *in vitro* methods to differentiate these cells in controlled fashions are limited<sup>2</sup>. This study explores the use of light stimulated photovoltaics and static magnetic fields to induce DPSC differentiation. For these experiments we used DPSCs genetically engineered to express enhanced Green Fluorescent Protein (eGFP) (strain: AV3-eGFP).

DPSCs for the photovoltaic experiment were grown on Poly(3-hexylthiophene-2,5-diyl) [P3HT] spun cast at thickness 20 or 60 nm, with or without exposure to a light intensity of 35,000 lux at a primary wavelength of 450 nm. DPSCs for the magnetic experiment were grown on Poly(Styrene-co-4-styrene sulfonic acid) [SPS] spun cast at thickness of 20 nm in the static magnetic field of strength 150 mT.

On tissue culture plastic (control), it was shown that the blue light initially inhibited cell proliferation due to high energy light inhibiting cellular metabolism (*Figure 1*)<sup>2</sup>. The P3HT was also found to further stunt stem cell growth, demonstrating possible cytotoxicity. Cells exposed to light on P3HT spun cast on 20 nm films were larger and had lower proliferation rates compared to those on 60 nm thick P3HT (*Figure 2*)<sup>2</sup>. Cells plated on 60 nm thick P3HT films with light had similar proliferation rates and cell morphology to cells plated on the same substrate without light, thus demonstrating that electricity has a counter-effect on the inhibitory actions of blue light.

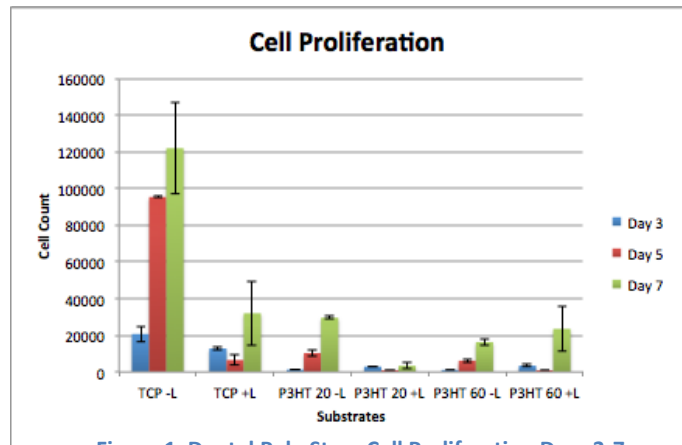


Figure 1: Dental Pulp Stem Cell Proliferation Days 3-7

Atomic force microscopy revealed that cell modulus was lowered when exposed to light, suggesting inhibited differentiation. During early incubation, exposure to magnetism showed inhibition of proliferation both on SPS and TCP control. Further experimentation will include calcification tests and qualitative biomineralization analysis using scanning electron microscopy (SEM) and energy dispersive X-ray spectroscopy (EDX).

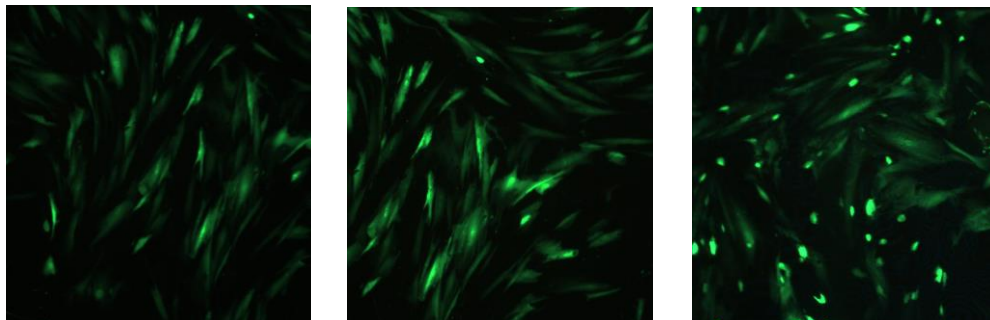


Figure 2: Fluorescent Microscopy for Day 14. Left: cells plated on 60 nm thick P3HT without light, Middle: 60 nm P3HT with light, Right: 20 nm P3HT with light

<sup>1</sup>Luciano Casagrande, Mabel Cordeiro, Silvia A. Nor Jacques E. Nor. Dental pulp stem cells in regenerative dentistry. *Odontology*. 2011;99:1-7

<sup>2</sup>Wilner, J. The Effects of Photostimulation on Stem Cell Proliferation and Differentiation. B.A. Dissertation, Tufts University, 2010

# Dental Pulp Stem Cell Mobility in the Cornell Polymer

Sanket Desai<sup>1</sup>, Juyi Li<sup>2</sup>, Yingjie Yu<sup>2</sup>, Dr. Myungwoong Kim<sup>3</sup>,

Dr. Christopher K. Ober<sup>3</sup>, Dr. Miriam Rafailovich<sup>2</sup>

<sup>1</sup>Ward Melville High School, East Setauket, NY 11733

<sup>2</sup>Department of Materials Science & Engineering, Stony Brook University, Stony Brook, NY 11794

<sup>3</sup>Department of Materials Science and Engineering, Cornell University, Ithaca, NY 14853

Dental pulp stem cells (DPSC) are an encouraging potential tool for tissue regeneration. Due to their many favorable characteristics, including ease of access compared to that of stem cell from embryos, DPSC have garnered much attention for therapeutic potential. Thus, there is a need to better understand the mobility of these stem cells as well as develop a way to move these stem cells to their target in the body.

Arginylglycylaspartic acid (RGD) peptide receptors are used for cell communication as well as gene expression, and have been used for studies with apoptosis, drug therapy, and cancer.<sup>1</sup> These have also been used for cell adhesion between cells and extracellular matrix.<sup>2</sup> These features of the RGD peptide receptors were used with Poly(methacrylic acid) (PMAA) to synthesize PMAA-RGD-PMAA block copolymer or “Cornell Block Copolymer”. It is useful for studying its effect on cell mobility. Thus, we examined the effect of the Cornell Polymer on fluorescent DPSC migration.

There are three types of the Cornell block copolymer; the #5 polymer has the lowest molecular weight and it has a RGD (arginine-glycine-aspartic acid) sequence. The #6 and #7 polymer have the same molecular weight, but the #6 polymer has a RGD sequence, while the #7 polymer has an RDG (arginine-aspartic acid-glycine) sequence. The RDG sequence is known to induce faster cell migration than RGD. We wanted to compare the effect of each type of Cornell polymer on the movement of the DPSC to see which one is ideal for mobility.

We started our work with the Cornell Polymer by making a 20mg/mL solution of each polymer type. In order to test the mobility and viability of the DPSC on this type of copolymer, the cells were plated in spun cast #6 polymer thin film. From figure 1, we can see DPSC grow normally on spun cast PMAA-RGD-PMAA thin film. Cell migration was measured by determining the cell velocity from confocal image recording. On average, velocity in the #6 spun cast polymer thin film is determined to be 0.00163  $\mu\text{m/s}$ . In

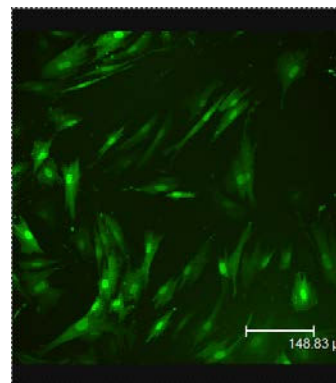


Figure 1: Confocal image of fluorescent DPSC on PMAA-RGD-PMAA copolymer thin film on day 1

addition, micro-printing technology was employed here to make thin film patterned with RGD peptide. First, polydimethylsiloxane (PDMS) stamp with certain pattern is made from adding PDMS solution onto micro-pattern imprinted silicon surface. PDMS stamp is dipped into Cornell polymer solution, and it was dried by nitrogen air. Then, PDMS stamp were placed on the 1cm \* 1 cm silicon wafer surface and were gently pressed to ensure a conformal contact. The stamped silicon wafer surface and PDMS stamp were checked by optical microscope (Figure2). In future work, several methods will be employed to optimize the stamping result, such as using UV light during the stamping process.



Figure 1: Cornell Polymer stamped on a silicon wafer	Figure 2: PDMS stamp from a rectangular silicon wafer	Figure 3: PDMS stamp from a weight and a square silicon wafer
--	---	---

Figure 2: Optical microscope image of stamp with pattern

## References:

1. Peptides International, Inc. (2012). RGD Peptides, Retrieved from <http://pepnet.com/products/rgdpeptides.pdf>
2. Ruoslahti (1996). RGD and other recognition sequences for integrins. Retrieved from <http://www.ncbi.nlm.nih.gov/pubmed/8970741>

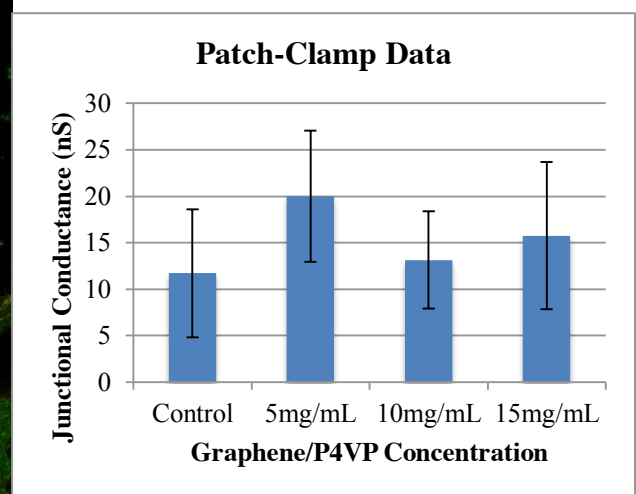
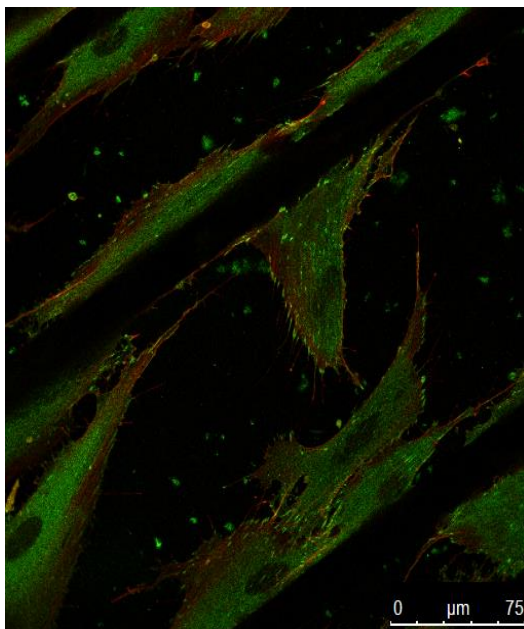
# SESSION 6 – CELL JUNCTIONS AND CELL MIGRATION

MENTORS: SISI QIN

KAO LI

FAN YANG

KUAN-CHE FENG



# Sustained Drug Delivery of Silver-Curcumin Nanoparticles for Wound Healing in Dermal Fibroblasts

Daphne Chen, Palm Harbor University High School, Palm Harbor, FL, 34683

Kuan-Che Feng, Shilpi Goenka, Dr. Miriam Rafailovich, Department of Materials Science and Engineering, Stony Brook University, Stony Brook, NY 11794

Dr. Marcia Simon, School of Dental Medicine, Stony Brook University, Stony Brook, NY,

Curcumin (CC) is a hydrophobic, polyphenolic drug derived from the *Curcuma longa* plant. It has a wide range of biological uses, including antibacterial, anticancer, antioxidant, anti-inflammatory, and wound healing abilities. CC induces wound healing by enhancing the proliferative phase of granulation tissue growth. [1] Recent medical developments have shown promise for CC drug applications. However, because of its poor water solubility, photosensitivity, and high instability, previous studies have had difficulty in effectively administering CC. [1]

Silver (Ag) nanoparticles (NPs) have excellent antibacterial and wound healing properties. [2] They offer various medical advantages in wound dressings. Interest in Ag NPs has recently increased, as the greater surface area of NPs improves the interaction between the drug and the affected surface. Poly(lactic-co-glycolic acid)(PLGA) encapsulated CC particles were used to test sustained drug release.

Currently, there is a need for a wound healing drug with enhanced efficiency. Past studies have shown that both Ag and CC have good wound healing properties. Understanding how Ag NPs and CC react together in a low dosage is critical to determining the efficacy and potential of the composite for use as medicine. Ag NPs in combination with CC provide potential use for biomedical applications in wound healing. However, both materials have been shown to be toxic to cells when administered in high concentrations. The study uses a 72-hour cytotoxicity assay with human dermal fibroblasts to determine the feasibility of Ag-CC NPs in wound healing treatment.

Pure CC was dissolved in DMSO and PBS at concentrations of 0, 2, 4, 6, 8, and 10  $\mu\text{M}$ . The solutions underwent ultraviolet-visible spectroscopy to obtain an absorption spectrum of CC. The resulting data points for each absorption curve were used to calculate the concentration of CC to use for the cytotoxicity assay.

For the PLGA-CC cytotoxicity assay, cells were plated for 2  $\mu\text{M}$  pure CC, 10  $\mu\text{M}$  pure CC, blank PLGA NPs, PLGA-CC 4.38  $\mu\text{g}/\text{mg}$ , PLGA-CC 8.28  $\text{mg}/\text{mg}$ , and a control group. Cell count after 72 hours showed a decrease to  $2.81 \times 10^4$  cells/well (Figure 2) from the control group ( $7.69 \times 10^4$  cells/well) (Figure 1), which confirms the cytotoxicity of CC at high concentrations. 2  $\mu\text{M}$  CC, PLGA, and PLGA-CC (at both concentrations) had no cytotoxic effect.

Cells were plated for a control group and three experimental groups (2  $\mu\text{M}$  CC, 40  $\mu\text{L}/\text{mL}$  Ag NP, Ag-CC). In the next few days, the data will indicate whether Ag-CC is cytotoxic. The results will determine the use of Au-CC composite for use in wound healing.

## References:

[1] Chereddy KK, Coco R, Membanga PB, Ucar B, Des Rieux A, Vandermeulen G, & Pr at V. (2013). "Combined effect of PLGA and curcumin on wound healing activity." *Journal of Controlled Release*, 171(2), 208-215. doi: 10.1016/j.jconrel.2013.07.015.

[2] Varaprasad K, Mohan YM, Vimala K, & Raju KM. (2010). Synthesis and Characterization of Hydrogel-Silver Nanoparticle-Curcumin Composites for Wound Dressing and Antibacterial Application. *Wiley Online Library*, # (#), ###-###. doi: 10.1002/app.33508.

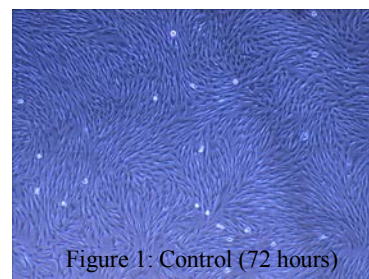


Figure 1: Control (72 hours)

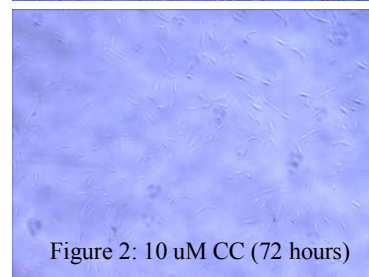


Figure 2: 10  $\mu\text{M}$  CC (72 hours)

## Increased Junctional Conductance and Intercellular Channel Formation in Cx43 Human Cervical Adenocarcinoma (HeLa) Cells Exposed to Graphene

Abigail Wax<sup>1</sup>, Karena Etwaru<sup>2</sup>, Sneha Chittabathini<sup>3</sup>, Evelyn Abramov-Kandov<sup>3</sup>, Nick Spiezio<sup>3</sup>, Dr. Miriam Rafailovich<sup>3</sup>, Dr. Tatsiana Mironava<sup>3</sup>, Dr. Peter Brink<sup>3</sup>, Dr. HZ Wang<sup>3</sup>, and Dr. Chris Gordon<sup>3</sup>  
<sup>1</sup>Harborfield High School, Greenlawn, NY; <sup>2</sup>Half Hollow Hills High School East, Dix Hills, NY; <sup>3</sup>SUNY Stony Brook University, Stony Brook, NY

Gap junctions are clusters of intercellular channels that enable cellular communication by sharing of ions, second messengers, and small metabolites (Bruzzone, R., et. al.)<sup>1</sup>. Recent research suggests gap junction channels can also be used for delivery of small interference RNA (siRNA) for gene suppression in cancer treatment. This method circumvents problems associated with dilution in the extracellular matrix, thus enhancing siRNA transfer. Previous studies have indicated that the connexin 43 facilitates successful gap junction formation (Valiunas, V, et. al.)<sup>2</sup>.

Because of cell-material interaction, materials can be used to enhance cell-to-cell communication. To further increase the efficacy of intercellular human cervical adenocarcinoma (HeLa) cells transfected with Cx43 were exposed to graphene to observe the effect on junctional conductance. Graphene is a single layer of carbon atoms with numerous biomedical applications because of its physical, mechanical, and chemical properties, one of which includes high electrical conductivity due to the atomic structure. Several methods of experimentation including the patch-clamp, hemocytometer, atomic force microscopy, optical microscopy, and confocal microscopy were used to determine the effect of graphene on the HeLa cells. The Cx43 HeLa cells were exposed to graphene in one of two conditions: cells were cultured in media containing graphene or cells were grown on spun-cast graphene substrates. For the first condition, Cx43 HeLa cells were plated and 24 hours later, the media was changed to the graphene-containing media at concentrations of 0.1, 0.5, and 1.0mg/mL. For the latter, solutions with graphene, poly(4-vinylpyridine) (P4VP), and DMF at concentrations of 5, 10, and 15mg/mL graphene to P4VP were spun-cast on to 1mm glass cover slips. Then, the glass cover slips were placed in the 24 well plates for culturing. The growth curves drawn from the cell counting data show graphene is not cytotoxic as the cell number continued to increase, even in the presence of the highest graphene concentrations. However, a significant decrease in cell number was found at the higher concentrations of graphene-containing media whereas increased cell growth was observed on the graphene substrates when compared to the P4VP control. We therefore infer that P4VP may adversely affect Cx43 HeLa cell growth. Furthermore, dual patch-clamping was performed to investigate differences in junctional conductance. Graphene did increase the gap-junctional

conductance of the cells grown on the substrates. The highest conductance was found in the 5mg/mL with 20ns, while the control without graphene had the lowest conductance, 11.71ns [Figure 1]. These data suggest graphene increases intercellular channel formation, thus increasing junctional conductance in Cx43 HeLa cells.

We plan to perform confocal microscopy on the cells exposed to graphene to examine the cell morphology and connexin expression. Furthermore, we intend to continue research to determine the exact mechanism by which graphene increases junctional conductance.

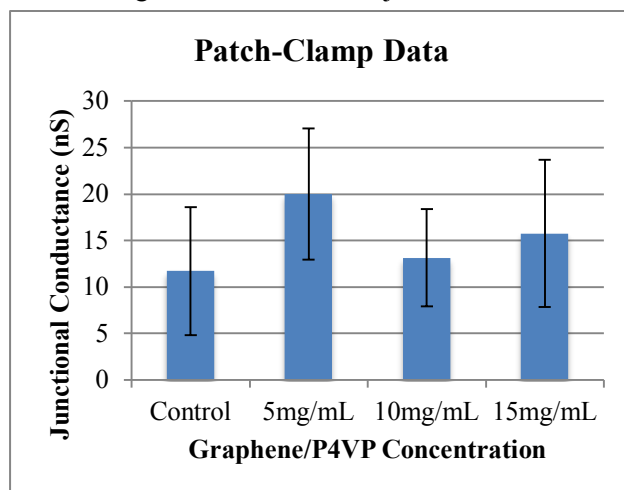


**Figure 1:** Graph illustrating the increase in junctional conductance of Cx43 HeLa cells grown on spun-cast graphene substrates.

<sup>1</sup>Bruzzone, R. et. al. "Connections with Connexins: The Molecular Basis of Direct Intercellular Signaling." *European Journal of Biochemistry*. (1996). 238 (1): 1-27.

<sup>2</sup>Valiunas, V, et. al. "Connexin-Specific Cell-to-Cell Transfer of Short Interfering RNA by Gap Junctions." *Journal of Physiology*. (2005). 568 (2): 459-468.

## Identifying the Age-Dependency of Human Dermal Fibroblast Uptake and the Cytotoxic Response to Gold Nanoparticles of Varying Concentrations

Emily Braverman, Clayton HS, Clayton MO, 63105; Elizabeth Varghese and Anna Vaynrub, Plainview HS, Plainview NY, 11804; Dr. Tatsiana Mironava, Fan Yang, Kuan-Che Feng, Yingjie Yu and Dr. Miriam Rafailovich, Stony Brook University, Stony Brook NY, 11794

The medical significance of gold nanoparticles lie in their versatility: AuNPs are novel agents in cancer therapy, imaging, and gene therapy<sup>1</sup>. Although the cytotoxic effects of AuNPs on human dermal fibroblasts (HDFs) have been well documented, few to no studies exist that detail the difference in AuNP toxicity on cells of different ages<sup>2</sup>. This project examines the response of human dermal fibroblasts of “young” and “old” age groups to AuNPs in regards to cell death and AuNP uptake. Additionally, the project aims to compare cell membrane rigidity and modulus between “young” and “old” cells.

The AuNPs were identified as gold using UltraViolet Visible Spectroscopy to determine a peak absorbance of 529 nm, characteristic of atomic gold. The average zeta potential of the AuNPs was -37.68, indicating moderate stability of the suspension, and TEM analysis determined the average diameter of the AuNPs to be 16.8 nm. Twenty-four hours after treating young HDFs with AuNPs with a concentration of 100  $\mu\text{L}/\text{mL}$ , the average proliferation reduction was 25.5%, while for old HDFs, the reduction was 17.6%. At a concentration of 150  $\mu\text{L}/\text{mL}$ , the young HDFs had an average proliferation reduction of 24.5%, yet the reduction was 9.78% for old HDFs.

Previous studies have indicated that as cells increase in age, their membranes increase in rigidity<sup>3</sup>. The greater rigidity of older plasma membranes may interfere with and deprive the cell of the elasticity required for receptor-mediated endocytosis--the mechanism responsible for AuNP uptake. The rigidity of the HDF cell membrane will be determined using atomic force microscopy (AFM).

The results thus far indicate that as the concentration of nanoparticles increases, cell death increases. Interestingly, the old HDFs have shown a greater resistance to AuNP toxicity. In contrast to the young cells, we observed an increase in the number of surviving old cells from the 100  $\mu\text{L}/\text{mL}$  to the 150  $\mu\text{L}/\text{mL}$  concentration. The results will benefit the nanotechnology industry by illustrating the differences in how older humans will react to AuNP treatment when compared to young humans, thus allowing for the development of more efficient and customized nanoparticle therapy.

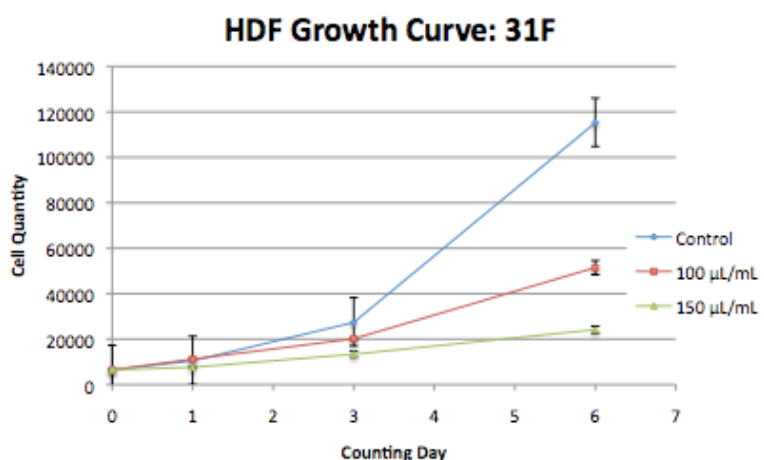


Figure 1. 31F HDF Growth Curve

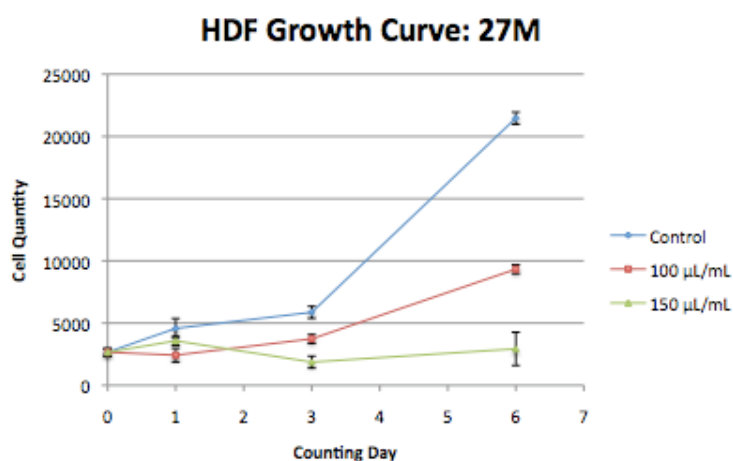


Figure 2. 27M HDF Growth Curve

<sup>1</sup> Liu, Z., et al. (June 2014). Effects of Internalized Gold Nanoparticles with Respect to Cytotoxicity and Invasion Activity in Lung Cancer Cells. *PLoS ONE*, 9, 1-11.

<sup>2</sup> Mironava, T., et al. (March 2010). Gold nanoparticles cellular toxicity and recovery: Effect of size, concentration and exposure time. *Nanotoxicology*, 4, 120-137.

<sup>3</sup> Schroeder, F., et al. (March 1984). Sex and age alter plasma membranes of cultured fibroblasts. *European Journal of Biochemistry*, 142, 183-191.

## Mechanisms of Migration of Human Dermal Fibroblasts on various topographically distinct scaffolds and when treated with the p12 peptide

Eliana Krim<sup>1</sup>, Mairead Milan<sup>2</sup>, Naomi Shapiro<sup>3</sup>, Kao Li<sup>4</sup>, Sisi Qin,<sup>4</sup> Dr. Miriam Rafailovich<sup>4</sup>

1. Ma'ayanot Yeshiva High School for Girls, Teaneck, NJ, 07666 2. South Side High School, Rockville Centre, NY, 11570 3. Yeshivah of Flatbush, Brooklyn, NY 11230 4. Department of Material Science and Engineering, State University of New York at Stony Brook, Stony Brook, NY, 11790

Human Dermal Fibroblast migration and the factors that influence their potency are critical components in understanding the human wound healing process. For the healthy reformation of epithelial tissue over a wound, fibroblasts must migrate efficiently.<sup>1</sup> Apparent in the elderly dermis is a temporal delay in wound closure and epithelization.<sup>2</sup> As the elderly stand to be the most susceptible group to trauma and alternatively derived chronic wounds, it is of particular clinical relevance to expedite fibroblast migration, thus minimizing the risks that open wounds exhibit. The purpose of this experiment is to investigate the migration of both young and older fibroblasts on different topographies, when treated with the p12, a peptide of nebulous understandings.

To create topographically distinct scaffolds for testing, the polymer Poly (methyl methacrylate or PMMA) was chosen to create the physical structures of flat and fibrous locales. PMMA was then spuncast onto glass wafers to assemble flat film scaffolds. After the scaffolds were annealed, PMMA was further electrospun on select flat films to achieve a fibrous surface. To induce the biocompatibility of a PMMA scaffold all scaffolds were covered in fibronectin. To evaluate the varying rates of cell migration, human dermal fibroblasts were farmed from a group of humans of various ages CF27 and AGAF09603.

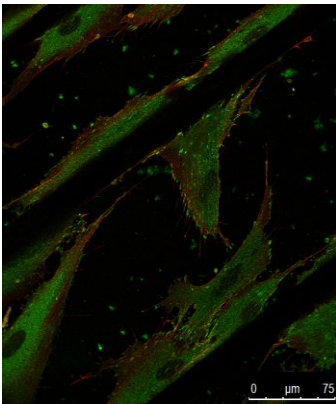


Figure 1: Actin and Vinculin Stains on AGAF09603 Flat

The dermal fibroblasts from each subject was then placed onto both flat films coated with a PMMA polymer solution and electrospun fibers made of PMMA. At the start of our experiment, we originally plated the scaffolds with cells to test the effect of topographies on their migration by analyzing the cells using single-cell migration. However after results displayed anomalous trends (results using CF31 and AGF09603), certain aspects of our original design were forsaken. To eliminate the influence of overcrowded cells we covered our next scaffolds with Agarose gel in order to measure en-masse cell migration. We plated young cells of a 31 year old human (CF-31) and old cells of an 84 year old human (AG-11744) on thin film scaffolds as well as fibrous scaffolds. We then plated additional old cells on thin film and fibrous scaffolds with an added peptide, P12, which is suspected of promoting cell migration, but isn't clearly understood. Cells were viewed and measurements were taken using Meta Morph.

Results thus far were collected from our original plated cells. Average velocities per hour old cells on thin films showed old cells on thin films migrating the fastest with  $56.7(\pm 9.2)$   $\mu\text{m}$  per hours, followed by old/fibers, young/fibers, young/ thin. These results signify anomalous findings. Samples from each group were stained for Vinculin and Actin. Results under the Confocal Microscope displayed a great concentration of Actin and Vinculin near fibers, which shows that the cells have strong adherence to the fibers. Figure 1 shows a sample of old cells on flat, thin film moving freely. The Image also displayed a more splayed concentration vinculin receptors on flat film fibroblasts. Initial data showed that fibroblasts on vinculin have more, smaller vinculin receptors, and that older cells had significantly less vinculin receptors than younger cells. If the data suggests that the younger and older cells migrate on the polymer fibers at a faster rate than those on flat films, then the study will prove that cell migration – and consequently wound healing – is promoted in fibrous surfaces. If the data on p12 treated AG11744 shows an increase in velocity, hence ultimately reducing the amount of time needed to heal wounds.

### References:

- 1 S. Guo and L.A. DiPietro. *Factors Affecting Wound Healing*
2. DiPietro, L. A., & Gosain, A. (2004, February). *Aging and wound healing*. World Journal of Surgery

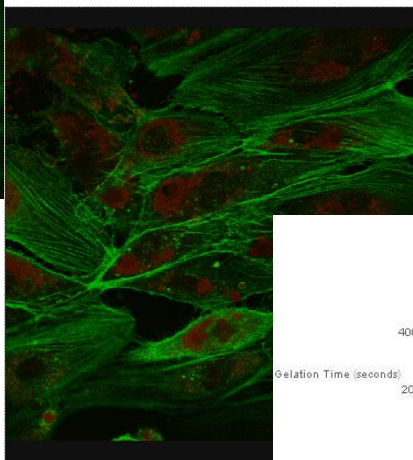
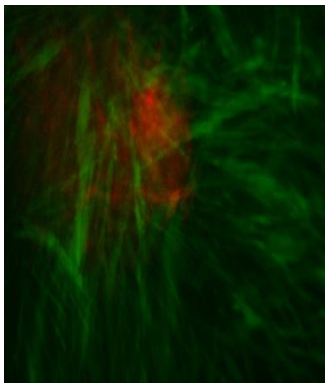
# SESSION 7 – THE INFLUENCE OF HYDROGEL SCAFFOLDS ON CELL BEHAVIOR

MENTORS: CLEMENT MARMORAT

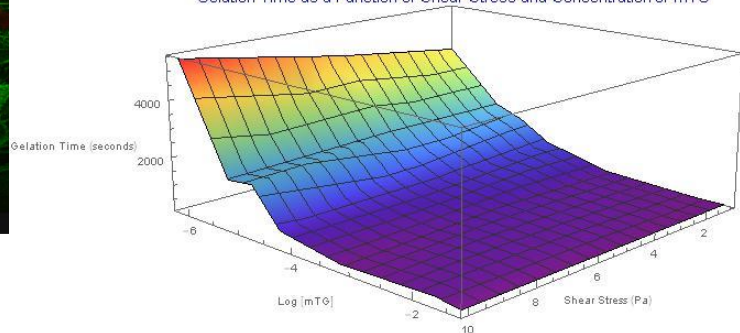
SISI QIN

YAN XU

KAO LI



Gelation Time as a Function of Shear Stress and Concentration of mTG



# Engineering Hydrogel Scaffolds for the Culture of Endothelial Cells and Applying Titanium Dioxide Nanoparticles to Regulate Proliferation

Pinelopi Margeti<sup>1</sup>, Aaron Gochman<sup>2</sup>, Clément Marmorat<sup>3</sup>, Yan Xu<sup>3</sup>, Dr. Miriam Rafailovich<sup>3</sup>

<sup>1</sup>Archimedean Upper Conservatory, Miami, FL, 33183

<sup>2</sup>Undergraduate, Stony Brook University

<sup>3</sup>Dept. of Material Science and Engineering, Stony Brook University

Currently, endothelial cells are cultured *in vitro* on matrigels, protein mixtures derived from Engelbreth-Hoth-Swarm mouse sarcoma cells<sup>1</sup>. Matrigels are difficult to synthesize and are expensive. Inexpensive viable alternatives to matrigels, such as hydrogels that can act as scaffolds and are viscoelastic, biodegradable, and exhibit biocompatible properties are sought. In this study, hydrogels were created with a gelatin (type A) matrix covalently cross-linked with microbial Transglutaminase (mTG), allowing the gelatin to be thermally stable and resistant at physiological temperatures<sup>2</sup>. Elastic modulus is to determine temperature and mechanical/shear stress resistant of hydrogels. Analysis of hydrogels with varying concentrations of mTG to gelatin (1:200, 1:125, 1:25, 1:3 ratio) revealed that the 1:25 ratio gel had the greatest and most stable elastic modulus ( $\bar{x}$  10,933 Pa at 10 Pa shear stress) and therefore served as the best candidate as a cellular scaffold. In addition, the relationship between the elastic modulus of the gels and their mTG concentrations generated a Gaussian distribution, in which extremities that deviated from the ideal 1:25 were not favored.

Using the hydrogels of 1:25 mTG to gelatin ratio (with Endothelial Growth Media *EGM*) as scaffold, the proliferation of endothelial cells was examined. After 48 hours of incubation, the endothelial cells survived, continued to develop, and showed indicated evidence of tubulogenesis or capillary formation. Additionally, the effect of titanium dioxide nanoparticles (rutile and anatase) on the proliferation of endothelial cells was examined. Hydrogels of 1:25 mTG to gelatin ratio consisting 0.1 mg/mL Rutile weakened the actin fibers of the endothelial cells and consequently lessened cell to cell contact as determined by confocal and optical microscopy. In contrast, 0.1 mg/mL anatase lysed the endothelial cells and inhibited tubulogenesis.

This study shows that hydrogels of a 1:25 mTG to gelatin ratio can effectively promote proliferation and differentiation of endothelial cells. Moreover, titanium dioxide nanoparticles can stifle development of these cells.

Figure 1

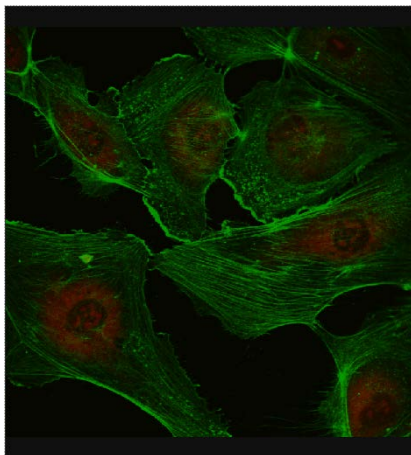


Figure 2

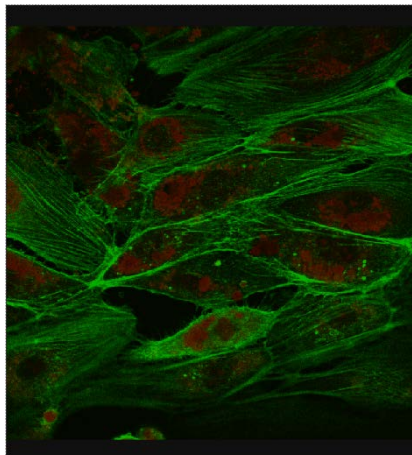


Figure 3

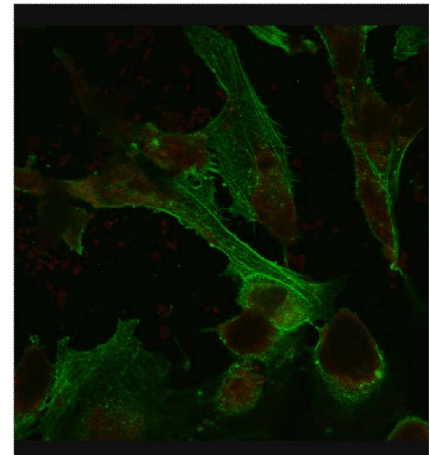


Figure 1. Confocal Microscopy. Endothelial Cell on hydrogel with EGM. (control) Tight, dense, actin fibers, and multiple solid cell to cell connections.

Figure 2. Confocal Microscopy. Endothelial Cell on hydrogel with EGM and Rutile. Weakened actin fibers and fewer contact between cells.

Figure 3. Confocal Microscopy. Endothelial Cell on hydrogel with EGM and Anatase. Cytoplasm lysis, no actin fibers present, and impaired nuclei.

<sup>1</sup>Hughes, C., Postovit, L., & Lajoie, G. (2010). Matrigel: A complex protein mixture required for optimal growth of cell culture. *PROTEOMICS*, 10(0), 1886-1890.

<sup>2</sup>Yung, C., Wu, L., Tullman, J., Payne, G., Bentley, W., & Barbari, T. (2007). Transglutaminase crosslinked gelatin as a tissue engineering scaffold. *Journal of Biomedical Materials Research Part A*, 83A(4), 1039-1046.

# The Modelization and Characterization of Hydrogel Cross-linking using Microbial Transglutaminase as a Cross-linking Agent

Jaymo Kang<sup>1</sup>, Joshua Lederer<sup>2</sup>, Clement Marmorat<sup>3</sup>, Miriam Rafailovich<sup>3</sup>

<sup>1</sup>Adlai E. Stevenson High School, Lincoln Shire, Illinois

<sup>2</sup>Hebrew Academy of the Five Towns and Rockaway High School, Cedarhurst, NY

<sup>3</sup>Department of Material Science and Engineering, Stony Brook University, Stony Brook, NY

A hydrogel is a type of biodegradable, biocompatible polymeric-like material that can be used in many biological applications, including drug delivery, cell scaffolding, and tissue engineering<sup>1</sup>. However, there is very little known about the dynamics of hydrogel cross linking. This project attempts to shed light upon the mechanisms behind hydrogel formation and how various factors, such as shear stress and concentration of *Microbial Transglutaminase* (mTG) affect the rate and strength of cross-linking. Hydrogels were prepared with mTG to gelatin volumetric ratios of 1:3, 1:5, 1:25, 1:75, 1:125, 1:200, and 1:500. Using dynamic rheology, it was determined that as the mTG to gelatin ratio decreased from 1:3 to 1:500, the gelation time increased tenfold. Furthermore, as sheer stress increased from 1 pascal to 10 pascals, the difference in gelation time between the 1:3 and 1:500 samples increased about 50% for each concentration of mTG.

Using Wolfram Mathematica, a 3-dimentional model was constructed to show the relationship between shear stress, concentration of mTG, and gelation time ( Figure 1).

In addition, a generalized model was constructed to describe how the viscosity of the hydrogel changed as a function of time (Figure 2). It was determined that the shape of the viscosity vs. time curves highly resembled an exponential curve  $A * e^{k*t}$  after a lag time, with gels of higher concentrations of mTG exhibiting shorter lag times. Furthermore, after the lag time, the k parameter also increased as the concentration of mTG increased, suggesting that higher concentrations lead to faster cross linking. Future questions that will be answered will answer how the A parameter changes such as temperature or volume of total solution, and whether or not both parameters can be modeled as functions of mTG concentration.

**Figure 1: Evolution of gelation time as shear stress and concentration of mTG varies**

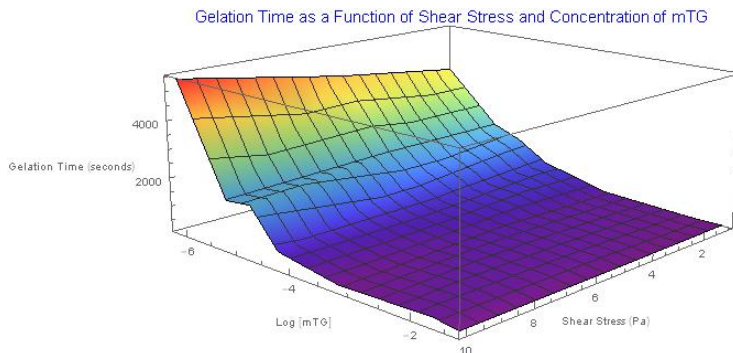
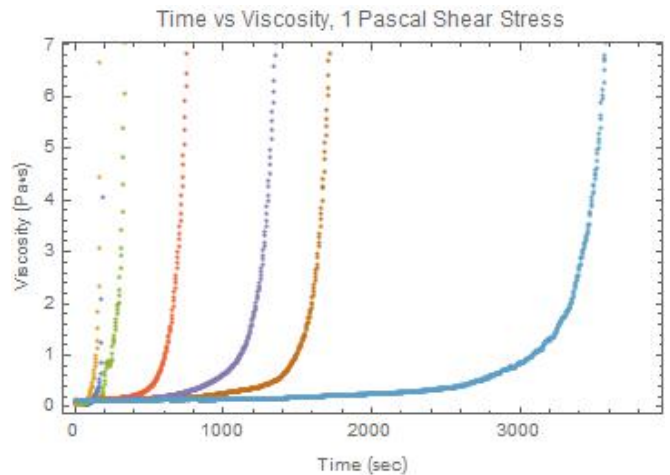


**Figure 2: Viscosity vs time graphs over varying concentrations of mTG**



## References:

- [1] N. A. Peppas, J. Z. Hilt, A. Khademhosseini and R. Langer, *Adv. Mater.*, 2006, 18, 1345–1360.
- [2] A. Fernandez-Barbero, I. J. Suarez, B. Sierra-Martín, A. Fernandez-Nieves, F. J. de las Nieves, M. Marquez, J. Rubio-Retama and E. Lopez-Cabarcos, *Adv. Colloid Interface Sci.*, 2009, 147–148, 88–108.
- [3] N. A. Peppas, P. Bures, W. Leobandung and H. Ichikawa, *Eur. J. Pharm. Biopharm.*, 2000, 50, 27–46.

# Crosslinked Hydrogels as a Platform for Mineralization with Dental Pulp Stem Cells

Tiffanie Yang<sup>1</sup>, Heesu Shin<sup>1</sup>, Clément Marmorat<sup>2</sup>, Dr. Adriana Pinkas-Sarafova<sup>3</sup>, Dr. Miriam Rafailovich<sup>2</sup>

<sup>1</sup> Half Hollow Hills High School East, Dix Hills, NY,

<sup>2</sup>Dept. of Material Science and Engineering, Stony Brook University,

<sup>3</sup>Dept. of Oral Biology and Pathology, Stony Brook University

Transglutaminase crosslinked gelatin hydrogels are biodegradable and biocompatible materials that can serve as scaffolds for promoting the growth and differentiation of stem cells. These hydrogels also offer a three-dimensional scaffold for biomineralization (deposits of calcium phosphate).<sup>1,2</sup> This study examines the mineralization potential of hydrogels of different elastic modulus. For this purpose hydrogels were prepared using gelatin crosslinked with microbial transglutaminase (mTG) at ratios of 25:1 to generate hydrogels of medium elastic modulus (“medium”) and 200:1 to generate hydrogels of low elastic modulus (“soft”). Biomineralization was evaluated using dental pulp stem cells (DPSC) that had been genetically engineered to express enhanced Green Fluorescent Protein (eGFP) (strain: AV3-GFP) in media with and without dexamethasone (Dex) as an inducer of differentiation and biomineralization.<sup>3</sup>

For the experimental set up, there were duplicate samples of four groups: 1. DPSC on soft hydrogels ± Dex; 2. DPSC on medium hydrogels ± Dex; 3. DPSC on tissue culture plastic; and 4. soft and medium hydrogels ± Dex with no cells. To measure the impact on cell mechanics, atomic force microscopy [AFM] was carried out 5-days post-plating, and to measure mineralization cultures were stained with xylenol-orange at days 7 and 14 post-plating. AFM data shows that the difference in moduli of the cells plated on the soft and medium gels with and without Dex is negligible. This indicates that contrary to expectations, the elastic moduli of the gels have little effect on the cells moduli. The differing amounts of mineralization in the gels plated with cells could therefore be explained by the idea that mineralization is influenced not by cell modulus but rather the ability of the cells to form bonds with the gels (Figure 1). Scanning electron microscopy is to be conducted after twenty-eight days.

Prior to cell plating, rheology tests were done on the two different gels to determine their respective elastic modulus and visco-elastic domain. The medium gel had a higher elastic modulus (12,000 Pa) than the soft gel (5,000 Pa). These elastic moduli are important for understanding how changes in surface mechanics and topography influence cell functions (e.g., differentiation and proliferation), and matrix mineralization. In the presence of Dex small calcium deposits were observed by day 7 in groups 1 (“soft”), 2 (“medium”), and 3 (tissue culture plastic). In the absence of Dex, mineral deposits were found only in group 3. In the experiment conducted without Dex, at day 14 small mineral deposits were observed in groups 2 and 3, but not in group 1 (Figure 2).

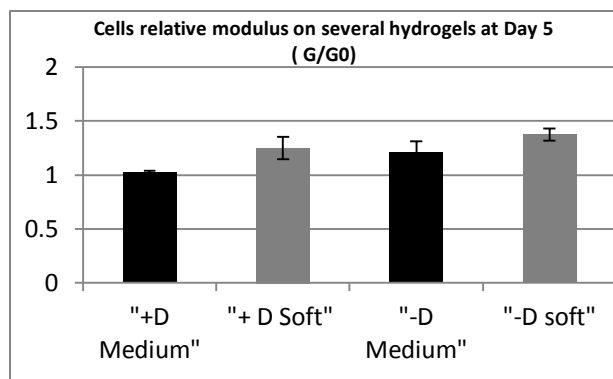


Figure 1: Variations of cell modulus from AFM

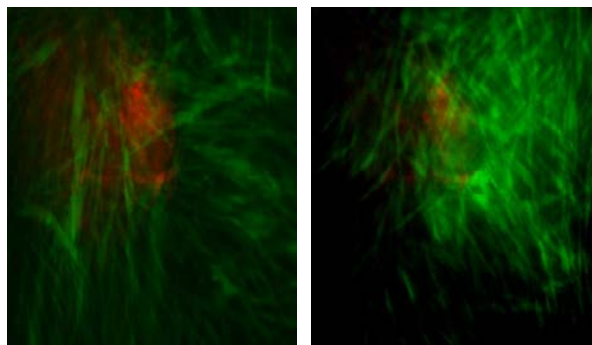


Figure 2: Image showing calcium phosphate deposits (red) on medium hydrogels with DPSCs (green) at day 14. A: -Dex, B: +Dex

[1] Divya Bhatnagar, PhD Thesis (2012) Stony Brook University

[2] Case Western Reserve University. "Stem cell proliferation and differentiation observed within hydrogel." ScienceDaily. ScienceDaily, 11 April 2013. <[www.sciencedaily.com/releases/2013/04/130411194915.htm](http://www.sciencedaily.com/releases/2013/04/130411194915.htm)>.

[3] Gronthos S(1), Brahim J, Li W, Fisher LW, Cherman N, Boyde A, DenBesten P, Robey PG, Shi S. Stem cell properties of human dental pulp stem cells. J Dent Res. 2002 Aug;81(8):531-5

# Optimizing Conditions to Proliferate Hematopoietic Stem Cells without Differentiation

Ruth Kopyto<sup>1</sup>, Sici Qin<sup>2</sup>, Dr. Jerell Aguila<sup>2</sup>, Dr. Miriam Rafailovich<sup>2</sup>

1. HAFTR HS, Cedarhurst, NY, 11516

2. Stony Brook University, Stony Brook, NY, 11794

Hematopoietic Stem Cells (HSCs) are multipotent and are able to differentiate into any hematological cell. They can be used to treat leukemia and lymphoma (Hematopoietic et. al., 2011)<sup>2</sup>. However, they are few in number, thus finding optimal conditions in which the HSCs can proliferate while maintaining stemness is the ultimate goal.

HSCs proliferate when two cells get close. To cause proliferation, the jagged and delta of one cell must cut the notch ligand of the other cell to allow the NICD to enter the cell. Once cut, the NICD triggers a chain of reactions, which ultimately causes the cell to undergo mitosis (Bigas et. al., 2012)<sup>1</sup>. Thus, finding an appropriate surface in which cells can move smoothly, close together will help assist in the proliferation process. HSCs on three different conditions were tested-a hard hydrogel (1:3-mTG:gelatin), a soft hydrogel (1:125), and a plain Petri dish (control). The average cell movement was recorded (see figure 1); as seen on the pictures the hard had multiple clumps of cells, and on the control the HSCs were very far apart, and on the soft gel the HSCs were evenly spread from the main circle of cells. Then for further testing, varying hydrogels were made out of gelatin (10.0% by concentration in PBS) and mTG-crosslinker(10% by concentration in PBS). Using a rheometer, a sheer stress was applied to each gel and the elastic modulus was measured. Tests on the rheometer were also done to see how the elastic modulus is affected in room temperature versus incubator temperature (37C) (see figure 2). These tests were performed to find optimal stable conditions in gels. From this research we found that very stiff gels were unstable and over crosslinked. Hence, a soft and stable gel may provide consistent cell movement and proliferation. Thus, for continuing research there will be six groups- Petri dish control, 1:125 hydrogel, 1:500 hydrogel, and the other three will be the same, except they will have lentivirus. Lentivirus transfects the cells so that it creates only the NICD, thus making the cells independent from one other, not needing the jagged or delta in order to proliferate.

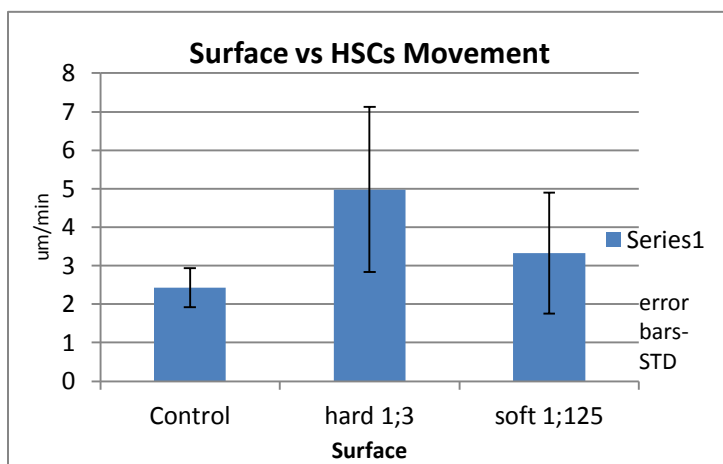


Figure 1: Cell velocity on different substrates

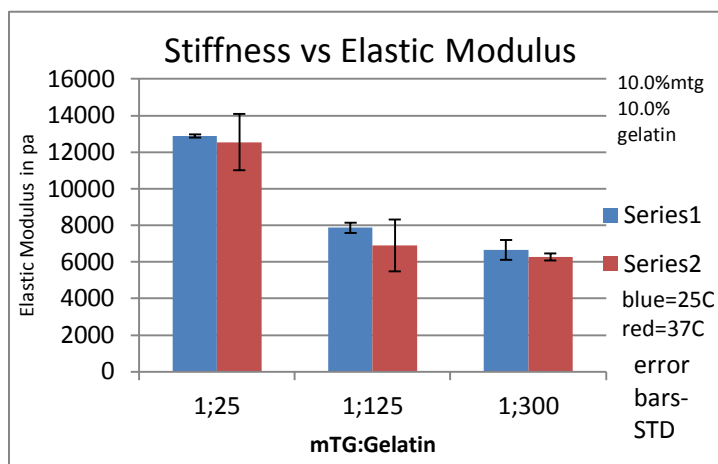


Figure 2: Gel Moduli at different temperatures

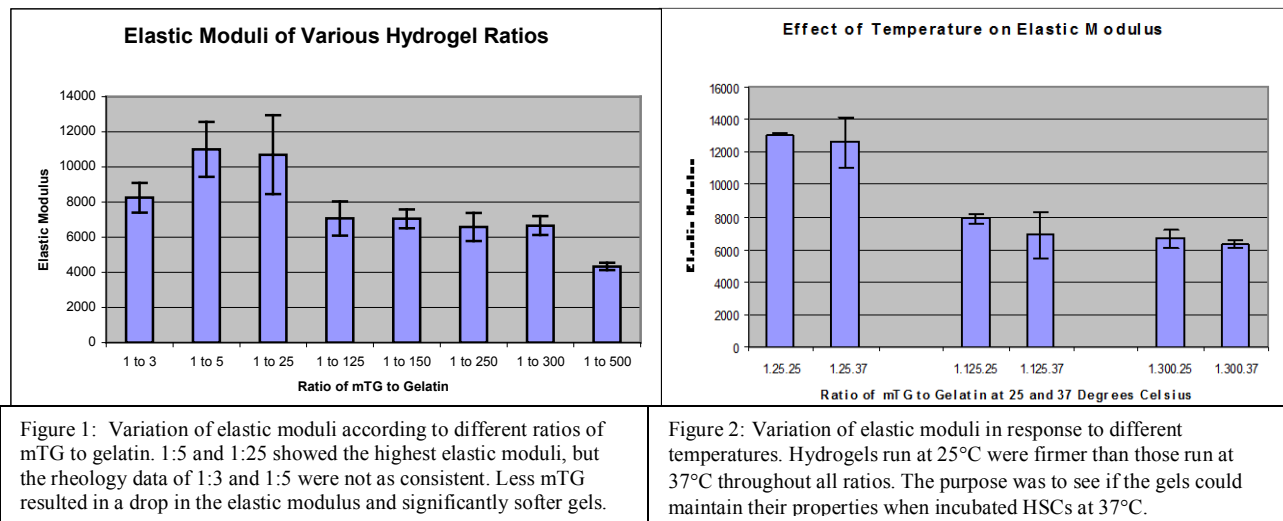
1. Bigas, A., and Espinosa, L. (2012). Hematopoietic stem cells: to be or Notch to be. *Blood*, 119(14), 3226-3235.
2. Hematopoietic Stem Cells . In *Stem Cell Information*. Bethesda, MD: National Institutes of Health, U.S. Department of Health and Human Services, 2011

## The Effects of Various Substrate Interfaces and Stemregenin 1 on Hematopoietic Stem Cell Proliferation and Stemness in Vitro

Henry Dong, Irvine HS, Irvine, CA, 92604; Sisi Qin, Stony Brook University, Stony Brook, NY, 11794; Dr. Yupo Ma, Dr. Miriam Rafailovich, Stony Brook University, Stony Brook, NY, 11794

It is commonly understood that hematopoietic stem cells (HSCs) have extensive self-renewal capabilities in vivo, and this phenomenon is exploited in practices such as clinical transplantation to treat disease-related bone marrow failure. However, these practical therapeutic purposes still remain generally limited – in comparison to their potential – by the loss of these capabilities in vitro (Lutolf et. al., 2008)<sup>1</sup>. There has been significant interest in imitating and modeling the stem cell niche for cell renewal to expand HSC populations in vitro. Recently, researchers have begun to utilize hydrogel plates as artificial niches imitating marrow architecture to assess the effects characteristic of the in vivo microenvironment (Sharma et. al., 2012)<sup>2</sup>.

The purpose of this study was to examine the properties of gelatin based hydrogels and use these gels – among other substrates – to develop a scaffold to maximize proliferation of HSCs. Multiple hydrogels were prepared with a 10% gelatin to PBS solution and were cross-linked with a 10% microbial transglutaminase (mTG) to PBS solution in ratios of 1:3, 1:5, 1:25, 1:125, 1:150, 1:250, 1:300, and 1:500 mTG to gelatin. Each gel was run under a rheology with 25°C and 37°C temperature controls to examine how the relative amount of mTG and the contrast of temperature affected the elastic modulus and the shear stress under which the gels broke. As shown in Figure 1, we found that the 1:25 ratio produced the firmest gels and highest elasticity, and we generally witnessed a collapse of its properties – when the elastic and viscous moduli crossed – at around a shear stress between 847.9 and 1209. The 1:125 ratio produced the next stiffest gels, and the following ratios produced softer gels with much lower elastic moduli and different properties, especially considering the fact that the elastic and viscous moduli did not cross. The 1:3 and 1:5 ratios were unstable in comparison, with lower elastic moduli than expected, likely due to the excess of mTG after all bonds had been cross-linked, resulting in weaker hydrogels. Additionally, the 37°C temperature control resulted in lower elastic moduli throughout (Figure 2). We selected the 1:25 and 1:300 ratio as our hard and soft samples, respectively, for cell plating. CD34+ and CD38+ HSCs were cultured on four surfaces – the two hydrogels, a spincoated poly(methyl methacrylate) (PMMA) thin film on glass, and a control sample with only the plastic petri dish. Each individual surface had two samples, one with the presence of the chemical stemregenin 1 (SR1) and one without in order to examine the chemical’s effect on proliferation and stemness. The cell incubation is currently in progress.



<sup>1</sup>Lutolf, M., Doyonnas, R., Havenstrite, K., Koleckar, K., & Blau, H. (2008). Perturbation of single hematopoietic stem cell fates in artificial niches. *Integrative Biology*, 1, 59-69.

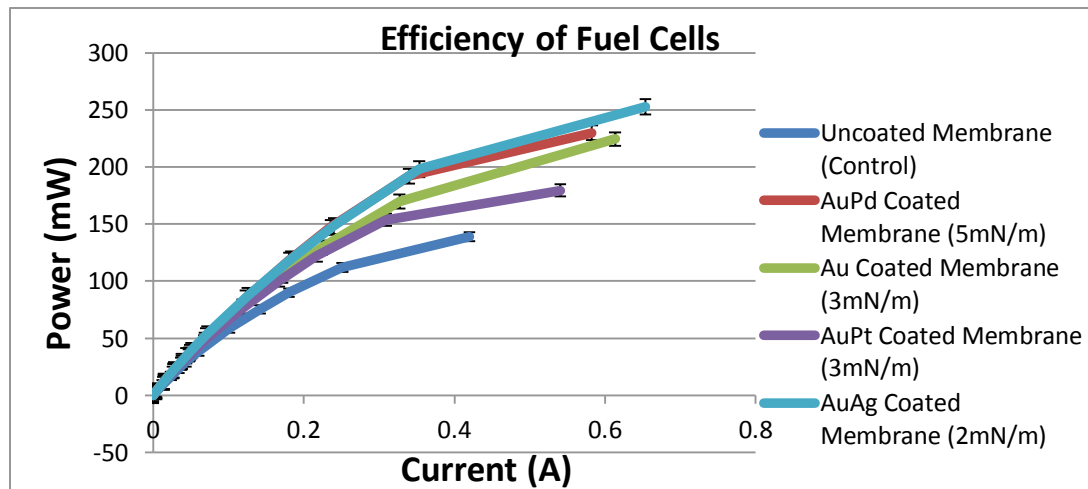
<sup>2</sup>Sharma, M., Limaye, L., & Kale, V. (2012). Mimicking the functional hematopoietic stem cell niche in vitro: Recapitulation of marrow physiology by hydrogel-based three-dimensional cultures of mesenchymal stromal cells. *Haematologica*, 651-660.

# SESSION 8

# FUEL CELLS

MENTORS: LONGTAO HAN

HONGFEI LI



## Increasing the Performance of PEM Fuel Cells with Nanoparticle Alloys on the Nafion<sup>®</sup> Membrane

Akash Wasil, Half Hollow Hills High School East, Dix Hills, NY, 11746

Roshan Patel, Ward Melville High School, East Setauket, NY, 11733

Will Fried, Ramaz High School, New York, NY, 10075

Hongfei Li, Longtao Han, and JinYing Lin, Stony Brook University, Stony Brook, NY, 11794

Polymer electrolyte membrane fuel cells (PEMFCs) can potentially be a viable alternative to fossil fuels. However, commercial usage of PEMFCs is limited due to high production costs and low power output<sup>[1]</sup>. Currently, expensive platinum nanoparticles are most commonly used to catalyze the transfer of protons across the proton exchange membrane<sup>[2]</sup>. The purpose of this study is to reduce costs and increase power output of PEMFCs by coating the Nafion<sup>®</sup> membrane with cheaper nanoparticle alloys.

Nanoparticle alloys containing a 1:1 ratio of Au/Pt, Au/Pd, and Au/Ag, were prepared using the Brust Two-Phase Method<sup>[3]</sup>. After synthesizing the nanoparticles, a Langmuir-Blodgett (LB) trough was used to coat the membrane with the particles in a monolayer, which was confirmed by Transmission Electron Microscopy (TEM). A H-tec fuel cell kit was used and the various membranes were inserted into the fuel cells. Power output was measured at various external resistances (Figure 1).

As predicted, the fuel cells with nanoparticles coated membranes performed substantially better than the fuel cells with uncoated membranes. The overall power output increased by 64% for the Au/Ag particles, 56% for the Au/Pd particles, 31% for the Au/Pt particles, and 44% for the pure Au particles. Using a 1:1 flow rate of H<sub>2</sub> and CO<sub>2</sub>, the fuel cell's efficiency of the fuel cells was also examined. The performances of all fuel cells exposed to the H<sub>2</sub>/CO<sub>2</sub> mixture significantly decreased, likely due to the formation of catalyst-poisoning CO from CO<sub>2</sub> and O<sub>2</sub><sup>[4]</sup>. However, this effect was least detrimental to the Au/Ag coated membrane, which performed 42% more efficiently than the uncoated control membrane.

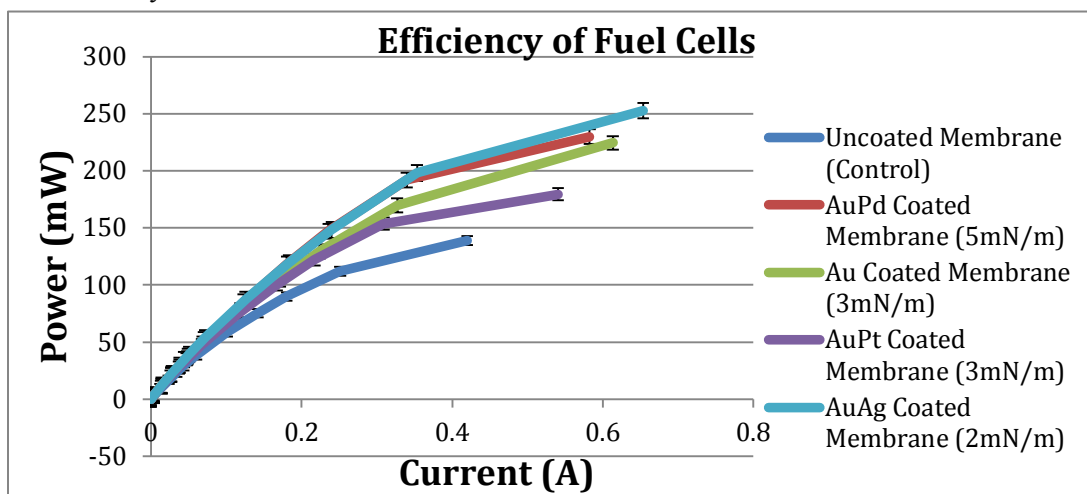


Figure 1: Power vs. Current for membranes coated with various nanoparticles. The membrane coated with Au/Ag particles produced the greatest power output.

[1] Saibuathong, N., Saejeng, Y., Pruksathorn, K., Hunsom, M., & Tantavichet, N. (n.d.). Catalyst electrode preparation for PEM fuel cells by electrodeposition. *Journal of Applied Electrochemistry*, 903-910.

[2] Gasteiger, H., Kocha, S., Sompalli, B., & Wagner, F. (n.d.). Activity benchmarks and requirements for Pt, Pt-alloy, and non-Pt oxygen reduction catalysts for PEMFCs. *Applied Catalysis B: Environmental*, 9-35.

[3] Mathias Brust, Meryll Walker, Donald Bethell, David J. Schiffrin and Robin Whyman. *J. Chem. Soc., Chem. Commun.*, 1994, 801-802

[4] Nachiappan, N., Kalaignan, G., & Sasikumar, G. Effect of nitrogen and carbon dioxide as fuel impurities on PEM fuel cell performances. *Ionics*, 19, 351-354

## Effects of Carbon Chain Length in Thiol-Functionalized Gold Nanoparticles Coating a Nafion® Membrane on PEM Fuel Cell Efficiency

**Ilana Radinsky**, Stella K. Abraham HS for Girls, Hewlett Bay Park, NY, 11557; **JinYing Lin**, Stony Brook University, Stony Brook, NY, 11794; **Hongfei Li**, Stony Brook University, Stony Brook, NY, 11794; **Longtao Han**, Stony Brook University, Stony Brook, NY, 11794; **Dr. Miriam Rafailovich**, Stony Brook University, Stony Brook, NY 11794

The recent energy crisis has taken the world by storm. Fossil fuels, on which the world relies most heavily for energy production, are hazardous to human health and the environment, and are predicted to be depleted in the coming years. Hydrogen fuel cells are a promising alternative to fossil fuels, because they produce water as the only byproduct, thereby eliminating health and environmental hazards, and because the world's hydrogen supply is virtually unlimited, so the fuel cell can be considered an infinite resource.

One of the major components of the hydrogen fuel cell is the electrolyte, for which a Nafion® membrane is most commonly used. Previous research has found that using a Nafion® membrane coated with gold nanoparticles improves the efficiency of a fuel cell. The gold nanoparticles serve as catalysts for the reverse electrolysis reaction that powers the fuel cell.<sup>1</sup> They also protect the platinum catalyst on the electrodes from being poisoned by carbon monoxide when using mixed H<sub>2</sub> and CO<sub>2</sub> gases to power the fuel cell instead of pure H<sub>2</sub>.<sup>2</sup>

These gold nanoparticles are functionalized with thiol, carbon chains ending in an SH- group, prior to coating. We hypothesize that the length of these carbon chains greatly affects fuel cell efficiency, because the lengths directly influence the dispersion of nanoparticles across the Nafion® membrane. To test this hypothesis, we used the Brust Two-Phase Method<sup>3</sup> to synthesize thiol-functionalized gold nanoparticles with 8-carbon chains, 12-carbon chains, and 18-carbon chains. We used the LB trough to coat three Nafion® membranes at three different surface pressures for each carbon chain length. We then tested the nine resulting Nafion® membranes in a fuel cell using both pure hydrogen gas and mixed hydrogen and carbon dioxide gases, and recorded the voltage and current. Based on this data, we were able to calculate the power output of the fuel cells at varying resistances as shown in figure 1. We determined the optimal carbon chain length for maximum fuel cell efficiency to be 12 carbons, as well as the optimal surface pressure for this carbon chain length to be 3 mN/m. We proved that carbon chain length does, in fact, directly impact hydrogen fuel cell efficiency.

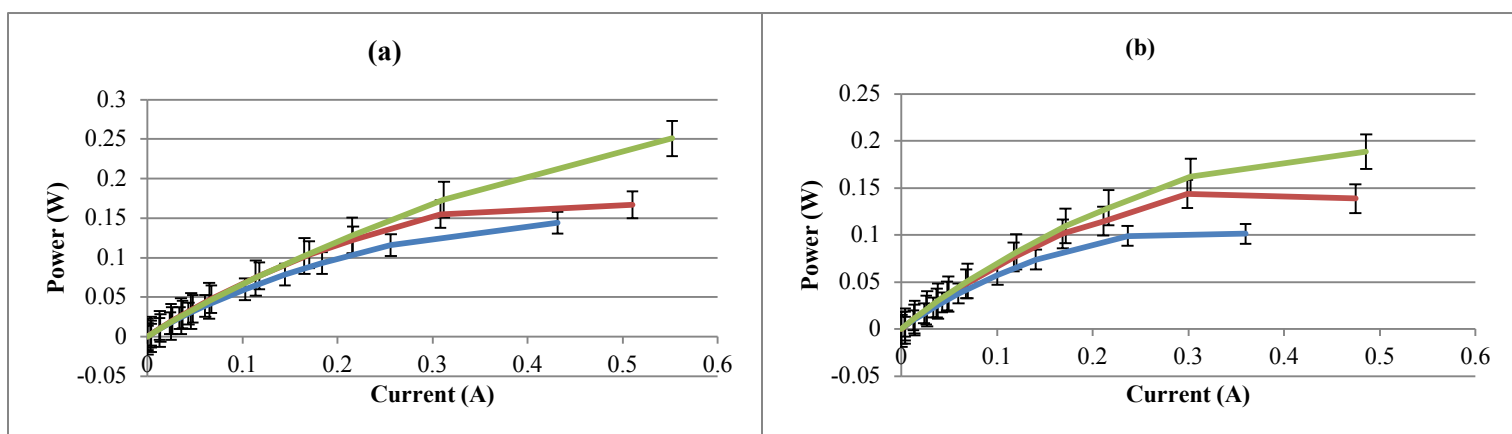


**Figure 1.** (a) Power output versus current using pure H<sub>2</sub> gas. (b) Power output versus current using mixed gas. For both graphs (a) and (b), blue: uncoated Nafion® membrane (control), red: Nafion® membrane coated with 8-C gold nanoparticles, green: Nafion® membrane coated with 12-C gold nanoparticles. For both graphs (a) and (b), the fuel cell using the Nafion® membrane coated with 12-C gold nanoparticles had the maximum efficiency.

<sup>1</sup> Green, Isabel Xiaoye, Wenjie Tang, Matthew Neurock, and John T. Yates. "Low-Temperature Catalytic H<sub>2</sub> Oxidation over Au Nanoparticle/TiO<sub>2</sub> Dual Perimeter Sites." *Angewandte Chemie International Edition* 50.43 (2011): 10186-0189. *Wiley Online Library*. Web. 31 July 2014.

<sup>2</sup> Green, I. X., W. Tang, M. Neurock, and J. T. Yates. "Spectroscopic Observation of Dual Catalytic Sites During Oxidation of CO on a Au/TiO<sub>2</sub> Catalyst." *Science* 333.6043 (2011): 736-39. Web.

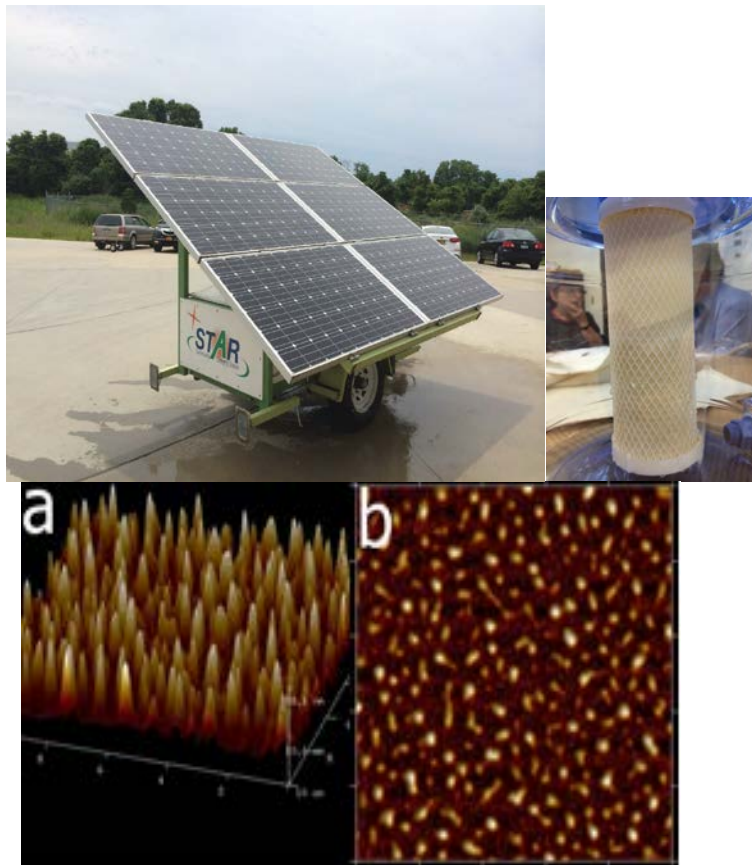
<sup>3</sup> Brust, Mathias, Merryl Walker, Donald Bethell, David J. Schiffrin, and Robin Whyman. "Synthesis of Thiol-derivatised Gold Nanoparticles in a Two-phase Liquid-Liquid System." *Journal of the Chemical Society, Chemical Communications* 7 (1994): 801. Web. 4 Aug. 2014.

# SESSION 9:

# SOLAR POWER

MENTORS: JOHN JEROME

ZHENHUA YANG



## Construction of the OPV Active Layer Using the LB Trough or Inducing Polymer Phase Separation to Improve Morphology and Efficiency

Wanying Fu<sup>1</sup>, Nicholas Han<sup>2</sup>, Andrew Chen<sup>3</sup>, Jinying Lin<sup>4</sup>, Zhenhua Yang<sup>4</sup>, Hong Fei Li<sup>4</sup>, Dr. Miriam Rafailovich<sup>4</sup>  
 1 Dougherty Valley High School, San Ramon, California 94582 2 Westview High School, Portland, Oregon 97229 3 Rice University, Houston, Texas 77005 4 Department of Materials Science, SUNY Stony Brook, Stony Brook, New York 11790

Our work attempts to enhance solar cell active layer morphology in two ways. The first is by introducing a photoactive polymer, Poly[*N*-9'-heptadecanyl-2,7-carbazole-*alt*-5,5-(4',7'-di-2-thienyl-2',1',3'-benzothiadiazole)] (PCDTBT), into the standard mixture of Poly(3-hexylthiophene-2,5-diyl) (P3HT) and [6,6]-Phenyl C<sub>61</sub> butyric acid methyl ester (PCBM) to induce polymer phase separation into columns that penetrate through the active layer, increasing donor-acceptor interface and shortening exciton travel length<sup>[1]</sup>. The second is by using the Langmuir-Blodgett (LB) trough to deposit alternating monolayers of P3HT and PCBM, allowing for precise organization of P3HT and PCBM where each layer is thin enough to allow all excitons to separate. By optimizing active layer morphology, we can improve overall solar cell efficiency<sup>[2]</sup>.

The P3HT:PCBM and P3HT:PCBM:PCDTBT blends were prepared by dissolving respective weights of the polymer displayed in **Table 1** in 1,2-dichlorobenzene. The solar cell was created by spin coating TiO<sub>2</sub> onto ITO glass. The respective polymer blends were then spin casted separately onto the TiO<sub>2</sub> layer. MoO<sub>3</sub> was deposited onto the sample. The Ag anode was deposited onto the MoO<sub>3</sub> layer in the same manner. Solar cell performance was evaluated using a 150W solar simulator with an AM 1.5G filter at a light intensity of 100 MW cm<sup>-2</sup>. Film morphology was analyzed using atomic force microscopy (AFM). For the LB trough construction of the active layer, solutions of PCBM, P3HT, and PCBM:P3HT were prepared in chlorobenzene all at a concentration of 5 mg/mL. The P3HT and PCBM were then deposited as four alternating monolayers on silicon wafers using the LB trough. In addition, the PCBM:P3HT solution was spun cast on silicon, and then four alternating monolayers on P3HT and PCBM were deposited on the spin cast layer. Half of the samples were annealed.

	P3HT:PCBM (1:1)	P3HT:PCBM:PCDTBT (11:15:4)
Efficiency (%)	1.10 ± .63	1.21 ± .06
J <sub>sc</sub> (mA/cm <sup>2</sup> )	7.50 ± 1.52	6.26 ± .23
V <sub>oc</sub> (V)	.297 ± .133	.393 ± .025
FF	.434 ± .083	.492 ± .014

Table 1: Device Performance of Polymer Blends  
 The experimental solar cells demonstrated higher V<sub>oc</sub>, FF, and overall efficiency than the control, but lower J<sub>sc</sub>.

The P3HT:PCBM:PCDTBT solar cells displayed a higher V<sub>oc</sub> of .393, higher fill factor of .492, and higher overall efficiency of 1.21% than the experimental cells did, but lower J<sub>oc</sub> of 6.26 mA/cm<sup>2</sup>. Phase separation was observed in the AFM images taken by the significant color contrast in **Figure 1.b**. The peaks on the film surface suggest the presence of desired columnar structures that could be responsible for the observed higher efficiency. However, TEM images of the samples must be obtained in order to verify the presence of such structures. AFM images of the LB trough-crafted samples must also be obtained in order to observe and compare film morphology.

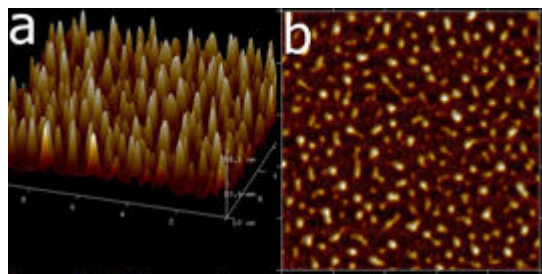


Figure 1. AFM images taken of the experimental solar cell blend. The high peaks of 58.1 nm in (a), a 3D view of the images, are demonstrated by the significant color contrast in image (b), a top view.

Future work includes altering the structure of the solar cell to improve J<sub>oc</sub>. Additional polymers such as PS or PMMA will be added to the active layer blend to induce further phase separation; its effects on active layer morphology and solar cell efficiency will be observed. In addition, the LB trough method will be tested in a

functional inverted solar device to observe actual efficiency.

[1] Pan, C.; Li, H.; Akgun, B.; Satijia, S. K.; Zhu, Y.; Xu, D.; Ortiz, J.; Gersappe, D.; Rafailovich, M. H. *Macromolecules* 2013, 46, 1812-1819.

[2] Hoppe, Harald, and Niyazi Sariciftci. "Morphology of Polymer/fullerene Bulk Heterojunction Solar Cells." *Journal of Materials Chemistry* 16.November (2005): 45-61. *Johannes Kepler University*. 28 Nov. 2005. Web. 6 Aug. 2014.

<[https://www.jku.at/JKU\\_Site/JKU\\_ipc/content/e166704/e175340/e177524/e177526/Publ2006.pdf](https://www.jku.at/JKU_Site/JKU_ipc/content/e166704/e175340/e177524/e177526/Publ2006.pdf)>.

# Creating a Solar-Powered Water Filtration System

Joshua Goldstein<sup>2</sup>, Daniel Foreman<sup>1</sup>, Steven Krim<sup>3</sup>, Gurkirat Singh<sup>3</sup>, Pierre Max Noldo Etienne<sup>4</sup>, Dr. Alvin Silverstein<sup>3</sup>, Dr. Stephen Walker<sup>3</sup>, Dr. John Jerome<sup>4</sup>, Veronica Burnett<sup>3</sup>, and Dr. Miriam Rafailovich<sup>3</sup>

1: Syosset High School NY 11791

2: North Shore Hebrew Academy High School Lake Success, NY, 11042

3: SUNY Stony Brook, Stony Brook NY 11790

4: Suffolk County Community College Selden, NY 11784

Tap water is something that we take for granted, especially in our country. In third world countries and post-natural disaster locations the primary need that must be addressed first is having a potable drinking water supply. The goal of our system is to provide this water supply efficiently, cheaply, and with little environmental cost, as well as providing an energy source. The system consists of a solar powered energy supply (STAR Trailer), which is hooked up to a water filtration setup



Figure 2. (Livinguard) Filter

that we designed around the (Livinguard) (Fig 2) filter specifications.<sup>1</sup> Our goal for the summer was to retrofit a filter system onto the STAR Trailer (Fig. 1) so that filter systems can be added to the trailer without major changes to its design. Since the STAR Trailer has already been deployed in places such as Haiti and Africa solely for



Figure 1. STAR Trailer



energy production, adding a water filtration system to it would benefit communities that use it already, even more.<sup>2</sup>

One part of our investigation was to see if the (Livinguard) filter is antibacterial, and if so, how. We placed  $1 \times 10^5$  staphylococcus aureus on one inch squares of the (Livinguard) filter and control cotton to see if the bacteria was killed. After a one day culture we found out that the (Livinguard) filter was able to exterminate all of the bacteria on contact (Fig 3). Because the (Livinguard) material was able to kill all the bacteria, we ran water tests with bacteria that was a  $2 \times 10^7$  lactobacillus/mL. ates were made from samples taken from the water that had and had not been passed through the (Livinguard) filter, and it was found that the water that had passed through the filter had no bacteria in it at all.

In the future, we need to make sure that the (Livinguard) filter does not leach out any of its antibacterial chemicals before we can give our approval to use the filter in the STAR Trailer system. It is also important to note that the filter would need necessary cleaning and upkeep, something that the person operating the STAR Trailer will be trained to do.

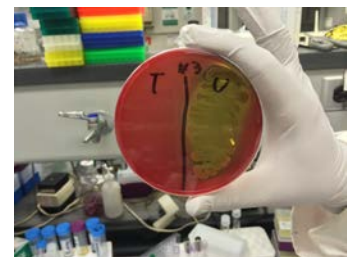


Figure 3. Bacteria Test Results

<sup>1</sup>Technology. (n.d.). Retrieved August 11, 2014.

<sup>2</sup> Wasserman, S. (2013, December 17). Solar Powered Water Purification for Orphanage in Haiti. Retrieved August 11, 2014.

# SESSION 10 : GRAPHENE

MENTORS: YING LIU

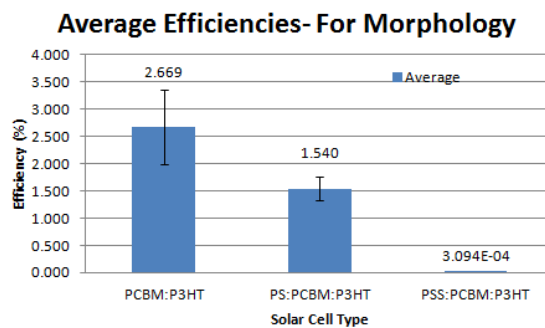
REBECCA ISSEROFF

ZHENHUA YANG

XIAOYU DI

MAXWELL PLAUT

HONGFEI LI



Blend	Avg PCE (%)	$J_{sc}$ (mA/cm <sup>2</sup> )	Voc (V)	FF (%)
PEDOT:PSS	0.346	1.69	0.455	45.0
GO	0.086	1.18	0.362	19.7
GO/PEDOT:PSS	0.872	4.08	0.435	49.1
r-GO/PEDOT:PSS	0.659	3.23	0.405	48.7
Au-GO/PEDOT:PSS	0.589	2.99	0.428	45.3
r-Au-GO/PEDOT:PSS	0.679	3.25	0.425	49.2
Pt-GO/PEDOT:PSS	0.358	3.30	0.328	43.9
r-Pt-GO/PEDOT:PSS	0.647	3.46	0.422	43.9

## Characterizing and Utilizing Silver Graphene and Iron Graphene Nanoparticles

**Jacqueline Barash**, Lawrence High School, Cedarhurst, NY, 11516 , **Rebecca Isseroff**, Lawrence High School, Cedarhurst, NY, 11516

Graphene, a single layer of carbon atoms structured in a honeycomb pattern, can be combined with any number of metals to produce nanoparticles that can serve many purposes, including water purification<sup>1</sup>, enhancing organic solar cell output, serving as an amphiphilic material used to combine two naturally incompatible polymers, etc.. Gold, platinum, and titanium metals are frequently tested with graphene for a multitude of purposes, however silver and iron graphene nanoparticles have never before been characterized for their properties.

In my research, my goal was to characterize iron and silver graphene nanoparticles, as well as find uses for these two nanoparticles. For my experiment, I needed vials of graphene oxide solution (GO), graphene solution, gold graphene oxide solution (Au-GO), and gold graphene solution (Au-Gr) for my constants, as well as silver graphene oxide solution (Ag-GO), silver graphene solution (Ag-Gr), iron graphene oxide solution (Fe-GO), and iron graphene solution (Fe-Gr) as variables (all solutions were made in 25:75 ethanol: H<sub>2</sub>O stock solution). Starting with GO solution, I added the metal salts and reduced half of the samples to create all my samples. The Ag-Gr, once reduced precipitated out of solution completely, and the Fe-Gr precipitated somewhat, but some stayed in solution (figures 1.1 & 1.2). All the samples were then split in order to make samples for FTIR, Raman spectroscopy, and confocal microscopy (the results for which are not available yet). A separate sample of Ag-Gr was then dried on two silicon wafers to be tested for anti-bacterial properties. 15mL of two types of bacteria, one for each slide, were placed on each slide and left for 24 hours. The next day the samples were dyed to prepare for confocal microscopy; the samples appeared to have no bubbles of bacteria on them. Confocal microscopy will Fe-Gr to see if it is a good medium for the mixing of polymers.



Figure 1.1- Fe-GO and Fe-Gr solutions



Figure 1.2- Ag-GO solution and Ag-Gr precipitate

1. TiO<sub>2</sub>-Graphene Nanocomposites. UV-Assisted Photocatalytic Reduction of Graphene Oxide, Graeme Williams, Brian Seger, and Prashant V. Kamat, *ACS Nano* **2008** 2 (7), 1487-1491

2. Transparent, Conductive Graphene Electrodes for Dye-Sensitized Solar Cells Xuan Wang, Linjie Zhi,\* and Klaus Müllen\* *Nano Letters* 2008 8 (1), 323-327

# Enhancing the Power Conversion Efficiency of Organic Photovoltaics via Exciton Energy Gap Reduction through the Integration of Functionalized Reduced Graphene Oxide and Phase Separated Polymer Morphology

Jessica Kim<sup>1</sup>, Zhenhua Yang<sup>2</sup>, Rebecca Isseroff<sup>3</sup>, Andrew Chen<sup>4</sup>, Dr. Miriam Rafailovich<sup>2</sup>

1) Manhasset High School, Manhasset, NY 11030, 2) Dept. of Materials Science and Engineering, Stony Brook University, NY 11794, 3) Lawrence High School, Cedarhurst, NY 11516, 4) Rice University, Houston, TX 77251

Organic solar cells are limited by recombination of excitons and excessive energy gaps within the active layer. The purpose of this study is to increase the efficiency of organic solar cells by 1) improving morphology with a nonconductive polystyrene (PS) column structure and 2) reducing the energy gap between phenyl-C<sub>61</sub>-butyric acid methyl ester 'Bucky balls' (PCBM - electron acceptor) and Poly(3-hexylthiophene-2,5-diyl) (P3HT- electron donor) by introducing gold functionalized reduced graphene oxide (Au-rGO) nanoparticles, which migrate to the interface<sup>[1]</sup>.

To form a column structure, either PS or polystyrene sulfonate (PSS) was blended with P3HT and PCBM in a 1:1:1 ratio with a concentration of 10mg/ml solution to form the active layer of the inverted solar cell<sup>[2]</sup>. Solar simulation (100 mW/cm<sup>2</sup> AM 1.5G illumination) results show that the PS:PCBM:P3HT blend had a higher efficiency (≈1.5%) than the PSS:PCBM:P3HT blend (≈0.0003%). AFM images show that deeper columns formed in the PS blend, which allow charge transfer and yield higher efficiency. It is important to note that the control, PCBM:P3HT blend, had the highest efficiency (≈2.6%). However, because both PS and PSS comprise a majority of the active layer and are non-conductive, the efficiency would be lowered despite organized morphology.

Because PS channels are more effective than PSS channels, PS channels were used in conjunction with Au-rGO to further reduce energy gaps. The polymer blends used, and their corresponding efficiencies, is shown in the table below. In two samples, 1.7% or 0.85% PSS was added because it was theorized that gold nanoparticles on a reduced graphene oxide sheet would bind with the sulfur on PSS and P3HT, while the PSS would integrate into the PS channels. This would further improve morphology. The results show that there was no significant difference (p>0.05) between the control (P3HT:PCBM) and the PS:PCBM: Au-rGO + 0.85%PSS:P3HT. This is encouraging because Au-

Blend:	Efficiency (%)	Jsc (mA/cm <sup>2</sup> )	Voc (V)	Fill Factor
P3HT:PCBM	1.269	6.976	0.462	0.395
PCBM: Au-rGO:P3HT	0.999	6.230	0.430	0.376
PS:PCBM: Au-rGO:P3HT	0.044	0.391	0.350	0.325
PS: 1.7%PSS- Au-rGO:PCBM:P3HT	0.265	1.721	0.435	0.356
PS:0.85%PSS- Au-rGO:PCBM:P3HT	1.342	5.451	0.572	0.433
0.85%PSS:PCBM: Au-rGO:P3HT	0.006	0.042	0.395	0.348

Table 1: Solar Simulation. The highest efficiencies were the control and the 0.85% PSS Au-rGo blends.

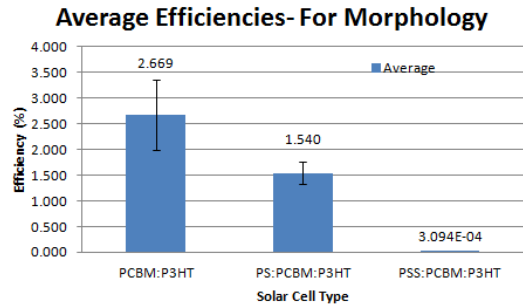


Fig. 1 shows that while the PCBM: P3HT blend has the highest efficiency, the PS and PSS blends have lower efficiencies because they are non-conductive.

rGO was only partially dissolved after stirring for one day. Perhaps, in the future, if the Au-rGO is dissolved for a longer period of time, the efficiency of the device would increase due to superior solution and film quality.

[1] Pan, Cheng, Hongfei Li, Bulent Akgun, Sushil K. Satijia, Yimei Zhu, Di Xu, Joseph Ortiz, Dilip Gersappe, and Miriam H. Rafailovich. "Enhancing the Efficiency of Bulk Heterojunction Solar Cells via Templated Self-Assembly." *Macromolecules* 46.5 (2013): 1812-819.

[2] He, Zhicai, Chengmei Zhong, Shijian Su, Miao Xu, Hongbin Wu, and Yong Cao. "Enhanced Power-conversion Efficiency in Polymer Solar Cells Using an Inverted Device Structure." *Nature Photonics* 6.9 (2012): 593-97.

# Optimizing Hole Extraction Layers of OPV Cells with Functionalized Graphene Derivatives

Michael Meng<sup>1</sup>, Jeffrey Cheng<sup>2</sup>, Michael Qu<sup>3</sup>

Andrew Chen<sup>4</sup>, Zhenhua Yang<sup>5</sup>, Dr. Miriam Rafailovich<sup>5</sup>

<sup>1</sup>Irvington High School, Fremont, CA 94538 <sup>2</sup>Clayton High School, St. Louis, MO 63105 <sup>3</sup>Oakton High School, Vienna, VA 22181 <sup>4</sup>Rice University, Houston, TX 77005 <sup>5</sup>Dept. of Material Science and Engineering, Stony Brook University, Stony Brook, NY 11790

Growing energy demands necessitate a cheap, efficient alternative to contemporary sources. Organic photovoltaic cells (OPVCs) provide a potential solution by virtue of low manufacturing cost, light weight, and mechanical flexibility.

This project seeks to modify Poly(3,4-ethylenedioxythiophene) polystyrene sulfonate (PEDOT:PSS) as a hole extraction layer (HEL), with functionalized graphene derivatives, in order to improve power conversion efficiencies (PCEs) and stability in OPVCs. Previous research has shown that the incorporation of graphene oxide (GO) into the PEDOT:PSS HEL enhances hole transport due to the improved hole conductivity and improved electron insulation. This study began with two hypotheses aimed at improving PCE: first, that reduction of GO would increase hole conductivity; and second, that functionalizing reduced GO (rGO) with gold (Au) and platinum (Pt) nanoparticles (NPs) would increase PCE by way of improving hole conductivity, tuning work function, and improving OPVC photocurrents due to an excitation of localized surface plasmon resonance<sup>[1]</sup>.

GO was synthesized using a modified Hummer's method, then reduced with NaBH<sub>4</sub> in the presence of gold and platinum salts. The functionalized GO derivatives were characterized using FTIR, Raman Spectroscopy, and TEM. Then, PEDOT:PSS was incorporated into each of the six solutions in a 2:1 [PEDOT:PSS]:[GO / GO derivative] volume ratio to create a homogeneous thin film when spincoating the HEL. The photovoltaic performance of these devices shown in **Table 1** was tested using a solar simulator with an AM 1.5G filter under light with an intensity of 100 mW/cm<sup>2</sup>.

The fabricated OPVCs yielded successful results in that the HEL mixtures of GO or GO derivatives with PEDOT:PSS consistently resulted in higher PCEs compared to HELs of GO alone or PEDOT:PSS alone. The test confirmed one hypothesis in particular: Au nanoparticles increased the PCE of rGO-based HEL layers. Moreover, the results demonstrated that the reduced Au-GO and reduced Pt-GO had higher short-circuit currents ( $J_{sc}$ ) and higher PCEs than their respective unreduced counterparts, indicative of metal NPs tuning the work function of rGO while maintaining rGO's conductivity. However, the GO and PEDOT:PSS composite layer had the highest  $J_{sc}$  out of all tested HELs, illustrating that tuning the work function to match the highest occupied molecular orbital of commonly used electron donor materials is more important than conductivity when optimizing electron hole transport.

Future work includes the incorporation of multi-walled carbon nanotubes (MWCNTs) into functionalized GO and PEDOT:PSS composite HELs; previous studies have shown that MWCNTs are effective in controlling the quality of polymer dispersion<sup>[2]</sup>, an aspect crucial to making homogenous conductively filled films.

Blend	Avg PCE (%)	$J_{sc}$ (mA/cm <sup>2</sup> )	V <sub>oc</sub> (V)	FF (%)
PEDOT:PSS	0.346	1.69	0.455	45.0
GO	0.086	1.18	0.362	19.7
GO/PEDOT:PSS	0.872	4.08	0.435	49.1
r-GO/PEDOT:PSS	0.659	3.23	0.405	48.7
Au-GO/PEDOT:PSS	0.589	2.99	0.428	45.3
r-Au-GO/PEDOT:PSS	0.679	3.25	0.425	49.2
Pt-GO/PEDOT:PSS	0.358	3.30	0.328	43.9
r-Pt-GO/PEDOT:PSS	0.647	3.46	0.422	43.9

**Table 1: Device Performance of Various HEL Blends**

[1] G.Q. Fan, Q.Q. Zhuo, J.J. Zhu, Z.Q. Xu, P.P. Cheng, Y.Q. Li, X.H. Sun, S.T. Lee, J.X. Tang, *Plasmonic-enhanced polymer solar cells incorporating solution-processable Au nanoparticle-adhered graphene oxide*, 2012, 1, 15614-15615.

[2] J. Kim, V.C. Tung, and J.X. Huang, *Advanced Energy Materials*, 2011, 1, 1052-1057.

## Investigating Novel Antibacterial Properties of Graphene, TiO<sub>2</sub> nanoparticles, and PDMS and EVA-based Phase Separated Polymer Blends

**Devorah Saffern**, Ma'ayanot Yeshiva High School, Teaneck, NJ, 07666, **Julie Vaughn**, Canyon Crest Academy, San Diego, CA, 92130, **Allison Lee**, University of Maryland, College Park, MD, 20742, **Dr. John Jerome**, Dept. of Mathematics, Suffolk Community College, Selden, NY, 11784, **Dr. Miriam Rafailovich**, **Dr. Ying Liu**, Dept. of Material Science and Engineering, Stony Brook University, Stony Brook, NY 11794, **Dr. Steven Walker**, Department of Oral Biology and Pathology, Stony Brook University, Stony Brook, NY 11794

Bacteria is a major source of a variety of diseases, and may adapt to chemical inhibitors at a relatively rapid pace. If a mechanical means of destroying bacteria could be developed, a greater variety of bacteria could be targeted through antibacterial coatings, which in turn may have a lesser impact on the environment than a chemical method. In this study, the bactericidal properties of phase separated polymer blends, polydimethylsiloxane (PDMS), titanium dioxide nanoparticles, and graphene were investigated across two bacterial species, *Staphylococcus aureus* and *Klebsiella pneumoniae*.

Phase separated polymer blends are shown to form microstructures after annealing according to their relative immiscibility<sup>1</sup>. In this study, the phase separation induced microstructures were meant to resemble the tall, approximately 200 nm columns found on the antibacterial wings of *Psaltoda claripennis* (cicadas)<sup>2</sup>, which are shown to kill Gram negative bacteria through a mechanical mechanism. Solutions of polystyrene (PS) to ethylene-vinyl acetate (EVA) and poly(styrene-co-4-bromostyrene) (PBrxS) to EVA were prepared at different relative concentrations, and then annealed for 90 hours. Microstructure formation in these samples, while highly visible through atomic force microscopy, did not have a high enough

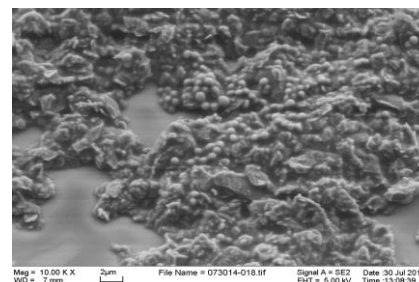


**Figure 1. SEM image of *S. aureus* on a graphene deposit**

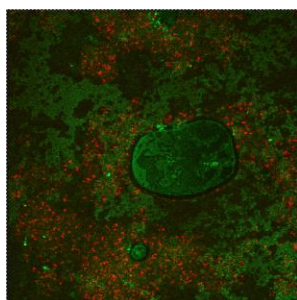


**Figure 2. Confocal image showing significant cell death due to graphene coating**

aspect ratio to be comparable to the columnar structure of the cicada wings. Further research involving the efficacy of polymer blends involving PDMS is currently being conducted, as well as experiments to determine if PDMS on its own possesses mechanical or chemical antibacterial properties.

According to previous research, titanium dioxide nanoparticles may have antibacterial properties when exposed to UV light, but the data of this experiment suggests that they are in fact not bactericidal on their own. Gram positive *Staphylococcus aureus* cells were stained (in a similar manner to all of the samples discussed here) using a bacteria viability dye (a mixture of propidium iodide and STYO 9) and confocal microscopy was utilized to reveal that the vast majority of cells were still alive after a 24 hour incubation.

Graphene, consisting of a carbon sheet one atom thick, was believed to have antibacterial properties, based on previous research, although studies resolved inconsistently<sup>3</sup>. In order to confirm graphene's antibacterial properties and gain information about the means of its destruction, a test was conducted in which *S. aureus* was placed on the surface of graphene (deposited via vapor deposition on a polyisoprene spin-coated silicon substrate). The cells were imaged with SEM to reveal that the bacteria clung to the surface of graphene (Fig. 1). Use of confocal microscopy was necessary to determine whether the bacteria had been killed. A large amount of dead bacteria was found in comparison to the control, confirming graphene's ability to kill bacteria (Fig 2). In the future, work will ideally be conducted to determine the exact mechanisms of graphene's antibacterial properties as well as better characterization of the different surfaces' morphologies.

<sup>1</sup> Karim, A., T. M. Slawecki, S. K. Kumar, J. F. Douglas, S. K. Satija, C. C. Han, T. P. Russell, Y. Liu, R. Overney, J. Sokolov, and M. H. Rafailovich. "Phase-Separation-Induced Surface Patterns in Thin Polymer Blend Films." *Macromolecules* 31.3 (1998): 857-62. Web

<sup>2</sup> Pogodin, S., Hasan, J., Baulin, V., Webb, H., Truong, V., Nguyen, T. H. P., Boshkovikj, V., Fluke, C., Watson, G. S., Watson, J. A., Crawford, R., & Ivanova, E. (2013) Biophysical Model of Bacterial Cell Interactions with Nanopatterned Cicada Wing Surfaces. *Biophysical Journal*, 104(4), 835-840.

<sup>3</sup> Liu, S., Zeng, T. H., Hofmann, M., Burcombe, E., Wei, J., Jiang, R., Kong, J., & Chen, Y. (2011). Antibacterial Activity of Graphite, Graphite Oxide, Graphene Oxide, and Reduced Graphene Oxide: membrane and Oxidative Stress. *ACS Nano*, 5(8), 6971-6980.

## Coating Hydrogen Fuel Cell Membranes with Different Functionalizations of Graphene Oxide and Reduced Graphene Oxide to Optimize Polymer Electrolyte Membrane Fuel Cell Efficiency

Lee Blackburn, Lawrence HS, Cedarhurst, NY, 11516, Arthur Chen, Lawrence HS, Cedarhurst, NY, 11516, Justin Lish, HAFTR HS, Cedarhurst, NY, 11516, Hongfei Li, Stony Brook University, Stony Brook, NY, 11794, Mrs. Rebecca Isseroff, Lawrence HS, Cedarhurst, NY, 11516

There is an increasing demand for an alternative clean source of energy, as the supply of fossil fuels diminishes and the temperature of Earth's atmosphere slowly rises. Hydrogen fuel cells are a promising clean source of energy still under development. Currently hydrogen fuel cells are not widely utilized, partly due to the inefficiency of the membrane since it can only operate at temperatures lower than 80 degrees Celsius. This decreases the performance of the fuel cell because of slow electrode kinetics and virtually no CO tolerance. The goal of this project is to coat the membrane with various forms of graphene to remove any CO poisoning, while increasing proton conductivity. In previous experiments, graphene oxide (GO), reduced graphene oxide (RGO), gold GO and gold RGO, platinum GO and platinum RGO were coated on the membrane of hydrogen fuel cells. This increased the power efficiency of the fuel cell, and out of all the samples tested previously, the gold graphene was most successful. In this new study, the effect of Gold-Platinum GO and Gold-Platinum RGO on the polymer electrolyte membrane has been examined. GO was synthesized and then prepared in a solution of ethanol and water. Gold and platinum were then individually and simultaneously conjugated in the GO using  $\text{KAuCl}_4$  and  $\text{K}_2\text{PtCl}_4$  salts. Next, a portion each Au-GO/Pt-GO/Au-Pt-GO solution was reduced using sodium borohydride. Data from Fourier Transform Infrared Spectroscopy (FTIR), determined that some functional groups remained on the Pt-RGO, specially OH and COOH. In addition, Au-RGO contained OH groups on after being reduced. The Au-Pt-GO sample had a small amount of functional groups left, while Au-PT-RGO still had all of its functional groups. According to the FTIR data, the functional groups on the GO were successfully removed, producing RGO and thus showing a successful reduction. For comparison, the FTIR spectra for graphene oxide and reduced graphene oxide samples are displayed below in figures 1 and 2.

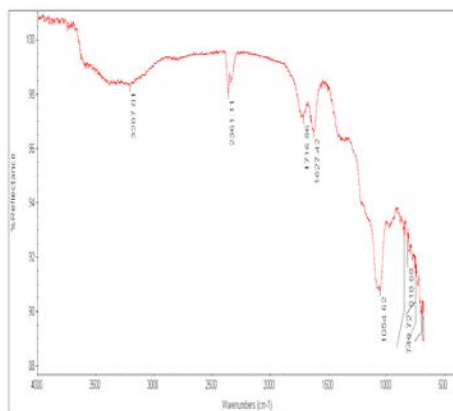


Fig. 1 plots the Fourier Transform Infrared Spectroscopy spectrum produced by the graphene oxide sample.

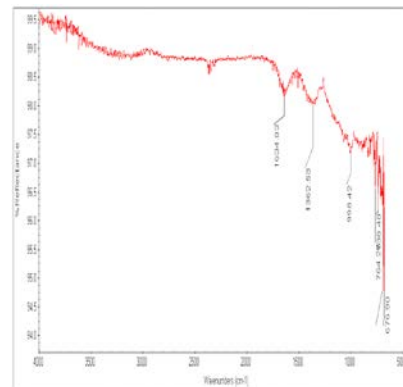


Fig. 2 plots the Fourier Transform Infrared Spectroscopy spectrum produced by the reduced graphene oxide sample.

Jalani, Nikhil H. *Development of Nanocomposite Polymer Electrolyte Membranes for Higher Temperature PEM Fuel Cells*. Thesis. Worcester Polytechnic Institute, 2006. N.p.: n.p., n.d. *Electronic Theses and Dissertations*. 1 Mar. 2006. Web. 06 Aug. 2014.

Majsztrik, Paul W. *MECHANICAL AND TRANSPORT PROPERTIES OF NAFION® FOR PEM FUEL CELLS; TEMPERATURE AND HYDRATION EFFECTS*. Thesis. Princeton University, 2008. N.p.: n.p., n.d. *MECHANICAL AND TRANSPORT PROPERTIES OF NAFION® FOR PEM FUEL CELLS; TEMPERATURE AND HYDRATION EFFECTS*. Web. 6 Aug. 2014.

## Compatibilization of Thin Film Binary Polymer Blends Using Pure and Oxidized Graphene

Omkar Sreekanth, The Charter School of Wilmington, Wilmington DE, 19807, Evan Lander, Plainview Old-Bethpage John F. Kennedy HS, Plainview NY, 11803, Maxwell Plaut (Stony Brook University), and Xiaoyu Di (Stony Brook University)

Thin film polymer blends are a key area in polymer research because they have various applications in multi-color photographic printing, paints, adhesives, and protective coatings.<sup>1,2</sup> Polymers are generally immiscible with each other, and when they blend, the result is a material that has a weak interfacial adhesion.<sup>3</sup> Compatibilizers, when added to an immiscible polymer blend, alter the blend's interfacial character and stabilize its morphology.<sup>4</sup> In this study, the effect of using graphene and graphene oxide as compatibilizers to reduce phase separation in a well-known binary polymer blend system: polystyrene (PS)/poly(methyl methacrylate) (PMMA) was investigated. PS and PMMA phase separate because of their difference in intermolecular forces. Graphene was tested as a compatibilizer because of its large aspect ratio and incredible mechanical strength. Contact and Neumann angle measurements were obtained using atomic force microscopy (AFM) and were used to determine the interfacial tension of PS:PMMA (1:3) blends. The blends were annealed for 24, 48, and 72 hours. The blends containing graphene and graphene oxide were shown to have a lower contact angle as the annealing time increased (Figure 1). The lower the contact angle measures are, the more effective the compatibilizers are. Thus, a positive correlation can be established between annealing time and effectiveness of compatibilizers. The PS:PMMA blends had average contact angle measures of 8.00, 7.87, and 7.65 degrees after 24, 48, and 72 hours of annealing, respectively. The blends containing graphene had average contact angle measures of 5.74, 5.17, and 4.70 degrees. The blends containing graphene oxide had average contact angle measures of 4.85 (Figure 2) and 4.19 degrees. Blends containing both graphene and graphene oxide worked as compatibilizers as shown by the decreasing contact angle. Overall, both graphene and graphene oxide were shown to be effective compatibilizers, but with graphene oxide shown to be more effective.

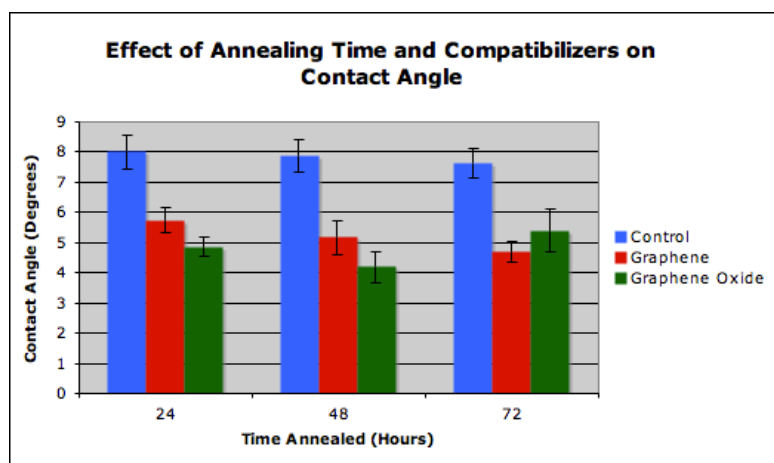


Figure 1: Bar graph of compatibilization vs. annealing time. There is a positive correlation between annealing time and compatibilization as shown by the decline in contact angle measures as annealing time increases.

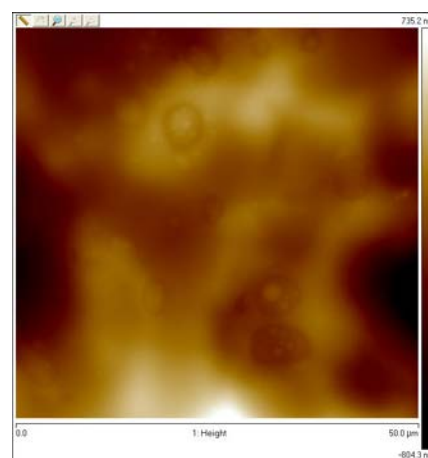


Figure 2: AFM image of sample containing PS:PMMA 1:3 with graphene oxide annealed for 24 hours showing less phase separation than graphene and control samples.

<sup>1</sup> Ade, H.; Smith, A. P.; Qu, S.; Ge, S.; Sokolov, J.; Rafailovich, M. Phase segregation in polymer thin films: Elucidations by X-ray and scanning force microscopy. *Europhys. Lett.* **1999**, *45*, 526.

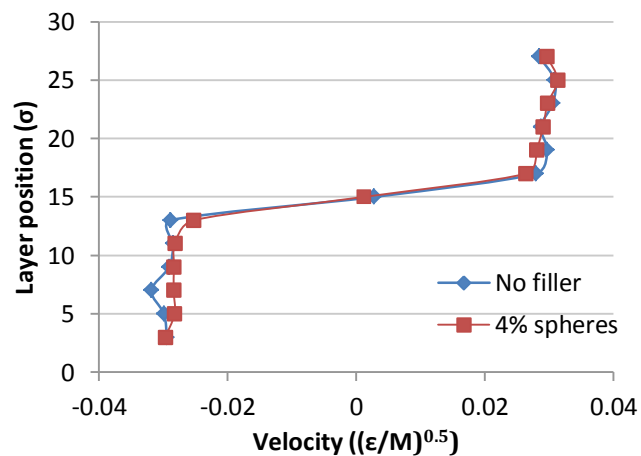
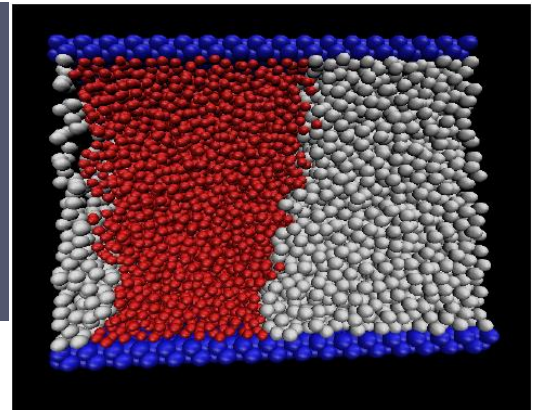
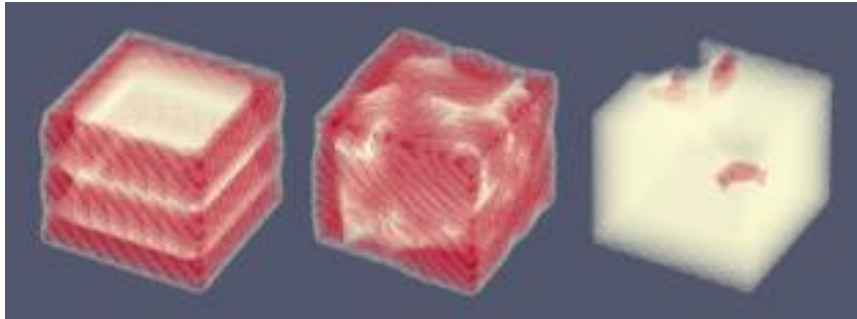
<sup>2</sup> Tsui, Ophelia Kwan Chui, and Thomas P. Russell, eds. *Polymer Thin Films*. Vol. 1. Singapore: World Scientific, 2008. Print.

<sup>3</sup> Karim, A.; Slawacki, T. M.; Kumar, S. K.; Douglas, J. F.; Satija, S.; Han, C. C.; Russell, T. P.; Liu, Y.; Overney, R.; Sokolov, J.; Rafailovich, M. H. Phase-Separation-Induced Surface Patterns in Thin Polymer Blend Films. *Macromolecules* **1998**, *31*, 857.

<sup>4</sup> S. Park and R. S. Ruoff. The chemistry of graphene oxide. *Nat. Nanotechnol.* **2009**, *4*, 217–224.

# SESSION 11 : SIMULATION AND MODELLING

MENTORS: NING SUN  
DI XU



## Using Nanofillers To Strengthen Polymer Blends

Matthew Wu<sup>1</sup>, Di Xu<sup>2</sup>, Dr. Dilip Gersappe<sup>2</sup>, Dr. Miriam Rafailovich<sup>2</sup>

<sup>1</sup>Naperville Central High School, Naperville, IL

<sup>2</sup>Dept. of Materials Science and Engineering, Stony Brook University, Stony Brook, NY

Polymer blends promise to be an easier, cheaper way to develop materials with desirable physical properties.<sup>1</sup> Unfortunately, most polymer blends are immiscible and tend to phase separate, leading to a material with poor mechanical properties.<sup>2</sup> Compatibilization is the act of increasing the miscibility of blend components, thereby reducing phase separation and strengthening the blend. Several studies have shown that the addition of nanofillers, such as spherical carbon black nanoparticles and sheet-like graphene<sup>2</sup> or organoclays,<sup>3</sup> can help compatibilize a polymer blend. Molecular dynamics (MD) is the simulation of a many-body system using classical mechanics. MD helps us understand how compatibilization works on a molecular level, a degree of precision difficult to attain in an experimental setting. In this project, we use MD to simulate the compatibilizing and strengthening ability of spheres and sheets, modeled after their real-world counterparts.

We use the LAMMPS Molecular Dynamics Simulator to perform MD simulations. Pairs of atoms interact through a Lennard-Jones (LJ) potential.  $\sigma$  and  $\epsilon$ , parameters from the LJ potential equation, and  $M$ , the mass of one atom, are used as units of length, energy, and mass in our simulation. Bonds are modeled by a finitely extensible non-linear elastic (FENE) potential. The simulation box of size  $(x, y, z) = (15\sigma, 15\sigma, 30\sigma)$  is bounded in the  $z$ -dimension by walls, while periodic boundary conditions are used in the  $x$ - and  $y$ -dimensions. Shear is applied by moving the top wall in the  $+x$  direction and the bottom wall in the  $-x$  direction, each at a velocity of  $0.03 (\epsilon/M)^{0.5}$ . Our system consists of two types of polymers, each modeled as chains of 57 atoms, with adjacent atoms connected by FENE bonds. Sphere nanofillers, when present, are modeled as single atoms. Before shear is applied, the polymer blend is allowed to phase separate so that one polymer type is located at the bottom half of the simulation box and the other is located at the top half, with an interface at a  $z$ -position of  $15\sigma$ .

Simulations were performed with no nanofiller and with 4% sphere filler. While shear is applied, the velocity profile is plotted for each simulation in Figure 1. In both cases, there is a large difference in the velocity of polymer atoms above and below the interface, characteristic of a strongly phase-separated polymer blend.<sup>4</sup> When a blend is compatibilized, the interfacial velocity difference should decrease. However, the velocity profile of the blend with sphere filler shows little improvement over that of the control. This may be because of large voids at the interface, which hinders the ability of spheres to span the interface and reduce the interfacial tension.

We hope to continue to test sphere nanofillers at various concentrations and shear rates. Afterward, we seek to test sheet nanofillers, examining their location and orientation in a polymer blend under shear.

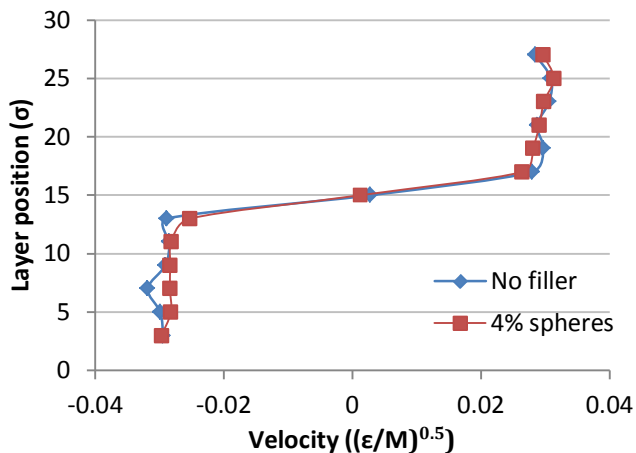


**Figure 1.** Velocity profile of polymer blends under shear, with no nanofiller and with 4% sphere filler. The simulation box is divided along the  $z$ -dimension into 15 layers, each  $2\sigma$  thick. The average velocity of polymer atoms in each layer is graphed against the  $z$ -position of each layer.

[1] Utracki, L. A. History of commercial polymer alloys and blends. *Polymer Engineering & Science*. **1995**, *35*, 2.

[2] Cao, Y.; Zhang, J.; Feng, J.; Wu, P. Compatibilization of Immiscible Polymer Blends Using Graphene Oxide Sheets. *ACS Nano*. **2011**, *5*, 5920-5927.

[3] Si, M.; Araki, T.; Ade, H.; Kilcoyne, A. L. D.; Fisher, R.; Sokolov, J. C.; Rafailovich, M. H. Compatibilizing Bulk Polymer Blends by Using Organoclays. *Macromolecules* **2006**, *39*, 4793-4801.

[4] Adhikari, N. P.; Goveas, J. L. Effects of Slip on the Viscosity of Polymer Melts. *J. Polym. Sci.* **2004**, *42*, 1888-1904.

# Designing Tablets for Personalized Medicine

Gina Yuan<sup>1</sup>, Ning Sun<sup>2</sup>, Dilip Gersappe<sup>2</sup>, Miriam Rafailovich<sup>2</sup>

<sup>1</sup>Dougherty Valley HS, San Ramon, CA, 94582

<sup>2</sup>Department of Materials Science and Engineering, Stony Brook University, Stony Brook, NY, 11794

Patient responses to identical treatments can be highly variable. Personalized medicine aims to use genetics or other molecular mechanisms to create a targeted therapy for the specific patient. Orally-administered tablets can be designed to have the appropriate dosage and drug release mechanism by altering the shape and the component ratios. The USP 2 paddle apparatus is currently the only method for predicting *in vivo* tablet dissolution. Although the test is generally accepted as valid, the apparatus has also been shown to produce unpredictable and inconsistent results.<sup>1</sup> A computer model has the advantages of being able to accurately, repeatedly, and quantitatively observe the system fluid dynamics and the dissolved tablet concentration. In this study, the fluid dynamics of the USP 2 model were developed in C++ using Palabos software, which employs the Lattice Boltzmann Method and parallel computing to create an efficient program.

To ensure the theoretical model's fluid dynamics reflect that of the real paddle apparatus, the morphology of the system was established according to the standardized dimensions of the USP 2, followed by coupled fluid velocity and advection-diffusion lattices to model fluid and particle movement. In this model, the tablet dissolves only by means of diffusion and solid-liquid mass transfer. The dissolution rate increases with paddle speed (Figure 1). Moreover, the dissolution behavior in the single component model (Figure 2) appears to match empirical studies<sup>2</sup>.

Several multicomponent morphologies were also studied with this simulation (Figure 3). Multiple parameters of each component can be changed to reflect the behavior of actual pharmaceuticals. If the dissolution of multicomponent tablets using various parameters on this computer model can be shown to quantitatively and qualitatively reflect experimental data, then this system can potentially be applied to testing oral drugs for personalized medicine in a convenient and cost-effective manner.

<sup>1</sup>Rowe, C.; Katstra, W.; Palazzolo, R.; Teung, P.; Giritlioglu, B.; Cima, M. J. Multimechanism oral dosage forms fabricated by three dimensional printing™. *J Control Release*. **2000**, *66*, 11-17.qq

<sup>2</sup>Mauger, J.; Ballard, J.; Brockson, R.; De, S.; Gray, V.; Robinson, D. Intrinsic Dissolution Performance Testing of the USP Dissolution Apparatus 2 (Rotating Paddle) Using Modified Salicylic Acid Calibrator Tablets: Proof of Principle. *Dissolut. Technol.* **2003**, *10*, 6-15.

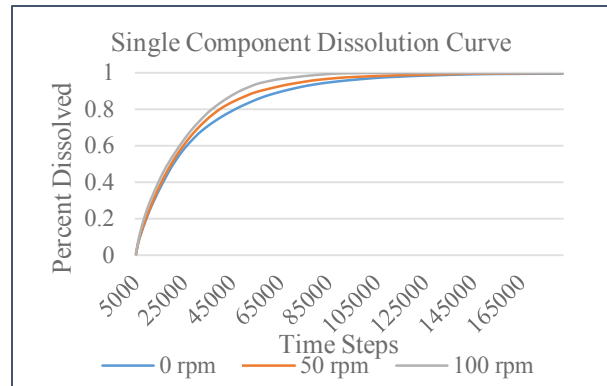


Figure 2. Dissolution curves of a single component tablet in this model at 0, 50, and 100 rpm.

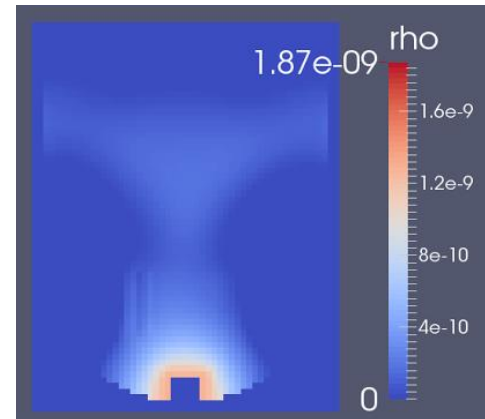


Figure 2. Model advection-diffusion lattice at 50 rpm.

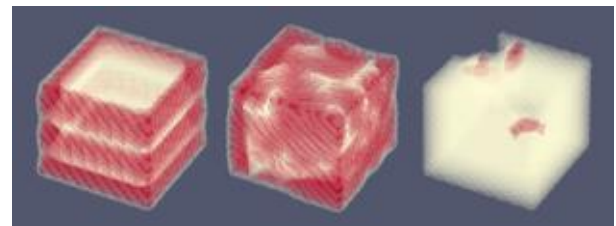


Figure 3. Morphologies of multicomponent tablets from left to right: layered tablet, homogenous tablet, coated tablet.

## Optimizing the Morphology of Organic Solar Cells

Constance Lam<sup>1</sup>, Di Xu<sup>2</sup>, Dilip Gersappe<sup>2</sup>, Miriam Rafailovich<sup>2</sup>

<sup>1</sup>Scarsdale High School, Scarsdale, NY

<sup>2</sup>Dept. of Materials Science, Stony Brook University, Stony Brook, NY

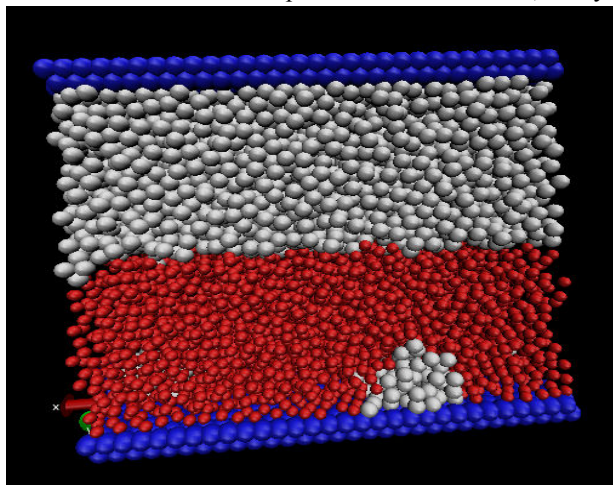


Figure 1a

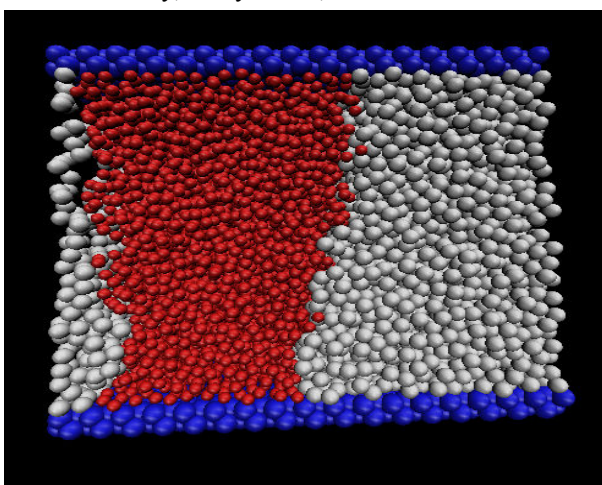


Figure 1b

Figure 1a: An example of a 30x30x25 control simulation trial 1 where polymer blends split into bilayers

Figure 1b: An example of a 30x30x25 control simulation trial 2 where polymer blends split into columns

The world's increasing energy consumption requires renewable and sustainable sources of energy. Inorganic solar cells are viable alternatives, however expensive because of the high production cost of crystalline silicon material. While organic solar cells have grown to be feasible alternatives to inorganic cells, commercially available organic solar cells only have the average power conversion efficiency (PCE) of 1.5%-2.5% due to low external quantum efficiency<sup>1</sup>. For greater solar efficiency, bulk heterojunction photovoltaic cells, whose electron donor and acceptor are mixed together to form a polymer blend, are promising solutions. However, the optimal morphology and composition of these cells are yet to be found.

In this research, two computer simulation programs were utilized to digitally model solar cells to find the optimal blend of polymers and nanofillers for organic solar cells: LAMMPS (Large-scale Atomic Molecular Massively Parallel Simulator) and Molecular Dynamics. LAMMPS was used to input atoms and depict their movements through calculating the Lennard-Jones' potentials that affect the movements of other atoms. Using Molecular Dynamics, the LAMMPS data visually displayed the atoms in three dimensions. The goal of the research is the morphology control of columnar phases in the solar cell, which will provide the maximum energy efficiency<sup>2</sup>. The controls were solar cells of different sizes without nanofillers (Figure 1a, 1b). Then, through varying nanofiller types, simulation sizes, polymer lengths, and nanofiller amounts, the cell structure was tested to see if nanofillers can successfully stabilize a columnar structure. The results demonstrate that as the simulation box got larger, the columns were more likely to become a bilayer structure. Furthermore, tests showed, as predicted, that spherical nanofillers aid in the compatibilization of polymer blends. In the future, the research project also will test graphene nanofillers, a novel approach to the conventional organic solar cell. Furthermore, the simulation will help pinpoint the exact optimal conditions for the maximum power conversion efficiency in bulk heterojunction cells.

<sup>1</sup>Scharber, M.C., and N.S. Sariciftci. "Efficiency of Bulk-heterojunction Organic Solar Cells." *National Center for Biotechnology Information*. U.S. National Library of Medicine, 03 June 0006. Web. 06 Aug. 2014.

<sup>2</sup>Pan, Cheng, Hongfei Li, Bulent Akgun, Sushil K. Satijia, Yimei Zhu, Di Xu, Joseph Ortiz, Dilip Gersappe, and Miriam H. Rafailovich. "Enhancing the Efficiency of Bulk Heterojunction Solar Cells via Templated Self-Assembly." *Macromolecules* 46.5 (2013): 1812-819. Web.



The Garcia Program gratefully acknowledges support from:

The Louis Morin Charitable Trust  
 National Science Foundation  
 Starbucks